Active control of sound absorption

Dipl.-Ing. Marco Norambuena

Von der Fakultät V - Verkehrs- und Maschinensysteme
der Technischen Universität Berlin
zur Erlangung des akademischen Grades

Doktor der Ingenieurwissenschaften
- Dr.-Ing. -

genehmigte Dissertation

Promotionsausschuss:

Vorsitzender:	Prof. Dr. sc. Jörn Sesterhenn
Gutachter:	Prof. Dr.-Ing. Michael Möser
	Dr.-Ing. André Jakob

Tag der wissenschaftlichen Aussprache: 21 Juni 2012

Berlin 2012
D 83

Contents

Introduction **1**

1 Theoretical background **4**
1.1 Wave decomposition 4
1.2 Power absorption by a secondary source 5
1.2.1 Infinite tube 6
1.2.2 Semi-infinite tube 8
1.2.3 Semi-infinite tube with a variable impedance at the end 12
1.3 Modal model of a rectangular enclosure 15
1.4 Control criterion 18
1.4.1 Cost function 19
1.4.2 Unidirectional control 20
1.4.3 Three-dimensional control 24
1.5 Absorption mechanism of real loudspeakers 26
1.6 Absorption coefficient of an array of secondary sources 26
1.7 Total acoustic potential energy 28
1.8 Reverberation time 29

2 Numerical results - Simulations **31**
2.1 Validation of simulations 31
2.2 Sound pressure field within a two-dimensional enclosure 33
2.2.1 Distance between secondary source and control point 33
2.2.2 Comparison against ANC system 36
2.2.3 Different distribution of primary sources 37
2.3 Sound pressure field within a three-dimensional enclosure 38
2.3.1 Control sources over six walls of the enclosure 40
2.3.2 Control sources over only selected walls of the enclosure 44
2.3.3 Absorption behavior at resonant frequencies 45
2.3.4 Comparison against ANC systems 46
2.4 Absorption coefficient and intensity in front of an array of secondary sources 49
2.4.1 Different number of secondary sources and sensors 51
2.5 Free field approximation inside a room 52
2.6 Frequency response within the enclosure 56
2.7 Acoustic potential energy 59
2.8 Direct control of the absorption coefficient α 62

3 Experimental results **65**
3.1 Control system 65
3.1.1 Manual control 65

3.1.2 Adaptive control 66
Secondary path $\widehat{\mathbf{c}}$ estimation 68
3.2 Active absorption in a one-dimensional waveguide 69
3.2.1 Pure tone excitation 71
Manual control 71
Absorption coefficient and Gain-Phase relationship 73
Adaptive control 76
3.2.2 Broadband excitation 76
Manual control 76
Adaptive control 87
3.3 Microphone pair transfer function 89
3.4 Active absorption of a single source mounted over a panel 93
3.4.1 Absorption coefficient 94
Pure tone excitation 94
Broadband excitation 94
3.4.2 Sound pressure map in front of the secondary source 96

4 Concluding remarks **105**

Appendix **109**

Bibliography **111**

Acknowledgements

At the end of this work I want to express my gratitude to all the people that collaborated throughout this adventure. In first place, I want to thank Professor Michael Möser not only for his guidance and supervision but also for his continuous encouragement and support.

Special thanks to André Jakob for sharing his knowledge and experience in active control systems and most importantly for having the infinite patience of answering my *short questions*. A big thanks goes to Rafael Piscoya for all the hours reviewing this thesis and the countless discussions over the years about these (and many other) subjects.

I also want to thank all the staff of the Institute of Fluid Mechanics and Engineering Acoustics which in one way or the other contributed to carry out this work. I want to specially thank my colleagues and friends at the Department of Engineering Acoustics who not only helped along the years in work but also made my stay in Berlin much more pleasant, Ricardo Alzugaray, Daniel Mena, Gianfranco Zuazo and, in the final stage, Jose Luis Barros.

From the distance, I want to thank my parents and all my family for the unconditional love and support that I have always received from all of them, this was one of the forces that kept me moving forward during this journey. And last, but definitely not least, my deepest gratitude to Anna for having the heart to join me in this adventure, you made all this much easier.

Abstract

The work presented here introduces a novel mathematical model for a multichannel active absorption system based on the wave separation method of Nishimura. The theoretical background of the active absorption system is presented in combination with a large set of simulations. Experiments confirm the behavior described by the simulations. The wave separation method is combined with the modal model of a three-dimensional room in order to obtain the controlling parameters of the active system.

Several parameters are simulated to study their influence over the performance of the active absorption, e.g. the density of secondary sources, the distance between sources and sensors, the distribution of sources, etc.

It is found that the equivalent absorption coefficient generated by active system reaches an optimal point when the density of sources approaches to three sources per wavelength (of the primary excitation). Under optimal conditions it is possible to generate an equivalent absorption coefficient of $\alpha = 1$. Moreover, it is shown that it is also possible to generate arbitrary values of the absorption coefficient between 0 and 1.

The active absorption system is not only able to modify the sound pressure field generated by a primary source inside an enclosure but, more importantly, it is able to efficiently damp the normal modes. Measurements and simulations show the damping of the normal modes as an *homogenization* of the pressure field which means that the differences between maxima and minima tend to vanish. The effect of modes damping is also reflected in the reduction of the acoustic potential energy. In the extreme case where the active system covers all surfaces of the rigid enclosure, it was proven that is possible to generate a free field radiation condition.

The active absorption method introduced in this work it is compared with the widely known *active noise control* (ANC) method in order to establish their differences.

Zusammenfassung

Die hier vorgestellte Arbeit gibt einen kurzen Einblick in ein neues mathematisches Modell eines Systems zur aktiven Mehrkanalabsorption, welches auf der Wellen-Trennung von Nishimura basiert. Der theoretische Hintergrund des aktiven Absorptionsystems wird in Kombination mit einer Vielfalt von Simulationen präsentiert. Versuche belegen das in den Simulationen beschriebene Verhalten. Die Methode der Wellenseparation wird mit einem modalen Modell eines dreidimensionalen Raumes kombiniert, um die das aktive System kontrollierenden Parameter zu erhalten.

Einige Parameter werden simuliert, um ihre Auswirkungen auf die Leistung der aktiven Absorption zu untersuchen, z.B. die Dichte der sekundären Quellen, der Abstand zwischen Quelle und Sensor, Quellenverteilung etc.

Es wird gezeigt, dass der vom aktiven System generierte äquivalente Absorptionsgrad, einen optimalen Punkt erreicht, wenn die Dichte der Quellen gegen 3 Quellen pro Wellenlänge (aus der ersten Erregung) läuft. Unter Idealbedingungen ist es möglich, einen äquivalenten Absorptionsgrad von $\alpha = 1$ zu erzeugen. Darüber hinaus wird gezeigt, dass es ebenfalls möglich ist, für den Absorptionsgrad beliebige Werte zwischen 0 und 1 zu generieren.

Das aktive Absorptionssystem ist nicht nur in der Lage, das von der primären Quelle in einem geschlossenem Raum erzeugte Schalldruckfeld zu modifizieren, sondern vielmehr die entsprechende Moden effizient zu dämpfen. Messungen und Simulationen zeigen die Dämpfung der Moden als *Homogenisierung* des Druckfeldes, was soviel heisst, dass die Unterschiede zwischen Minima und Maxima dazu neigen zu verschwinden. Der Effekt der Modendämpfung spiegelt sich zudem in der Reduktion der Akustischen potentiellen Energie wieder. Im Extremfall, wo das aktive System alle Oberflächen des festen Begrenzung bedeckt, wurde nachgewiesen, dass es möglich ist, eine Freifeldbedingung zu erzeugen.

Die in dieser Arbeit vorgestellte aktive Absorptionsmethode wird mit der bereits bekannten ANC (Active Noise Control) verglichen, um ihre Unterschiede hervorzuheben.

Introduction

In architectural acoustics one of the most important parameters that defines the acoustic quality of a room is the reverberation time (RT_{60}). This parameter can be handled by means of modification of the absorption in the room. At middle and high frequencies it is rather easy to manage the absorption using passive materials like porous absorbers or resonators, however it is a major challenge to replicate the same degrees of absorption at low frequencies using these same passive absorbers. Mainly because the larger wavelength involved would require absorbers of huge dimensions, making them impractical for implementation. Therefor it becomes of major interest to address this problem and try to find a more effective solution.

The development of computers and embedded electronic chips in the last 30 years has opened a door offering new opportunities to solve problems as never before. And acoustics has not been a stranger to these new advances. The best examples of these are all the improvements fostered by the Digital Signal Processing (DSP) and all its branches that had allowed to have today faster and more powerful measurement and data analysis systems. But not only the acquisition and processing of data has been benefited by this technology, it has also been directly applied to provide new solutions. Probably one of the most favored area of this advances is the noise control, which has been able to successfully implement this technology to create feasible, efficient and relatively low cost active noise control (ANC) systems.

Considering all the background knowledge provided by years of research in ANC, it is valid to raise the questions: Is it possible to extrapolate the development of ANC systems to create *active absorption*?. Exists such a thing as *active sound absorption*?. If ANC *actively cancels sound*, how does this differs from *actively absorb sound*?. Would *active sound absorption* be able to provide an effective solution at low frequencies?. This work tries to answer these questions and provide a deeper understanding of the *active absorption*.

From the acoustic point of view, a passive absorbent material is such that over an impinging sound wave it is able to reduce the amplitude of the resulting reflected wave, where the difference between incident and reflected wave is partly transmitted and partly dissipated as heat. In physical terms, the energy of the incident part E_i of the wave must be equal to the sum of the reflected E_r, the dissipated E_d and the transmitted E_t parts, or

$$E_i = E_r + E_d + E_t.$$

If we simplify this model to consider that there is no transmission involved ($E_t \to 0$) and the material is only able to either reflect or dissipate the energy, the best absorbent material will be the one with the highest dissipative capabilities, and consequently will minimize the reflected part of the energy E_r. Thus, an *active absorption system* must be able to mimic this exactly same behavior, i.e. dissipate energy and minimize only

the reflected part of the sound. This behavior differs clearly from an ANC system whose objective is to minimize the sound pressure at a given control point and hopefully its surrounding area. However this minimization is certainly not able to discriminate if it is an incident or a reflected part of the sound field that is being observed. Moreover, there is no energy absorption involved in this process but only a spatial shifting of the sound energy. Even though the surrounding area of the control point becomes quieter, there will be other points in space where the sound pressure will be undoubtedly incremented.

A literature research reveals that in recent years new techniques developed from the active noise control world have been used to provide solutions in the area of active sound absorption. Four main methodologies can be found throughout the literature: impedance control, Kirchhoff-Helmholtz integral equation, energy-power minimization control and wave separation.

Orduña-Bustamante [1] presents a one-dimensional feed-forward adaptive system using an impedance control method. This method aims to change the acoustical impedance of the control source to a desired value in a way to avoid the sound reflection. A year later, Wu [2] presented a similar work where he also uses a state-space feedback model to modify the impedance and report simulations for a one-dimensional wave propagation case.

Takahashi [3, 4] and later Takane [5] worked in active absorption systems using the Kirchhoff-Helmholtz boundary integral equation method which uses a large number of sensors and sources to manage the reflection over an imaginary control surface.

Computer simulation by Clark [6] has been made with the method based on the control of the acoustic potential energy to achieve the sound absorption. Elliott [7] and Zimmermann [8] used the power minimization criterion to achieve absorption, implemented on digital and analog systems respectively. Ise [9] also presents a one-dimensional system based on the sound intensity control.

Guicking [10, 11], one of the precursors in this area, made the first attempt to create an active absorption device in 1983. He presented an analog absorption system based on a standing wave separator that years later Zhu [12] will call delay method of wave separation. Following the work of Guicking, Wenzel [13] tried to expand this method to work with an array of secondary sources using an adaptive digital controller.

Nishimura [14,15] experimented with three different approaches to build a one-dimensional active absorber, with two feed-forward and one analog feedback control system. In one of those approaches he introduced a new wave separation method. Zhu [12] took these wave separation methods from Guicking and Nishimura to create a thin panel speakers controller to modify reflection, absorption and transmission coefficients inside a tube. From these two methods, Zhu reported that the wave separation introduced by Guicking presents a large disadvantage since the wave separation is not complete and both components (incident and reflected) possess parts from each other. On the other hand, the wave separation procedure introduced by Nishimura is able to completely separate the incident p_i and the reflected p_r parts of the sound field.

All these past works have been mainly focused on the presentation of the electro-acoustic systems required to achieve the absorption and none of them has been able to provide an accurate and detailed mathematical model for the active sound absorption, with the exception of Takahashi and Takane where a two-dimensional model was presented. This, requires a Finite-Element-Method modeling and consequently an extra degree of complexity.

The work presented in this thesis introduces a novel mathematical model for an active sound absorption system based on the wave separation method of Nishimura since it proves to be a feasible approach, mathematically as well as also in practice. The wave decomposition method is combined with a modal model of a three-dimensional room in order to obtain the controlling parameters of the active system. Along with this theoretical background a real implementation of the active absorption system is presented.

This thesis is written with a simple structure of three main chapters: Theoretical background, Simulation and Measurement results. Naturally, a final chapter summarizes the discussion and findings.

Chapter 1 - Theoretical background: It sets out and develops all the equations necessary to describe the fundamentals of the active sound absorption. Describes how the wave decomposition is calculated and later on combined with the modal model of a room. Finally the active absorption system is included and the cost function is defined. The resulting system is solved to find the parameters that allow to achieve the active absorption.

Chapter 2 - Simulations: A large set of different conditions and parameters are simulated to obtain the maximum amount of information possible. Some of the simulations of the active absorption system are compared with a classical ANC system to establish their differences.

Chapter 3 - Measurements: This research was carried out in two stages where at the beginning focused in experiment with a one-dimensional wave guide to understand the fundamental about active absorption and later on extrapolate this to a more realistic, but still simplified, three-dimensional case. The results of both stages are presented.

Chapter 1

Theoretical background

This chapter begins describing the wave propagation inside a one-dimensional waveguide and how it is possible to decompose the steady-state sound field in two components, an incident and a reflected part. Then a brief description of the sound field within a rectangular enclosure is presented. A modal model of a room is introduced and a set of primary and secondary sources are included in the model to describe the active control system. In the last section the active control question is presented as an *optimization* problem where a cost function J is defined and the system is solved for a set of unknown coefficients β_i that minimize J. Each β_i corresponds to a *complex amplification coefficient* that defines the magnitude and phase for each secondary source. The definitions of the cost function J will be based on the decomposition method described below.

1.1 Wave decomposition

Considering a one-dimensional waveguide and a standing wave inside, it is possible to decompose the sound field in an incident p_i and a reflected p_r part, each of them propagating in opposite directions.

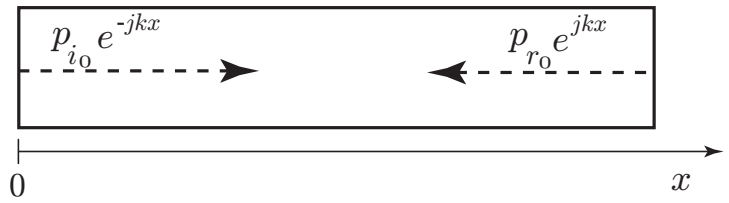

Figure 1.1: One-dimensional wave guide with two waves propagating in opposite directions.

For this case, the incident and the reflected parts of the sound field can be expressed as

$$p_i = p_{i_0}\, e^{j(\omega t - kx)} \tag{1.1}$$

$$p_r = p_{r_0}\, e^{j(\omega t + kx)}, \tag{1.2}$$

where ω is the angular frequency and k is the wave number. Now the particle velocity can be calculated for each of these components as

$$u_i = \frac{j}{\omega \varrho} \frac{\mathrm{d}p_i}{\mathrm{d}x} = p_{i_0} \frac{-j^2\, k}{\omega \varrho}\, e^{j(\omega t - kx)} = \frac{1}{\varrho c}\, p_i \tag{1.3}$$

$$u_r = \frac{j}{\omega\varrho}\frac{\mathrm{d}p_r}{\mathrm{d}x} = p_{r_0}\frac{j^2\,k}{\omega\varrho}\,e^{j(\omega t+kx)} = \frac{-1}{\varrho c}\,p_r, \tag{1.4}$$

where ϱ is the air density and c is the speed of sound in the medium. Thus, the total particle velocity u at some point will be the superposition of both components as

$$u = u_i + u_r = \frac{1}{\varrho c}(p_i - p_r). \tag{1.5}$$

Likewise, the total pressure p at some point will be the superposition of the individual pressures as

$$p = p_i + p_r. \tag{1.6}$$

Now combining eq. (1.5) and (1.6), the incident and the reflected part of the total sound field can be calculated using the total pressure and the particle velocity as

$$p_i = \frac{1}{2}\,(p + \varrho\,c\,u) \tag{1.7}$$

$$p_r = \frac{1}{2}\,(p - \varrho\,c\,u). \tag{1.8}$$

By this mean it is possible to decompose the sound field in these two components, p_i and p_r. These two simple equations will become of major importance later on since the cost function J is based on them. In practical terms, p_i and p_r can be measured using the well known method of sound intensity measurement developed by Fahy [16] using two pressure microphones (p_1, p_2) separated by a distance d_{pp} as

$$p(t) = \frac{p_1(t) + p_2(t)}{2} \tag{1.9}$$

and

$$u_x(t) = \frac{1}{\varrho}\int_{-\infty}^{t} \frac{p_1(\tau) - p_2(\tau)}{d_{pp}}\,d\tau. \tag{1.10}$$

However this is not the only way to obtain a measurement of pressure and velocity. Nowadays, an intensity probe based on a pressure microphone and a hot wire are able to directly provide both quantities for a single point in space [17, 18].

1.2 Power absorption by a secondary source

Every active control system consists of four basic components. A primary (or external) excitation that is wanted to be controlled, a sensor that is used for observability, a control actuator responsible to interact with the primary excitation and a digital or analog controller responsible to generate the adequate signals sent to the actuators. The controller uses the signal provided by the sensor as input information to generate the output signal sent to the control actuator, this input information is combined with a previously defined minimization criterion to generate its output. In active noise control, the most common control criterion used is the minimization of the sound pressure at a single or at multiple points. These points are usually called control points since they are used as reference for the pressure minimization. Microphones placed at every control point provide the necessary information about the evolution of the minimization process. If a digital controller

is used, this information is fed into an adaptive algorithm driven by the control criterion (or cost function). Both, the adaptive algorithm and the cost function are responsible for the generation of the controlling signals sent to all the control sources (or secondary sources). The sound source that is responsible for the primary excitation is also usually called primary source.

The next sections describes and quantifies how much power can be absorbed by a secondary source in a one-dimensional waveguide. The first case considers sound propagation in an infinite tube and shows that it is possible to absorb half of the energy radiated by the primary source.

The second case presents a semi-infinite tube, i.e. with a rigid termination in one end. Under this condition it is proven that it is possible to completely absorb incident energy and therefore completely minimize the reflected wave generated by the rigid end.

A more generalized third case is considered where in the same way as in the latter case, a semi-infinite tube is used but now instead of a rigid termination at the end, an arbitrary impedance Z_0 is assigned. Thus, the power flowing through the secondary source can be calculated as a function of the impedance Z_0 of the reflecting end.

1.2.1 Infinite tube

Acoustic sources had demonstrated to be not only generators of energy but also sinks [19]. To illustrate this concept, an infinite one-dimensional enclosure with a secondary source in the middle of it is considered. The secondary source is placed laterally in the enclosure as depicted in Figure 1.2.

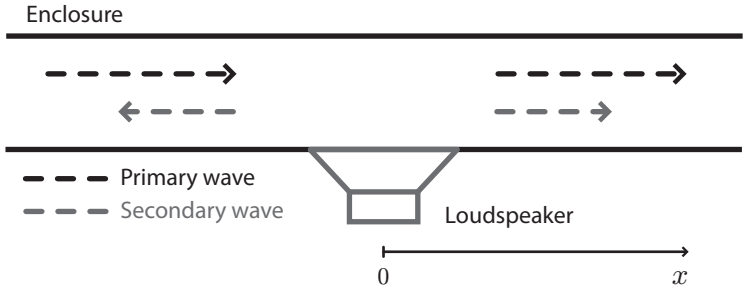

Figure 1.2: Diagram of the infinite tube and the traveling waves generated by the primary (black) and secondary (grey) sources.

From the left-hand side of the enclosure a primary source is radiating such that the generated wave travels only in the positive direction of the x axis. Since the secondary source is placed in the middle, it is able to radiate in both directions of the x axis, positive and negative. Thus, two zones of sound field are defined as:

- Zone 1: upstream of the secondary source, i.e. $x < 0$.
- Zone 2: downstream of the secondary source, i.e. $x > 0$.

For each one of these zones the total sound field is defined by

$$p_1(x) = p_0 \left[e^{-jkx} + \gamma\, e^{jkx} \right] \text{, for } x < 0 \tag{1.11}$$

$$p_2(x) = p_0 \left[e^{-jkx} + \gamma\, e^{-jkx} \right] \text{, for } x > 0, \tag{1.12}$$

where the first and second term of both equations corresponds to the waves contributed by the primary and secondary source respectively. The complex coefficient γ defines the relationship, in magnitude-and-phase, of the secondary source regarding to the primary source. Under these conditions the particle velocities for both zones are obtained as

$$v_1(x) = \frac{p_0}{\varrho\, c}\left[\, e^{-jkx} - \gamma\, e^{jkx}\right] \text{ , for } x < 0 \tag{1.13}$$

$$v_2(x) = \frac{p_0}{\varrho\, c}\left[\, e^{-jkx} + \gamma\, e^{-jkx}\right] \text{, for } x > 0 \tag{1.14}$$

and consequently the mean sound intensity $\overline{I}$ for the same zones will be given by

$$\overline{I}_1 = \frac{1}{2}\,\Re\{p_1\, v_1^*\} = \frac{p_0^2}{2\varrho\, c}\,\Re\Big\{1 - \gamma\gamma^* + \gamma\, e^{j2kx} - \gamma^* e^{-j2kx}\Big\} \tag{1.15}$$

$$\overline{I}_2 = \frac{1}{2}\,\Re\{p_2\, v_2^*\} = \frac{p_0^2}{2\varrho\, c}\,\Re\Big\{(1+\gamma)\, e^{-jkx}(1+\gamma^*)\, e^{jkx}\Big\} \tag{1.16}$$

or

$$\overline{I}_1 = \frac{p_0^2}{2\varrho\, c}(1 - \gamma\gamma^*) = \frac{p_0^2}{2\varrho\, c}(1 - |\gamma|^2) \tag{1.17}$$

$$\overline{I}_2 = \frac{p_0^2}{2\varrho\, c}(1+\gamma)(1+\gamma^*) = \frac{p_0^2}{2\varrho\, c}\,|1+\gamma|^2. \tag{1.18}$$

The sound power $P_{1,2}$ on each zone will be the respective intensity $\overline{I}_{1,2}$ times the cross section area S of the enclosure, $P_{1,2} = \overline{I}_{1,2} \cdot S$. If the power radiated only by the secondary source is defined as P_s, it is possible to write a simple energy balance equation as

$$P_1 + P_s = P_2, \tag{1.19}$$

assuming arbitrarily that the secondary source is introducing energy into the enclosure, in that case P_s is represented as an arrow pointing toward the inside as shown in Figure 1.3. But the actual direction of the energy flow will be defined by the coefficient γ, moreover, if an optimal γ_0 is chosen it could be possible to maximize the flow outward the enclosure. This would be the most interesting case since the secondary source will be acting as an active absorber.

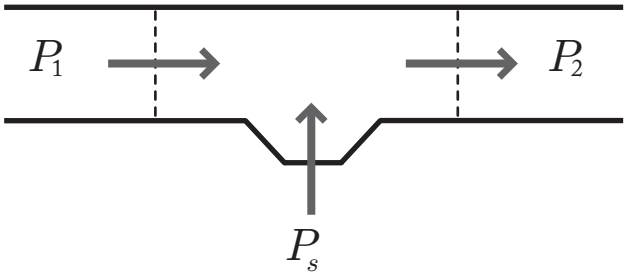

Figure 1.3: Diagram of the energy balance inside the infinite tube.

As already established, the power for each zone $P_{1,2}$ of the enclosure will be given by

$$P_1 = \frac{S p_0^2}{2\varrho\, c}\,(1 - |\gamma|^2) \tag{1.20}$$

$$P_2 = \frac{S p_0^2}{2\varrho\, c}\,|1+\gamma|^2 \tag{1.21}$$

and according to (1.19) the power introduced by the secondary source to the enclosure will be

$$P_s = \frac{Sp_0^2}{2\varrho\, c}\left[\,|1+\gamma|^2-(1-|\gamma|^2)\right] \tag{1.22}$$

$$P_s = \frac{Sp_o^2}{2\varrho\, c}\left[\gamma+\gamma^*+2\,\gamma\gamma^*\right]. \tag{1.23}$$

As it was said previously, γ is a complex coefficient that controls the amplitude and phase of the secondary source, however P_s is a real-valued function. This allows to treat the differentiation of P_s respect to the complex variable γ as a simple differentiation with respect to a real variable [20]. Thus,

$$\frac{\mathrm{d}P_s}{\mathrm{d}\gamma^*} = P_0\left[1+2\,\gamma\,\right] \tag{1.24}$$

where P_0 corresponds to the power of the primary source coming from the left-hand side of the enclosure

$$P_0 = \frac{Sp_0^2}{2\varrho\, c}. \tag{1.25}$$

Now solving equation (1.24) for γ it is possible to find the optimal value γ_0 that maximize the flow of energy of the secondary source as

$$\frac{\mathrm{d}P_s}{\mathrm{d}\gamma^*} = 0 \tag{1.26}$$

$$P_0\left[1+2\,\gamma_0\right] = 0 \tag{1.27}$$

$$\gamma_0 = -\frac{1}{2}, \tag{1.28}$$

replacing γ_0 in the general expression of P_s, equation (1.23), the power flowing through secondary source gives

$$P_{s,\max} = -\frac{P_0}{2}, \tag{1.29}$$

where the negative sign means that the power is flowing outward the enclosure and that under the best circumstances the secondary source is able to actively absorb the half of the power coming from the primary source.

1.2.2 Semi-infinite tube

This configuration consists of a semi-infinite one-dimensional waveguide, e.g. an extremely long tube with one closed end, a primary source at one end and a secondary source at some point near to the other rigidly closed end (given by the distance l) as shown in Figure 1.4.

Under these conditions the sound pressure equations within the tube can be written in a similar way as in the latter section (cf. Equations 1.11 and 1.12) except that now it is necessary to include the contribution of the reflection from the rigid end, provided by the term $r\,e^{jkx}$, where r represent the complex reflection coefficient at the end. Hence, the equations that describe the pressure will be

$$p_1(x) = p_0\left[e^{-jkx}+\gamma\,e^{jkx}+r\,e^{jkx}\right]\ \text{, for } x<0 \tag{1.30}$$

$$p_2(x) = p_0\left[e^{-jkx}+\gamma\,e^{-jkx}+r\,e^{jkx}\right]\ \text{, for } x>0. \tag{1.31}$$

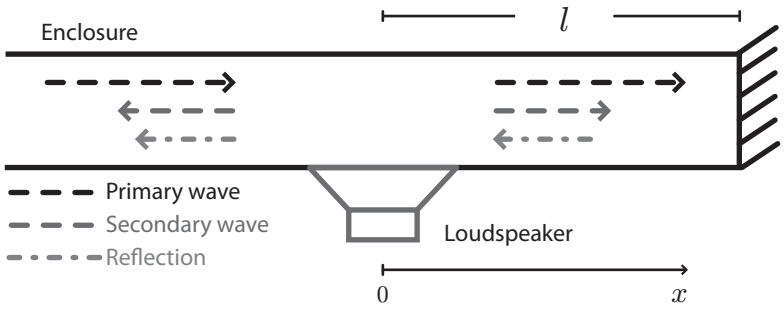

Figure 1.4: Diagram of the semi-infinite tube and the traveling waves generated by the primary source, secondary sources and the reflection due to the rigid end.

To solve these equations it is necessary to find the value of r. It is almost straightforward to calculate r using the pressure p_2 of the zone between the secondary source and the rigid end, but for completeness it will be proved that the same result is obtained using also p_1. The boundary condition used here, is that the particle velocity over the rigid surface is zero $v_2(l) = 0$, thus if

$$v_2(x) = \frac{p_0}{\varrho\, c}\left[(1+\gamma)\, e^{-jkx} - r\, e^{jkx}\right] \tag{1.32}$$

$$v_2(l) = \frac{p_0}{\varrho\, c}\left[(1+\gamma)\, e^{-jkl} - r\, e^{jkl}\right] = 0 \tag{1.33}$$

therefore

$$(1+\gamma)\, e^{-jkl} = r\, e^{jkl}$$

which results in

$$r = (1+\gamma)\, e^{-2jkl}. \tag{1.34}$$

Now replacing back the value of r into the equation of particle velocity of the zone 2, equation (1.32), gives

$$v_2(x) = \frac{p_0}{\varrho\, c}(1+\gamma)\left[e^{-jkx} - e^{-2jkl}\, e^{jkx}\right] \tag{1.35}$$

and the pressure p_2 will be

$$p_2(x) = p_0\,(1+\gamma)\left[e^{-jkx} + e^{-2jkl}\, e^{jkx}\right] \tag{1.36}$$

or

$$p_2(x) = p_0\left[e^{-jkx} + \gamma\, e^{-jkx} + (1+\gamma)\, e^{-j2kl}\, e^{jkx}\right]. \tag{1.37}$$

Now for the case upstream of the secondary source ($x < 0$), taking the general solution for steady state pressure in a one-dimensional field

$$p_1(x) = p_0\left[Ae^{-jkx} + Be^{jkx}\right] \tag{1.38}$$

and using the continuity condition given by

$$p_1(x)\Big|_{(x=0)} = p_2(x)\Big|_{(x=0)} \tag{1.39}$$

it is possible to obtain the first equation to find the constants A and B. Hence, equation (1.39) gives

$$A + B = (1+\gamma)\left[1 + e^{-j2kl}\right] \tag{1.40}$$

or

$$(1+\gamma)\Big[1+e^{-j2kl}\Big]-[A+B]=0. \tag{1.41}$$

The second boundary condition used to find A and B comes from the relationship between the particle velocity on both sides of the secondary source and the strength of the secondary source itself, a detailed description of this boundary condition is presented by Johansen [21] and Möser [22]. For this particular case this condition can be written as

$$v_2(0_+)-v_1(0_-)=\frac{2\,p_0\gamma}{\varrho\,c} \tag{1.42}$$

where 0_+ and 0_- represent the limit approach from the right and the left respectively to the position of the source in $x_s=0$. Since v_2 was already calculated in equation (1.35) it is only necessary to obtain v_1 from the pressure equation (1.38) and combine both into the boundary condition (1.42), giving

$$(1+\gamma)\Big[1-e^{-j2kl}\Big]-[A-B]=2\gamma. \tag{1.43}$$

Now, combining equations (1.41) and (1.43) it is possible to find A and B, giving as a result

$$A = 1 \tag{1.44}$$
$$B = \gamma+(1+\gamma)\,e^{-j2kl}. \tag{1.45}$$

Replacing now A and B into the equation (1.38), the final expression for the pressure p_1 upstream is obtained

$$p_1(x)=p_0\left[e^{-jkx}+\left\{\gamma+(1+\gamma)\,e^{-j2kl}\right\}e^{jkx}\right] \tag{1.46}$$

or

$$p_1(x)=p_0\big[\underbrace{e^{-jkx}}_{\text{prim.}}+\underbrace{\gamma\,e^{jkx}}_{\text{sec.}}+\underbrace{(1+\gamma)\,e^{-j2kl}\,e^{jkx}}_{\text{refl. at end}}\big]. \tag{1.47}$$

As expected, equation (1.47) is composed by three terms where each of them corresponds to the contribution of the primary source, secondary source and the reflection of the rigid end respectively.

The equations (1.37) and (1.47) differ only in the sign of the exponent of the second term, $\gamma\,e^{-jkx}$ and $\gamma\,e^{jkx}$ respectively, which is reasonable to expect since the secondary source radiates in both directions of the tube. Naturally, both equations share the same reflection coefficient $r=(1+\gamma)\,e^{-2jkl}$ in the third term.

Since the pressures in both zones of the enclosure p_1 and p_2 are known, it is possible now to estimate the power absorbed by the secondary source. A diagram of the power balance is shown in Figure 1.5.

In the same way as in the latter section, an equation of energy balance can be written once again for this case as

$$P_1+P_s=P_2, \tag{1.48}$$

which is identical to equation (1.19) but this time it is necessary to consider that in zone 2 there is a rigid end. This rigid boundary will generate a reflection which combined with the incident wave will create a stationary wave in that zone. As it is known, in a

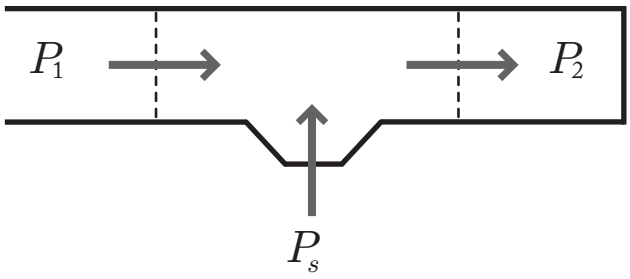

Figure 1.5: Diagram of the energy balance inside the semi-infinite tube.

stationary field the net intensity equals zero, which means that $P_2 = 0$. Hence, equation (1.48) will become

$$P_1 + P_s = 0. \tag{1.49}$$

The task now is to solve (1.49) to find the relationship between the power P_1, P_s and γ. The particle velocity v_1 can be calculated easily from the pressure p_1, equation (1.46). Thus v_1 will be

$$v_1(x) = \frac{p_0}{\varrho\, c}\left[e^{-jkx} - \left\{\gamma + (1+\gamma)\, e^{-j2kl}\right\} e^{jkx}\right], \tag{1.50}$$

and the sound intensity in the zone 1, $\overline{I}_1$, is calculated as

$$\overline{I}_1 = \frac{1}{2}\,\Re\{p_1\, u_1^*\} \tag{1.51}$$

$$\overline{I}_1 = \frac{p_0^2}{2\varrho\, c}\,\Re\left\{\left[e^{-jkx} + \left(\gamma + (1+\gamma)e^{-j2kl}\right) e^{jkx}\right]\left[e^{jkx} - \left(\gamma^* + (1+\gamma^*)e^{j2kl}\right) e^{-jkx}\right]\right\} \tag{1.52}$$

$$\overline{I}_1 = \frac{p_0^2}{2\varrho\, c}\, 2\,\Re\left\{\gamma\,(1+\gamma^*)\,(1+e^{j2kl})\right\}. \tag{1.53}$$

Hence, recalling from equation (1.25) that the power radiated by the primary source is

$$P_0 = \frac{S p_0^2}{2\varrho\, c}, \tag{1.54}$$

and replacing $\overline{I}_1$ into (1.49) gives

$$P_s = -P_1 \tag{1.55}$$

$$P_s = -\frac{p_0^2}{2\varrho\, c}\, 2\,\Re\left\{\gamma\,(1+\gamma^*)\,(1+e^{j2kl})\right\} \tag{1.56}$$

$$P_s = -\ P_0\ \ 2\,\Re\left\{\gamma\,(1+\gamma^*)\,(1+e^{j2kl})\right\}. \tag{1.57}$$

This equation relates the power flowing through the secondary source and the power radiated from the primary source.

If we assume that the secondary source is acting as an active absorber, the direct consequence is that no wave propagation upstream the tube will take place. This assumption means that the second term ($\left\{\gamma + (1+\gamma)\, e^{-j2kl}\right\} e^{jkx}$) of the sound pressure p_1 (1.46) must vanish. Therefore it is safe to assume that the optimal coefficient γ_0 that maximizes the absorption of the secondary source can be calculated using this condition. Hence, if the second term is zero

$$\left\{\gamma_0 + (1+\gamma_0)\, e^{-j2kl}\right\} e^{jkx} = 0 \tag{1.58}$$

then the optimal coefficient γ_0 will be

$$\gamma_0 = \frac{-1}{1 + e^{j2kl}}. \tag{1.59}$$

If the coefficient γ_0 is replaced back into equation (1.57), it becomes

$$P_{s,\max} = -P_0 \tag{1.60}$$

which means that the total incident power radiated by the primary source is absorbed by the secondary source.

Although γ_0 is able to provide the right magnitude and phase to drive the secondary source as an active absorber, there are certain points where γ_0 becomes unstable. This occurs when the denominator of equation (1.59) approaches to zero. It is possible to estimate when this singularity takes place, if

$$1 + e^{j2kl} = 0 \tag{1.61}$$

$$e^{j2kl} = -1 \tag{1.62}$$

then

$$2kl = (2n + 1)\,\pi\ , \quad \text{for } n = ..., -2, -1, 0, 1, 2, ... \tag{1.63}$$

it therefore follows that γ_0 is not defined when

$$\frac{l}{\lambda} = \frac{(2n + 1)}{4} \tag{1.64}$$

where n is an integer number.

Using equation (1.59), magnitude and phase of γ_0 are modelled in Figure 1.6. The curve of magnitude represent the relationship of amplification between primary and secondary source. The peaks in this curve illustrate the values where γ_0 becomes undefined, the physical meaning of these points is that the amplification of the secondary source should be infinitely larger than the primary source to be able to generate the active absorption. In this particular case, the problem can be easily solved by moving the secondary source closer to the rigid end, e.g. making $l = 0$, in that way the singularities are completely avoided.

1.2.3 Semi-infinite tube with a variable impedance at the end

A more generalized expression can be found for the pressure within the enclosure assigning an arbitrary impedance to the rigid end on the right side. This, moreover, allows to obtain a curve that describes the absorption generated by the secondary source as a function of the impedance Z_0 at the end of the tube.

It is possible to start the development of these equations using the same expression for the pressure $p_2(x)$ used in equation (1.31). This describes the sound field downstream $(x > 0)$ the secondary source as

$$p_2(x) = p_0 \left[(1 + \gamma)\, e^{-jkx} + r\, e^{jkx}\right] \tag{1.65}$$

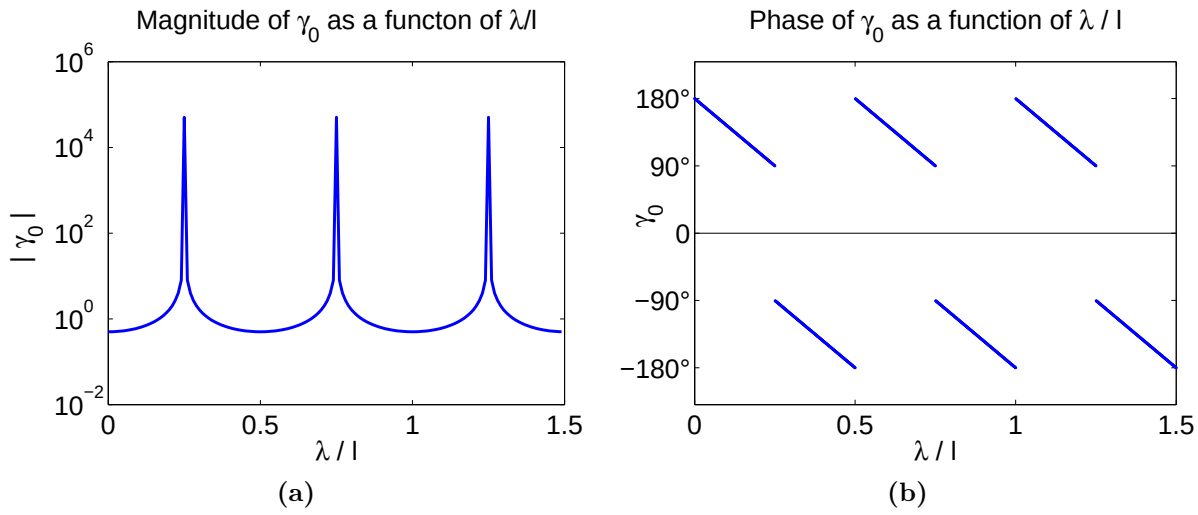

Figure 1.6: Magnitude and phase of the optimal coefficient γ_0.

where, as seen before, γ represents the complex coefficient that drives the secondary source and r is the reflection coefficient of the end of the tube that now has an impedance Z_0. This new boundary condition can be written simply as

$$\frac{p_2(l)}{v_2(l)} = Z_0, \tag{1.66}$$

where l is the distance between the secondary source and the end of the tube as depicted in Figure 1.4. Deriving the pressure $p_2(x)$, the expression for the particle velocity $v_2(x)$ results in

$$v_2(x) = \frac{p_0}{\varrho c}\left[(1+\gamma)\, e^{-jkx} - r\, e^{jkx}\right]. \tag{1.67}$$

Thus, combining $p_2(x)$ and $v_2(x)$ into equation (1.66) makes possible to obtain an expression that describes the reflection coefficient r as

$$r = e^{-j2kl}\,(1+\gamma)\,\frac{\left(\frac{Z_0}{\varrho c} - 1\right)}{\left(\frac{Z_0}{\varrho c} + 1\right)}. \tag{1.68}$$

Following a similar procedure as shown in the latter section, the pressure $p_1(x)$ and the particle velocity $v_1(x)$ can be found using the conditions given by equations (1.39) and (1.42), i.e.

$$p_1(0) = p_2(0)$$

and

$$v_2(0_+) - v_1(0_-) = \frac{2\, p_0 \gamma}{\varrho\, c}.$$

Hence,

$$p_1(x) = p_0\left[e^{-jkx} + \gamma\, e^{jkx} + e^{-j2kl}\,(1+\gamma)\,\frac{\left(\frac{Z_0}{\varrho c} - 1\right)}{\left(\frac{Z_0}{\varrho c} + 1\right)}\, e^{jkx}\right] \tag{1.69}$$

and

$$v_1(x) = \frac{p_0}{\varrho c}\left[e^{-jkx} - \gamma\, e^{jkx} - e^{-j2kl}\,(1+\gamma)\,\frac{\left(\frac{Z_0}{\varrho c} - 1\right)}{\left(\frac{Z_0}{\varrho c} + 1\right)}\, e^{jkx}\right]. \tag{1.70}$$

To obtain the optimal complex coefficient γ_0 that minimizes the reflected sound pressure, it is necessary to cancel the wave that propagates upstream to the tube. As seen before, this is obtained doing the second and third terms of equation (1.69) equal to zero. This is

$$\gamma_0 + e^{-j2kl}\,\zeta + \gamma_0\, e^{-j2kl}\,\zeta = 0 \tag{1.71}$$

where

$$\zeta = \frac{\left(\frac{Z_0}{\varrho c} - 1\right)}{\left(\frac{Z_0}{\varrho c} + 1\right)},$$

in this way the optimal coefficient γ_0 becomes

$$\gamma_0 = \frac{-\zeta}{\zeta + e^{j2kl}}. \tag{1.72}$$

Once again both parts of the mean intensity $\overline{I}_1$ and $\overline{I}_2$ can be obtained as

$$\overline{I}_1 = \frac{1}{2}\,\Re\left\{p_1\, v_1^*\right\} \tag{1.73}$$

$$\overline{I}_1 = \frac{p_0^2}{2\varrho\, c}\left[1 - \left(\gamma + \zeta(1+\gamma)\, e^{-j2kl}\right)\left(\gamma^* + \zeta(1+\gamma^*)\, e^{j2kl}\right)\right] \tag{1.74}$$

and

$$\overline{I}_2 = \frac{1}{2}\,\Re\left\{p_2\, v_2^*\right\} \tag{1.75}$$

$$\overline{I}_2 = \frac{p_0^2}{2\varrho\, c}\left[(1+\gamma)(1+\gamma^*)\left[1-\zeta^2\right]\right]. \tag{1.76}$$

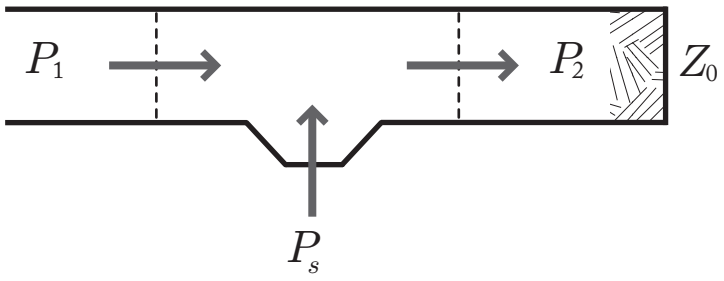

Figure 1.7: Diagram of the energy balance inside the semi-infinite tube.

According with Figure 1.7 the power balance equation can be written as

$$P_1 + P_s = P_2. \tag{1.77}$$

Therefore P_s can be obtained multiplying $\overline{I}_1$ and $\overline{I}_2$ by the cross section area S of the tube to get P_1 and P_2, and later on replacing these quantities into equation 1.77. Finally the power that flows through the secondary source P_s is given by

$$P_s = \frac{S\, p_0^2}{\varrho\, c}\,\Re\Big\{\gamma\,(1+\gamma^*)\left(1+\zeta\, e^{j2kl}\right)\Big\}. \tag{1.78}$$

If the optimal coefficient γ_0 is introduced in P_s, it is possible to find the dependency of the power of the secondary source with the impedance Z_0 of the rigid end. Figure 1.8 shows the relationship between Z_0, l/λ and P_s/P_0.

A couple of interesting facts arise from this result. In first place, the range of P_s/P_0 goes between -1 and 0. Considering the definition of the directions of the power flow made in Figure 1.7, a negative value of P_s tells that the power is flowing outward the tube. Second, when $Z_0 = \varrho c$ the resulting power is always $P_s = -\frac{P_0}{2}$, irrespective of the value of l/λ. This result is consistent with the maximum value of power $P_{s,\max}$ that the secondary source is able to absorb when the tube has an open end, as described in Section 1.2.1. Third, when the end of the tube has an extremely high or low impedance Z_0, the secondary source is able to completely absorb the incident power coming from the primary source, i.e. $P_s = -P_0$. Once again, this result is also consistent with the finding of Section 1.2.2 where the end of the tube is assumed to be rigid.

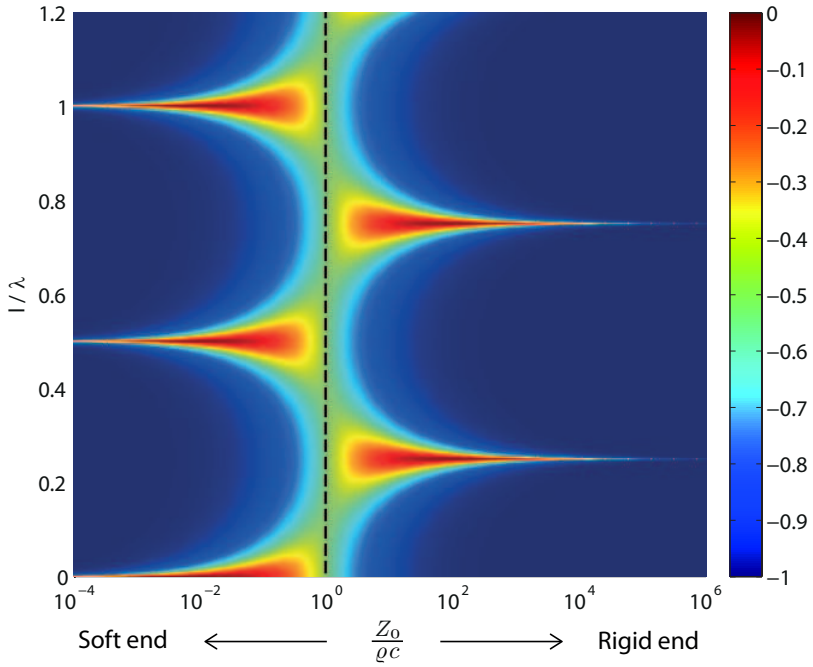

Figure 1.8: Normalized power flow through the secondary source P_s/P_0. Domain is defined as $Z_0/\varrho c$.

1.3 Modal model of a rectangular enclosure

To describe the sound field within a three-dimensional enclosure, the starting point is given by the homogenous wave equation [23]

$$\nabla^2 p(\vec{\mathbf{r}}) + k^2 p(\vec{\mathbf{r}}) = 0 \tag{1.79}$$

where, as usual, $k = \omega/c$ is the wave number of the excitation signal associated with the angular frequency $\omega = 2\pi f$ and the speed of sound c. The time convention is assumed in the equation (1.79), hence the time dependance $e^{j\omega t}$ is omitted. Considering the boundary conditions that all the walls that define the enclosure are completely rigid, i.e. that the

normal component of the particle velocity at each surface of the enclosure is zero

$$v_x(0) = v_x(l_x) = 0 \tag{1.80}$$
$$v_y(0) = v_y(l_y) = 0 \tag{1.81}$$
$$v_z(0) = v_z(l_z) = 0, \tag{1.82}$$

where l_x, l_y, l_z are the dimensions of the enclosure as depicted in Figure 1.9. The general solution of the wave equation (1.79) is given by

$$p(\vec{\mathbf{r}}) = \underbrace{\sum_{p=0}^{\infty}\sum_{q=0}^{\infty}\sum_{r=0}^{\infty}}_{\sum_{pqr}^{\infty}} A_{pqr}\Psi_{pqr}(\vec{\mathbf{r}}) \tag{1.83}$$

where $\vec{\mathbf{r}} = (x, y, z)$ defines any position within the enclosure, A_{pqr} is an arbitrary modal amplitude and $\Psi_{pqr}(\vec{\mathbf{r}})$ is the modal shape function that satisfies the boundary conditions, such that can be written as

$$\Psi_{pqr}(x, y, z) = \cos\left(\frac{p\pi x}{l_x}\right)\cos\left(\frac{q\pi y}{l_y}\right)\cos\left(\frac{r\pi z}{l_z}\right) \tag{1.84}$$

where p, q and r are modal indexes for each spatial coordinate.

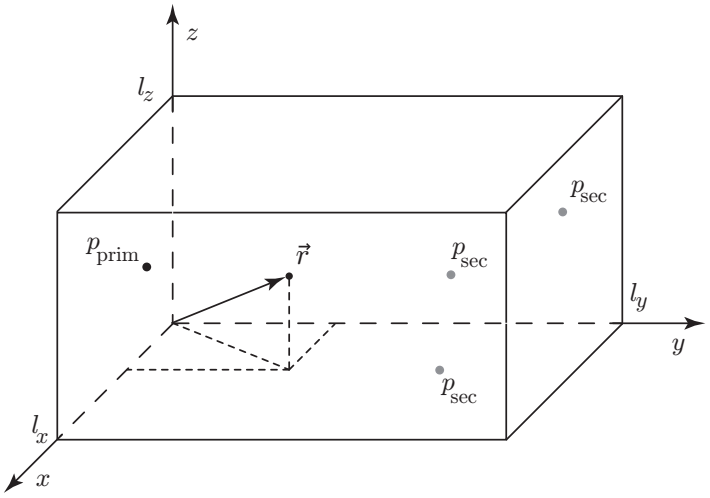

Figure 1.9: Sketch of a rectangular enclosure with a set of primary p_{prim} and secondary p_{sec} sources inside. The vector $\vec{\mathbf{r}} = (x, y, z)$ defines any position within the room.

The objective now is to find the adequate value of A_{pqr} that describes the sound field generated by a set of primary p_{prim} and secondary p_{sec} sources included within the enclosure. Thus, equation (1.79) becomes

$$\nabla^2 p(\vec{\mathbf{r}}) + k^2 p(\vec{\mathbf{r}}) = p_{\text{prim}}(\vec{\mathbf{r}}) + \sum_{i=1}^{I} \beta_i \; p_{\text{sec}}^{(i)}(\vec{\mathbf{r}}) \tag{1.85}$$

here the right-hand side takes into account the inclusion of those sources. Each secondary source is driven by a *complex coefficient* β_i which is a magnitude-and-phase shift regarding

the primary source. For simplicity, the right-hand side of equation (1.85) can be written in a more compact way as

$$= \sum_{i=0}^{I} \beta_i \; p^{(i)}(\vec{\mathbf{r}}) \tag{1.86}$$

with

$$\beta_0 = 1 \qquad \wedge \qquad p^{(0)}(\vec{\mathbf{r}}) = p_{\text{prim}}(\vec{\mathbf{r}}).$$

In general, $p^{(i)}(\vec{\mathbf{r}})$ can also be described as a modal expansion like

$$p^{(i)}(\vec{\mathbf{r}}) = \sum_{pqr}^{\infty} p_{pqr}^{(i)} \cos\left(\frac{p\pi x}{l_x}\right) \cos\left(\frac{q\pi y}{l_y}\right) \cos\left(\frac{r\pi z}{l_z}\right), \tag{1.87}$$

where the modal excitation $p_{pqr}^{(i)}$ contributed by each secondary source i can be found easily using the orthogonality property, i.e. multiplying both sides by a cosine factor and integrating over the whole volume. In that way the sum can be eliminated and $p_{pqr}^{(i)}$ can be obtained as

$$p_{pqr}^{(i)} = \frac{1}{\mu_{pqr}} \int_0^{l_z} \int_0^{l_y} \int_0^{l_x} p^{(i)}(x,y,z) \cos\left(\frac{p\pi x}{l_x}\right) \cos\left(\frac{q\pi y}{l_y}\right) \cos\left(\frac{r\pi z}{l_z}\right) \mathrm{d}x \, \mathrm{d}y \, \mathrm{d}z, \tag{1.88}$$

where

$$\mu_{pqr} = \mu_p \, \mu_q \, \mu_r \tag{1.89}$$

and

$$\mu_p = \begin{cases} l_x & \text{if } p = 0 \\ \frac{l_x}{2} & \text{if } p \neq 0 \end{cases} \qquad \mu_q = \begin{cases} l_y & \text{if } q = 0 \\ \frac{l_y}{2} & \text{if } q \neq 0 \end{cases} \qquad \mu_r = \begin{cases} l_z & \text{if } r = 0 \\ \frac{l_z}{2} & \text{if } r \neq 0 \end{cases}. \tag{1.90}$$

In equation (1.88), $p^{(i)}(x,y,z)$ defines the radiation characteristics of the sources located within the room. These sources can be selected to have any arbitrary radiation pattern, e.g. a point source, a velocity profile, etc. For simplicity in this development, point sources are chosen. This means that the radiation characteristic should be written as a combination of three Dirac's delta functions δ, one for each coordinate axis as

$$p^{(i)}(x,y,z) = \delta(x - x_i) \; \delta(y - y_i) \; \delta(z - z_i), \tag{1.91}$$

where (x_i, y_i, z_i) are the position coordinates of each i-th source in space. Thus, defining the sources in this manner makes equation (1.88) to become

$$\begin{aligned} p_{pqr}^{(i)} &= \frac{1}{\mu_{pqr}} \cos\left(\frac{p\pi x_i}{l_x}\right) \cos\left(\frac{q\pi y_i}{l_y}\right) \cos\left(\frac{r\pi z_i}{l_z}\right) \\ &= \frac{\Psi_{pqr}(x_i, y_i, z_i)}{\mu_{pqr}}. \end{aligned} \tag{1.92}$$

The last remaining step to solve equation (1.83) is to find the value of A_{pqr}. Replacing equation (1.83) into the inhomogeneous wave equation (1.85) and solving for A_{pqr} gives

$$\frac{1}{k^2} \sum_{pqr}^{\infty} \left[-\left(\frac{p\pi}{l_x}\right)^2 - \left(\frac{q\pi}{l_y}\right)^2 - \left(\frac{r\pi}{l_z}\right)^2 \right] A_{pqr} \Psi_{pqr}(x,y,z) + \sum_{pqr}^{\infty} A_{pqr} \Psi_{pqr}(x,y,z) = \sum_{i=0}^{I} \beta_i \sum_{pqr}^{\infty} p_{pqr}^{(i)} \Psi_{pqr}(x,y,z) \tag{1.93}$$

$$\frac{k^2 - \left(\frac{p\pi}{l_x}\right)^2 - \left(\frac{q\pi}{l_y}\right)^2 - \left(\frac{r\pi}{l_z}\right)^2}{k^2} A_{pqr} = \sum_{i=0}^{I} \beta_i \, p_{pqr}^{(i)}. \tag{1.94}$$

If the wave number component k_{pqr} is defined as

$$k_{pqr}^2 = \left(\frac{p\pi}{l_x}\right)^2 + \left(\frac{q\pi}{l_y}\right)^2 + \left(\frac{r\pi}{l_z}\right)^2 \tag{1.95}$$

and

$$\omega_{pqr}^2 = c^2 \, k_{pqr}^2 \tag{1.96}$$

then

$$A_{pqr} = \sum_{i=0}^{I} \beta_i \, \frac{p_{pqr}^{(i)}}{1 - \frac{\omega_{pqr}^2}{\omega^2}}. \tag{1.97}$$

The definition of k_{pqr} given in equation (1.95) considers an enclosure with only perfectly rigid walls, but this condition is not completely true in real rooms. Hence, to take this into account, it is necessary to include a loss factor η that comprises all the occurring losses. This loss factor can be used to include for instance the unavoidable absorption effect of the walls by viscothermal boundary layer damping. Usually η is simply defined as a small real constant. Thus, the new k_{pqr} will be given by

$$k_{pqr}^2 = (1 + j\,\eta) \left[\left(\frac{p\pi}{l_x}\right)^2 + \left(\frac{q\pi}{l_y}\right)^2 + \left(\frac{r\pi}{l_z}\right)^2 \right]. \tag{1.98}$$

Finally, putting together the modal amplitudes equation (1.97) and the wave number component equation (1.98) into the general solution of the sound field equation (1.83), the description of the entire sound field in the enclosure with a set of primary p_{prim} and secondary p_{sec} sources will be defined by

$$p(\vec{\mathbf{r}}) = \sum_{i=0}^{I} \beta_i \sum_{pqr}^{\infty} \frac{p_{pqr}^{(i)}}{1 - \frac{\omega_{pqr}^2}{\omega^2}} \, \Psi_{pqr}(\vec{\mathbf{r}}). \tag{1.99}$$

1.4 Control criterion

Despite the fact that the wave decomposition developed in Section 1.1 considers only a one-dimensional wave propagation, those equations can be extrapolated to be used in a three-dimensional propagation case. In the modal model of the room described in the latter section, the sound pressure within the enclosure is defined by the superposition of modes propagating independently along each spatial coordinate. Hence, it is possible to arbitrarily choose one direction of propagation to apply the same decomposition method and use the reflected pressure p_r for this particular direction as a parameter to be minimized by the active system. Following this same reasoning, if the reflected part of the sound field vanishes and only the incident part p_i remains, it is possible to ensure that sound absorption is generated for that chosen direction of the sound field.

1.4.1 Cost function

Every active control system needs a cost function to operate. This cost function is the criterion used to minimize certain parameter. This minimization is done by means of a control signal (generated by the system) that is sent to an actuator. The interaction of the actuator over the primary (or external) excitation creates a destructive interference that results in the minimization of the chosen parameter.

In a classical active noise control system (ANC), the cost function uses the sound pressure as minimization parameter. In this way, the active system generates an output signal that is fed into a secondary source that tries to minimize the sound pressure at a given control point in space.

As seen in the previous sections, the minimization of the reflected pressure propagating in a given direction proves to be an efficient parameter to generate active absorption. Hence, a cost function that uses this parameter can be used to drive the active system.

Initially, a cost function will be defined to generate active absorption only in one direction of propagation, this will allow to describe in details the fundamentals of the proposed active absorption system. Later on, this development will be expanded to cover total active absorption in one dimension, i.e. with wave propagation in both directions in space, and finally in three dimensions.

The minimization problem can be solved relatively easy using the *Hermitian quadratic form* introduced in active noise control theory by Nelson et al. [19, 24], which is widely used from then on. The *Hermitian quadratic form* can be written as

$$J = \boldsymbol{\beta}^H \mathbf{A}\, \boldsymbol{\beta} + \boldsymbol{\beta}^H \mathbf{b} + \mathbf{b}^H \boldsymbol{\beta} + c_h, \tag{1.100}$$

where J represents the cost function, the superscript ^{H} indicates the Hermitian transpose or complex conjugate transpose, $\mathbf{A}$ is an hermitian matrix (i.e. $\mathbf{A} = \mathbf{A}^H$), $\mathbf{b}$ and $\boldsymbol{\beta}$ are complex vectors and c_h is a real scalar value. The advantage of using the *Hermitian quadratic form* is that knowing the values of $\mathbf{A}$, $\mathbf{b}$ and c_h, the set of optimum coefficients $\boldsymbol{\beta}_{\text{opt}}$ that minimize the cost function J can be easily calculated. If $\mathbf{A}$ is positive definite (i.e. $\boldsymbol{\beta}^H \mathbf{A}\, \boldsymbol{\beta} > 0$) then J will have a unique global minimum J_0 for a given $\boldsymbol{\beta} = \boldsymbol{\beta}_{\text{opt}}$, and this minimum will be a real scalar value. Following the development of Nelson, the optimum set of coefficients $\boldsymbol{\beta}_{\text{opt}}$ can be obtained as

$$\boldsymbol{\beta}_{\text{opt}} = -\mathbf{A}^{-1}\mathbf{b} \tag{1.101}$$

and therefore the unique global minimum is given by

$$J_0 = c_h - \mathbf{b}^H \mathbf{A}^{-1} \mathbf{b}. \tag{1.102}$$

To take advantage of the *Hermitian quadratic form*, the squared reflected pressure must be used as a cost function. For our case, as stated in Section 1.3, each β_i represents a *complex amplification coefficient* that drives a single secondary source. If a number of I secondary sources is used then

$$\boldsymbol{\beta} = [\beta_1\ \beta_2\ \ldots\ \beta_{\text{I}}]^T. \tag{1.103}$$

1.4.2 Unidirectional control

The cost function introduced in this section will try to minimize the reflected pressure generated by an incident sound wave traveling in the positive direction of x when it impinges on the boundary of the enclosure. Thus, equation (1.8) is rewritten in terms of the selected direction simply as

$$p_r = \frac{1}{2}(p - \varrho\, c\, u_x), \tag{1.104}$$

where the only difference between both equations is that now (1.104) explicitly considers only the component x of the particle velocity. Before, this distinction was not set since the whole development of those equations considered wave propagation in only one dimension. Now, this distinction is required since there is propagation in three dimensions.

In almost every active control system, sensors are required to serve as input for observation. Here, a number of L sensors is used and each sensor is located at the position $\vec{\mathbf{r}}_\ell = (x_\ell, y_\ell, z_\ell)$, where $\ell = 1, 2, 3, \ldots, L$. Hence, the cost function that minimizes the sum of the reflected sound pressure at all L sensor positions is defined as

$$J_{x_p} = \sum_{\ell=1}^{L} \left|p_r(\vec{\mathbf{r}}_\ell)\right|^2 = \sum_{\ell=1}^{L} \left|\frac{1}{2}\Big[p(\vec{\mathbf{r}}_\ell) - \varrho\, c\, u_x(\vec{\mathbf{r}}_\ell)\Big]\right|^2 \stackrel{!}{=} \text{Minimum}, \tag{1.105}$$

where the subscript x_p in J_{x_p} denotes the minimization of the reflected component of the pressure p_r ; urify this, Figure 1.10

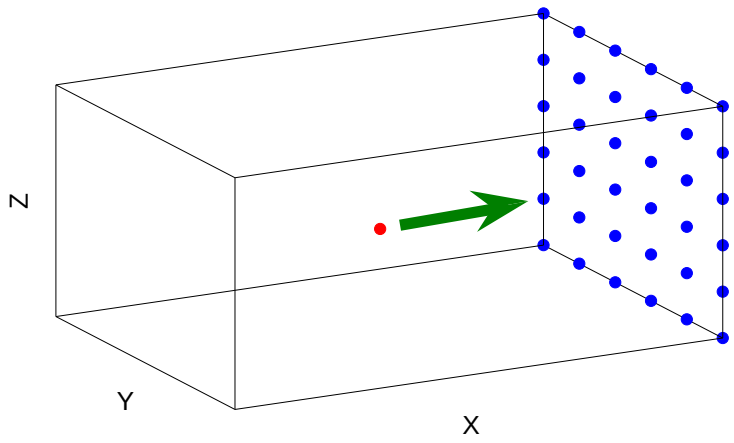

Figure 1.10: The red dot represents the primary source, the green arrow shows one component of the wave propagating in the positive direction of x and the blue dots represent an array of secondary sources placed over the wall.

Even though the enclosure is considered large enough to allow the primary source to radiate in the three dimensions of space, the active absorption system is able to decompose this sound field to *observe* each individual spatial component and apply the control accordingly. Which, for this case, will sense only the component of the sound field traveling along the x coordinate.

Likewise, one could choose any other direction to minimize p_r, e.g. y or z direction. The next section will present the expansion of this method to minimize p_r in a three-dimensional enclosure.

Now, to obtain the optimum set of coefficients $\boldsymbol{\beta}_{\text{opt}}$, it is necessary to further develop the cost function to reach an equation similar to the *Hermitian quadratic form*, as shown in equation (1.100).

Considering the general solution of the pressure field given in equation (1.99), the sound pressure at a given observability point $\vec{\mathbf{r}}_\ell$ within the enclosure will be

$$p(\vec{\mathbf{r}}_\ell) = \sum_{i=0}^{I} \beta_i \sum_{pqr}^{\infty} g_{pqr}^{(i)} \, \Psi_{pqr}(\vec{\mathbf{r}}_\ell), \tag{1.106}$$

where

$$g_{pqr}^{(i)} = \frac{p_{pqr}^{(i)}}{1 - \frac{\omega_{pqr}^2}{\omega^2}}. \tag{1.107}$$

The particle velocity u_x evaluated at the same point $\vec{\mathbf{r}}_\ell$ is obtained as

$$\begin{aligned} u_x(\vec{\mathbf{r}}_\ell) = \frac{j}{\varrho\,\omega} \frac{\partial p(\vec{\mathbf{r}})}{\partial x}\bigg|_{\vec{\mathbf{r}}_\ell} &= \frac{j}{\varrho\,\omega} \sum_{i=0}^{I} \beta_i \sum_{pqr}^{\infty} g_{pqr}^{(i)} \, \frac{\partial \Psi_{pqr}(\vec{\mathbf{r}})}{\partial x}\bigg|_{\vec{\mathbf{r}}_\ell} \\ &= \frac{j}{\varrho\,\omega} \sum_{i=0}^{I} \beta_i \sum_{pqr}^{\infty} g_{pqr}^{(i)} \, \Psi_{pqr}^{S}(\vec{\mathbf{r}}_\ell) \end{aligned} \tag{1.108}$$

with

$$\Psi_{pqr}^{S}(\vec{\mathbf{r}}_\ell) = \frac{\partial \Psi_{pqr}(\vec{\mathbf{r}})}{\partial x}\bigg|_{\vec{\mathbf{r}}_\ell} = -\frac{p\,\pi}{l_x} \, \sin\left(\frac{p\pi x_\ell}{l_x}\right) \cos\left(\frac{q\pi y_\ell}{l_y}\right) \cos\left(\frac{r\pi z_\ell}{l_z}\right). \tag{1.109}$$

Thus, combining pressure (1.106) and particle velocity (1.108), the reflected pressure p_r from equation (1.104) can be rewritten as

$$p_r(\vec{\mathbf{r}}_\ell) = \sum_{i=0}^{I} \beta_i \sum_{pqr}^{\infty} g_{pqr}^{(i)} \, \Phi_{pqr}(\vec{\mathbf{r}}_\ell), \tag{1.110}$$

where

$$\Phi_{pqr}(\vec{\mathbf{r}}_\ell) = \frac{1}{2}\left(\Psi_{pqr}(\vec{\mathbf{r}}_\ell) - \frac{j}{k}\Psi_{pqr}^{S}(\vec{\mathbf{r}}_\ell)\right) \tag{1.111}$$

and $\Psi_{pqr}(\vec{\mathbf{r}})$ was already defined in equation (1.92).

Now, replacing the new equation of the reflected pressure (1.110) into the cost function J_{x_p} (1.105), the latter can be expanded in terms of β_i and $g_{pqr}^{(i)}$ to obtain the values $\mathbf{A}$, $\mathbf{b}$ and c_h of the *Hermitian quadratic form* that defines the optimal set of *complex coefficients*

$\boldsymbol{\beta}_{\text{opt}}$. Thus, J_{x_p} becomes

$$\begin{aligned}
J_{x_p} &= \sum_{l=1}^{L} p_r(\vec{\mathbf{r}}_\ell) \cdot p_r^*(\vec{\mathbf{r}}_\ell) \\
&= \sum_{l=1}^{L} \left(\sum_{i=0}^{I} \beta_i \sum_{pqr}^{\infty} g_{pqr}^{(i)} \, \Phi_{pqr}(\vec{\mathbf{r}}_\ell) \cdot \sum_{j=0}^{I} \beta_j^* \sum_{lmn}^{\infty} g_{lmn}^{*(j)} \, \Phi_{lmn}^*(\vec{\mathbf{r}}_\ell) \right) \\
&= \sum_{i=1}^{I} \sum_{j=1}^{I} \beta_j^* \sum_{pqr}^{\infty} \sum_{lmn}^{\infty} g_{pqr}^{(i)} \, g_{lmn}^{*(j)} \, \Gamma_{pqrlmn}(\vec{\mathbf{r}}_\ell) \, \beta_i + \sum_{j=1}^{I} \beta_j^* \sum_{pqr}^{\infty} \sum_{lmn}^{\infty} g_{pqr}^{(0)} \, g_{lmn}^{*(j)} \, \Gamma_{pqrlmn}(\vec{\mathbf{r}}_\ell) \, \beta_0 \\
&+ \sum_{i=1}^{I} \beta_0^* \sum_{pqr}^{\infty} \sum_{lmn}^{\infty} g_{pqr}^{(i)} \, g_{lmn}^{*(0)} \, \Gamma_{pqrlmn}(\vec{\mathbf{r}}_\ell) \, \beta_i + \beta_0^* \sum_{pqr}^{\infty} \sum_{lmn}^{\infty} g_{pqr}^{(0)} \, g_{lmn}^{*(0)} \, \Gamma_{pqrlmn}(\vec{\mathbf{r}}_\ell) \beta_0
\end{aligned} \tag{1.112}$$

where

$$\Gamma_{pqrlmn}(\vec{\mathbf{r}}_\ell) = \sum_{l=1}^{L} \Phi_{pqr}(\vec{\mathbf{r}}_\ell) \, \Phi_{lmn}^*(\vec{\mathbf{r}}_\ell). \tag{1.113}$$

Note that the superscript * indicates complex conjugate.

The values of $\mathbf{A}$, $\mathbf{b}$ and c_h are extracted from the first, second and fourth term of J_{x_p}, given

$$\mathbf{A} = \sum_{pqr}^{\infty} \sum_{lmn}^{\infty} \Gamma_{pqrlmn}(\vec{\mathbf{r}}_\ell) \begin{bmatrix} g_{pqr}^{(1)} g_{lmn}^{*(1)} & \cdots & g_{pqr}^{(I)} g_{lmn}^{*(1)} \\ \vdots & \ddots & \vdots \\ g_{pqr}^{(1)} g_{lmn}^{*(I)} & \cdots & g_{pqr}^{(I)} g_{lmn}^{*(I)} \end{bmatrix}, \tag{1.114}$$

$$\mathbf{b} = \sum_{pqr}^{\infty} \sum_{lmn}^{\infty} g_{pqr}^{(0)} \, \Gamma_{pqrlmn}(\vec{\mathbf{r}}_\ell) \begin{bmatrix} g_{lmn}^{*(1)} \\ \vdots \\ g_{lmn}^{*(I)} \end{bmatrix} \tag{1.115}$$

and

$$c_h = \sum_{pqr}^{\infty} \sum_{lmn}^{\infty} g_{pqr}^{(0)} \, \Gamma_{pqrlmn}(\vec{\mathbf{r}}_\ell) \, g_{lmn}^{*(0)}. \tag{1.116}$$

For completeness it must be said that it is also possible to rewrite the latter set of equations in terms of matrices and vectors to make it more compact and easy to handle. In this way the general equation for the reflected sound pressure $p_r(\vec{\mathbf{r}}_\ell)$ at a given point $\vec{\mathbf{r}}_\ell$ (1.110) can be expressed as

$$p_r(\vec{\mathbf{r}}_\ell) = \boldsymbol{\beta}^T \mathbf{G}^T \boldsymbol{\Phi}_\ell \tag{1.117}$$

where $\boldsymbol{\Phi}_\ell$ is a complex vector given by all the possible combinations of the modal indexes p, q and r as defined by $\Phi_{pqr}(\vec{\mathbf{r}}_\ell)$ in equation (1.111). If each modal index p, q and r is truncated at a certain maximum value P, Q and R respectively, then the vector resulting from all the possible combinations will have a length of $P \cdot Q \cdot R$, therefore $\boldsymbol{\Phi}_\ell$ will have

dimensions of $[P\cdot Q\cdot R\times 1]$, thus

$$\mathbf{\Phi}_\ell = \frac{1}{2}\begin{bmatrix} 1 \\ \Psi_{001}(\vec{\mathbf{r}}_\ell) - \frac{j}{k}\Psi^S_{001}(\vec{\mathbf{r}}_\ell) \\ \Psi_{002}(\vec{\mathbf{r}}_\ell) - \frac{j}{k}\Psi^S_{002}(\vec{\mathbf{r}}_\ell) \\ \vdots \\ \Psi_{PQR}(\vec{\mathbf{r}}_\ell) - \frac{j}{k}\Psi^S_{PQR}(\vec{\mathbf{r}}_\ell) \end{bmatrix} \tag{1.118}$$

and $\mathbf{G}$ is a complex matrix that is defined by the individual values of $g^{(i)}_{pqr}$ given in equation (1.107). Its first column contains the modal amplitudes belonging to the primary source and the subsequent columns correspond to the modal amplitudes contributed by each i-th secondary source. Likewise as $\mathbf{\Phi}_\ell$, the number of rows is defined by all possible combinations of the trio of modal indexes p, q and r. Hence, its dimension is $[P\cdot Q\cdot R\times I+1]$.

$$\mathbf{G} = \begin{bmatrix} g^{(0)}_{000} & g^{(1)}_{000} & \cdots & g^{(I)}_{000} \\ g^{(0)}_{001} & g^{(1)}_{001} & \cdots & g^{(I)}_{001} \\ \vdots & \vdots & \ddots & \vdots \\ g^{(0)}_{PQR} & g^{(1)}_{PQR} & \cdots & g^{(I)}_{PQR} \end{bmatrix}. \tag{1.119}$$

In general, the reflected pressure $p_r(\vec{\mathbf{r}})$ for a number of L observation points within the enclosure will be given by

$$\mathbf{p_r} = \begin{bmatrix} p_r(\vec{\mathbf{r}}_1) \\ p_r(\vec{\mathbf{r}}_2) \\ \vdots \\ p_r(\vec{\mathbf{r}}_L) \end{bmatrix} = \begin{bmatrix} \mathbf{\Phi}_1^T \\ \mathbf{\Phi}_2^T \\ \vdots \\ \mathbf{\Phi}_L^T \end{bmatrix} \cdot \mathbf{G}\,\boldsymbol{\beta}, \tag{1.120}$$

moreover if the complex matrix Θ is defined as

$$\Theta = \begin{bmatrix} \mathbf{\Phi}_1^T \\ \mathbf{\Phi}_2^T \\ \vdots \\ \mathbf{\Phi}_L^T \end{bmatrix}^H \cdot \begin{bmatrix} \mathbf{\Phi}_1^T \\ \mathbf{\Phi}_2^T \\ \vdots \\ \mathbf{\Phi}_L^T \end{bmatrix} \tag{1.121}$$

then, the cost function J_{x_p} (1.112) can be rewritten as

$$\begin{aligned} J_{x_p} &= \sum_{l=1}^{L} \left| p_r(\vec{\mathbf{r}}_\ell) \right|^2 \\ &= \mathbf{p}_\mathbf{r}^H\, \mathbf{p_r} \\ &= (\mathbf{G}\,\boldsymbol{\beta})^H\, \Theta\ (\mathbf{G}\,\boldsymbol{\beta}). \end{aligned} \tag{1.122}$$

As before, $\boldsymbol{\beta}_{\text{opt}}$ can be obtained through $\mathbf{A}$, $\mathbf{b}$ and c_h from the expansion of the cost function, now the same development can be applied but with the difference that now it can be calculated in matrix terms.

Recalling from equation (1.103) that $\boldsymbol{\beta}$ is composed by the *complex amplification coefficients* of the primary β_0 and the secondary sources $\beta_{1,2,\ldots,I}$ and $\mathbf{G}$ is composed by a

combination of modal amplitudes of the primary and the secondary source, it is possible to expand the cost function J_{x_p} (1.122) to find the values of $\mathbf{A}$, $\mathbf{b}$ and c_h as

$$\begin{aligned} J_{x_p} &= (\mathbf{G}\,\boldsymbol{\beta})^H\,\Theta\;(\mathbf{G}\,\boldsymbol{\beta}) \\ &= \overline{\boldsymbol{\beta}}_I^H \underbrace{\overline{\mathbf{G}}_I^H \Theta\, \overline{\mathbf{G}}_I}_{\mathbf{A}} \overline{\boldsymbol{\beta}}_I + \overline{\boldsymbol{\beta}}_I^H \underbrace{\overline{\mathbf{G}}_I^H \Theta\, \mathbf{G}_0}_{\mathbf{b}} \beta_0 + \beta_0^H \underbrace{\mathbf{G}_0^H \Theta\, \overline{\mathbf{G}}_I}_{\mathbf{b}^H} \overline{\boldsymbol{\beta}}_I + \beta_0^H \underbrace{\mathbf{G}_0^H \Theta\, \mathbf{G}_0}_{c_h} \beta_0 \end{aligned} \tag{1.123}$$

where the first column of $\mathbf{G}$ is defined as $\mathbf{G}_0$ and all the rest of the columns as $\overline{\mathbf{G}}_I$, and $\overline{\boldsymbol{\beta}}_I$ corresponds to the sub-set $\beta_{1,2,\ldots,I}$ and $\beta_0 = \beta_0^H = 1$. This is,

$$\mathbf{G} = \Big[\mathbf{G}_0 \underbrace{\mathbf{G}_1\mathbf{G}_2 \ldots \mathbf{G}_I}_{\overline{\mathbf{G}}_I}\Big] \tag{1.124}$$

and

$$\begin{aligned} \boldsymbol{\beta} &= \Big[\beta_0\, \beta_1\, \beta_2 \;\ldots\; \beta_I\Big] \\ &= \Big[1 \underbrace{\beta_1\, \beta_2 \;\ldots\; \beta_I}_{\overline{\boldsymbol{\beta}}_I}\Big]. \end{aligned} \tag{1.125}$$

1.4.3 Three-dimensional control

As shown in the past section, the cost function J_{x_p} was defined to minimize the reflected component of the pressure p_r due to a wave propagating in the positive direction of x. However, in order to achieve total absorption in a particular dimension, lets say x, it is also essential to take into account the reflected component p_r due to a wave traveling in the negative direction of x. For that reason, a second cost function J_{x_n} must be defined for this case.

Thus, equivalent to Figure 1.10 where J_{x_p} is minimized, Figure 1.11 shows the combination of [illegible] al sound absorption i

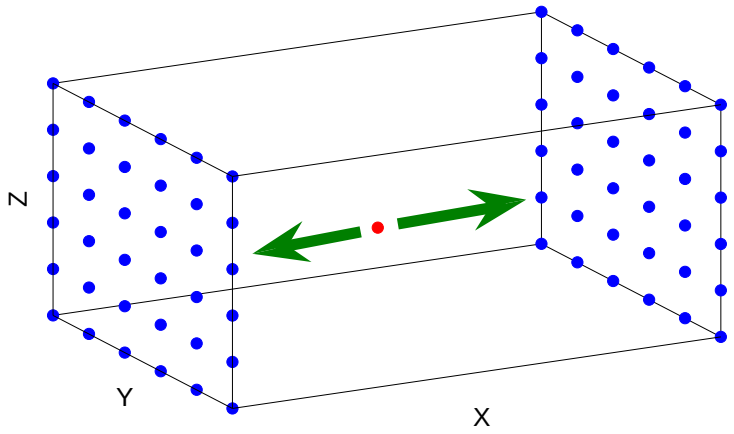

Figure 1.11: Secondary source must be placed in both, positive and negative, directions of propagation to control the absorption in the x dimension.

In Section 1.1, p_r was obtained according to the definitions given in Figure 1.1 where a source was placed on the left side of the tube and the rigid end on the right side.

Given this conditions, p_r travels in the negative direction of x. Under this premises J_{x_p} was developed and solved, as shown in Figure 1.10. Now it is necessary to obtain an expression for J_{x_n} that is required to solve the case depicted in Figure 1.11, where the total number of sources is now $2L$.

From the minimization point of view J_{x_p} and J_{x_n} are equivalent, the only fundamental difference is the spatial arrangement of sources. Recalling the diagram of Figure 1.1, if the loudspeaker now is placed on the right side of the tube and the left side is only a rigid termination, two new expressions p_i' and p_r' could be obtained as

$$p_i' = \frac{1}{2}\left(p - \varrho\, c\, u\right) \tag{1.126}$$

$$p_r' = \frac{1}{2}\left(p + \varrho\, c\, u\right) \tag{1.127}$$

where the only difference between these two equations and the equations (1.7) and (1.8) is the opposite sign in front of the particle velocity u. Using these new expressions as the starting point and following the same procedure described in Section 1.4.2 it is possible to obtain $\mathbf{A}$, $\mathbf{b}$ and c_h using the new cost function J_{x_n}, which takes the form

$$J_{x_n} = \sum_{\ell=L+1}^{2L} \left| \frac{1}{2}\Big[p(\vec{\mathbf{r}}_\ell) + \varrho\, c\, u_x(\vec{\mathbf{r}}_\ell)\Big] \right|^2 . \tag{1.128}$$

If the active system combines J_{x_p} and J_{x_n}, it is possible to generate total absorption in both directions of propagation along the x axis. Hence, a new cost function J_x that ensures total absorption for the x dimension is defined as

$$J_x = J_{x_p} + J_{x_n}. \tag{1.129}$$

Finally, to find the cost function that minimizes the reflected pressure for the other two dimensions, i.e. y and z, it is necessary to repeat the same procedures described before. The only difference is that now the particle velocities u_y and u_z must be replaced into equations (1.104) and (1.127). Thus, four new cost functions are obtained: J_{y_p}, J_{y_n}, J_{z_p} and J_{z_n}. Each of them minimizes the reflected pressure for the specified axis and direction.

In the best case scenario, one would want to place secondary sources in each of the six walls of the enclosure to obtain the best possible absorption. Under this conditions the total cost function J that minimizes the reflected pressure for the six directions of propagation inside the room will be given by the combination of all individual cost functions, this is

$$J = J_{x_p} + J_{x_n} + J_{y_p} + J_{y_n} + J_{z_p} + J_{z_n}. \tag{1.130}$$

Later on, in Section 2.2.2 and 2.3.4 the method described here will be contrasted with the classical method of active noise control (ANC) to compare how both systems perform from the absorption point of view. An ANC system locally minimizes the sound pressure p at a given number of sensor points $\vec{\mathbf{r}}_\ell$. The cost function for this criterion can be written as

$$J_{\text{ANC}} = \sum_{\ell=1}^{L} \left| p(\vec{\mathbf{r}}_\ell) \right|^2 \stackrel{!}{=} \text{ Minimum.} \tag{1.131}$$

1.5 Absorption mechanism of real loudspeakers

From the acoustical point of view, a loudspeaker working as an active absorption device can be seen as a membrane resonator. The mechanical analogy of a membrane resonator is based on a mass which vibrates in resonance on a spring, where the mass is given by the area density (mass per area) of the membrane, and the spring is given by the air layer in the cavity behind the membrane with a certain dynamic stiffness mainly defined by the volume. In a loudspeaker, the mass is given by the moving mass of the cone, and the spring by the combination of the mechanical resistance and compliance of the suspension of the cone.

In a membrane resonator the stiffness of the spring is fixed or tuned just for one value of resonance and therefore allowing a unique frequency, or narrow band, of maximal absorption. In contrast, the loudspeaker shall be able to easily change its mechanical response to obtain a wider range of effectivity if the right signal is fed into the loudspeaker, since the current flowing through the coil will be able to force the movement of the cone to the appropriate response.

On the other hand, an electro-mechanical analogy of the loudspeaker can be given to understand deeper the dissipation of energy. A simplified model of a loudspeaker can be defined by a rigid cone of mass M_m of area A with a suspension system of stiffness K_m and damping R_m. The cone is moved by the action of a coil where a current i is flowing. Hence, the motion equation of the cone is given by

$$j\omega M_m + R_m u + \frac{K_m u}{j\omega} = Bli - pA \tag{1.132}$$

where u is the complex cone velocity, p is the complex acoustic pressure which acts over the area A, Bl is the product of the magnetic flux density and the length of the coil, thus Bli represents the force transmitted to the cone by the action of the coil in the magnetic field. Following the development given by Nelson [19], it is possible to obtain the expression of the power dissipated W_e by the loudspeaker. The right hand side of equation (1.133) shows the three independent forms of power dissipation, i.e. electrical, mechanical and acoustical respectively. Nelson writes, *"It is entirely possible for the third of these, given by* $\Re\{pq^*\}$*, to take a negative value. Under these circumstances it is clear that less electrical power will be required to sustain a given piston velocity amplitude* $|v|$*"* [19]. This means that, if the cone of the loudspeaker is impinged by an incident sound wave, part of the energy is transferred to the coil. The force applied keeps the cone movement but using less current.

The dissipated power is given by

$$W_e = \frac{1}{2}|i|^2 R + \frac{1}{2}|v|^2 R_m + \frac{1}{2}\Re\{p\,q^*\} \tag{1.133}$$

where $q = vA$ is the total volume velocity produced by the cone velocity fluctuations.

1.6 Absorption coefficient of an array of secondary sources

The absorption coefficient α can be considered as a useful evaluation parameter in this study, since a single value can be directly associated to an array of secondary sources of a given area, in the same way as passive absorbers are qualified.

The ISO 354 [25] specifies an area $S = 10\ \mathrm{m}^2$ of sample of passive material to determine its absorption coefficient. Likewise, an array of secondary sources of the same area S can be used, with the difference that here the density of sources, or the number of sources per unit of area, can be freely modified. Figure 1.12 shows the area defined by the secondary sources and its change when the density is increased.

If the primary source radiates a signal with a given frequency f_0, a certain wavelength λ_0 is associated with this excitation. Thus, keeping the frequency constant but increasing the number of secondary sources within the area S, allows to define the parameter of *sources per* λ^2, which is also directly proportional to the number of *sources per* λ in only one direction. This is of course valid only if the sources are equally spaced lengthwise and widthwise.

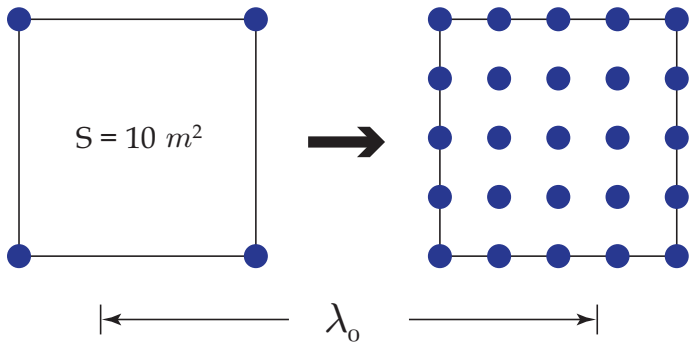

Figure 1.12: As the number of secondary sources is incremented within the area S, the number of source per wavelength also increases.

As seen, incident and reflected components of the pressure and the particle velocity can be calculated at any point within enclosure. Hence, an imaginary parallel plane $\mathbf{\Omega}$ near and in front of the array of secondary sources is defined and p_i, p_r, u_i and u_r are calculated over a number of M discrete points in the plane $\mathbf{\Omega}$, such that for each single element Ω_m of this plane, the incident I_{i_m} and reflected I_{r_m} sound intensity can be calculated as

$$I_{i_m} = \frac{1}{2}\Re\{p_{i_m}\, u_{i_m}^*\}, \tag{1.134}$$

$$I_{r_m} = \frac{1}{2}\Re\{p_{r_m}\, u_{r_m}^*\}. \tag{1.135}$$

Figure 1.13 shows a diagram of the plane $\mathbf{\Omega}$ with its corresponding Ω_m elements, in general the number of elements M is not related to the number of secondary sources used in the array.

Since the secondary sources control the perpendicular component of the impinging sound field, it is only necessary to compute the perpendicular component of the sound intensity that crosses the plane $\mathbf{\Omega}$. For example, if the plane $\mathbf{\Omega}$ is parallel to the axis y and z then u_{i_m} and u_{r_m} must be calculated using the component u_x of the particle velocity.

Now it is possible to obtain the mean reflection coefficient R over the plane $\mathbf{\Omega}$ as

$$R = \frac{I_r}{I_i}, \tag{1.136}$$

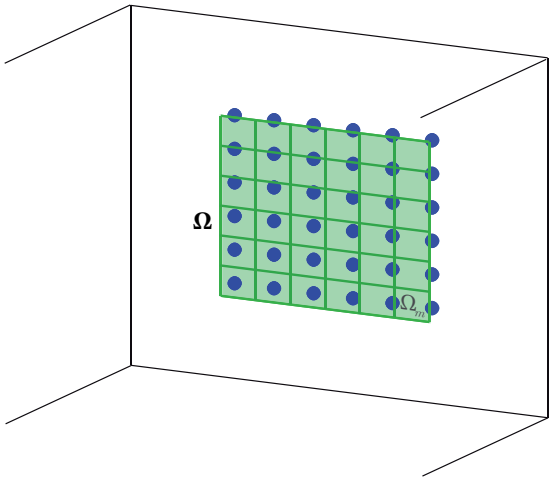

Figure 1.13: Plane $\mathbf{\Omega}$ and its Ω_m elements in front of an array of secondary sources.

where I_r and I_i are mean values of all I_{r_m} and I_{i_m} respectively,

$$I_r = \frac{1}{M}\sum_{m=1}^{M} I_{r_m} \tag{1.137}$$

$$I_i = \frac{1}{M}\sum_{m=1}^{M} I_{i_m}. \tag{1.138}$$

Subsequently the absorption coefficient α that can be associated to the array of secondary sources can be obtained as

$$\alpha = 1 - R. \tag{1.139}$$

By means of this procedure it is possible to associate a certain α with the number of secondary sources used. But even more interesting is to describe α as a function of the density of *secondary sources per* λ. Later on, in Chapter 2, simulations of the active system will be evaluated using the absorption coefficient to estimate the performance of the active absorption under different conditions.

1.7 Total acoustic potential energy

Although the active absorption acts over just one propagation direction, the whole sound field is modified. In order to assess the effect of the active absorption system, a global parameter is required to quantify its influence. The total time-averaged acoustic potential energy E_p describes the global energy of the sound field within the enclosure since it integrates the pressure over the whole space. Therefore it will quantify any change generated by the active system. The time-averaged potential energy [19] E_p is given by

$$E_p = \frac{1}{4\,\varrho\,c^2}\int_V \left|p(\vec{\mathbf{r}})\right|^2 \mathrm{d}V. \tag{1.140}$$

This expression can be developed further by replacing the pressure $p(\vec{\mathbf{r}})$ by the expression given in equation (1.110), hence

$$\begin{aligned} E_p &= \frac{1}{4\,\varrho\,c^2}\int_V p(\vec{\mathbf{r}})\,p^*(\vec{\mathbf{r}})\,\mathrm{d}V \\ &= \frac{1}{4\,\varrho\,c^2}\int_V \sum_{i=0}^{I}\beta_i\,\sum_{pqr}^{\infty} g_{pqr}^{(i)}\;\Psi_{pqr}(\vec{\mathbf{r}})\cdot\sum_{j=0}^{I}\beta_j^*\,\sum_{lmn}^{\infty} g_{lmn}^{*(j)}\;\Psi_{lmn}(\vec{\mathbf{r}})\;\mathrm{d}V \\ &= \frac{1}{4\,\varrho\,c^2}\sum_{i=0}^{I}\sum_{j=0}^{I}\beta_j^*\,\sum_{pqr}^{\infty} g_{pqr}^{(i)}\,\mu_{pqr}\,g_{pqr}^{*(j)}\;\beta_i, \end{aligned} \tag{1.141}$$

where μ_{pqr} is the integral of the squared modal shape $\Psi_{pqr}(\vec{\mathbf{r}})$, which it was already calculated in (1.89). Here, μ_{pqr} can be rewritten as a diagonal matrix $\boldsymbol{\mu}$ in the form

$$\boldsymbol{\mu} = \begin{bmatrix} \mu_0\,\mu_0\,\mu_0 & & & \mathbf{0} \\ & \mu_1\,\mu_1\,\mu_1 & & \\ & & \ddots & \\ \mathbf{0} & & & \mu_P\,\mu_Q\,\mu_R \end{bmatrix} \tag{1.142}$$

where the diagonal is constructed multiplying μ_p, μ_q and μ_r point by point. This is possible only if $P = Q = R$. Hence, $\boldsymbol{\mu}$ is a squared matrix of dimensions $[P \times P]$.

Finally, the total time-averaged acoustic potential energy E_p that includes the primary and secondary sources is expressed as

$$E_p = \frac{1}{4\,\varrho\,c^2}\,(\mathbf{G}\,\boldsymbol{\beta})^H\boldsymbol{\mu}\,(\mathbf{G}\,\boldsymbol{\beta}). \tag{1.143}$$

The value of potential energy when the active system is working in optimal conditions ($E_{p\,\mathrm{on}}$) can be easily calculated replacing $\boldsymbol{\beta}$ by $\boldsymbol{\beta}_{\mathrm{opt}}$.

1.8 Reverberation time

As it is widely known, the reverberation time (RT_{60}) is the time that takes to decrease the mean sound pressure level from a reference value by -60 dB. However, this is just a primary interpretation of a more deeper concept. The reverberation time describes the ratio of damping of the normal modes of a room as a function of time, and this ratio is dependant of the acoustic absorption of the enclosure. As pointed out by Crighton [26], *"There are two important practical consequences of absorption in a room. One is the influence on the reverberation time, the other is the influence on the average sound pressure"*, which summarizes the description given before, there is a direct relationship between reverberation time and the sound absorption of the room. But not only that, it is possible to infer that both characteristics are co-dependant and that is particularly important in this research.

The mathematical model described in the past sections was entirely developed in frequency domain, therefore it will require to rewrite the whole model in time domain to be able to study their effect over the reverberation time. To add an extra degree of complexity it must be considered that the reverberation time is a a transient phenomenon, far away from any possible steady state representation.

Nevertheless, it is possible to use the much simpler approach of Crighton to prove the influence of the active absorption system over the reverberation time. As we will see in the next chapter, it is possible to generate a precise equivalent absorption coefficient for an array of secondary source, where this value can be used directly to calculate the reverberation time. It will be proven later that the extreme case of $\alpha = 1$ can be achieved and moreover a free field condition can be generated inside the room.

Chapter 2

Numerical results - Simulations

2.1 Validation of simulations

The software Matlab was chosen as a tool for the development of the forthcoming simulation since it offers unique flexibility and a large mathematical library that allows to easily implement the model introduced in the first chapter. The major advantage is given by how quick the parameters of the model can be adjusted, for instance the dimensions of the enclosure, the number or the distribution of sources. It is of major interest to model the sound pressure field resulting from the combination of primary and secondary sources inside an enclosure, as given by equation (1.106). However, before getting started with the large set of simulations, it is crucial to validate the results generated by our model in Matlab.

A Finite Element Method (FEM) software is chosen to compare against since it provides the exact boundary conditions needed to describe this model, *Sound hard boundary* and *Total absorption*. But more importantly, it is widely used and accepted as a reliable modeling tool. Giving those reasons, one could ask, why not simply use FEM? The answer is that FEM models are difficult and slow to modify, even for the smallest changes.

This validation is made by comparing two identical cases, one simulated with Matlab and the other with the FEM software, specifically Comsol. Consequently, if similar results are obtained in both cases, the Matlab simulations can be considered fully valid.

The simulated model consisted of a two-dimensional rectangular enclosure with dimension $l_x = 5.5$ m and $l_y = 3.8$ m. A primary source was located in the upper left corner $x_s = 0$ and $y_s = 3.8$. According to equation (1.98), a small lost factor η was included in both cases. The right side boundary was defined as totally absorbent ($\alpha = 1$). In Matlab, this latter condition is implemented using a number of $I = 15$ secondary sources according to the mathematical model already developed in Chapter 1, whereas in Comsol this condition can be easily set using a Perfectly Matched Layer (PML) [27, 28]. According to the Comsol's documentation, *"A PML is strictly speaking not a boundary condition but an additional domain that absorbs the incident radiation without producing reflections"* [29]. Under these conditions, four different frequencies were simulated 75, 100, 200 and 300 Hz, Table 2.1 summarizes the results. In the Matlab figures, the small blue and yellow circles in the right side represent the secondary sources and the sensor points of the active system respectively.

As shown in the figures of Table 2.1, for each frequency the results obtained in both

cases are almost identical. Consequently, this result validates the simulations made using Matlab and additionally gives a first view about the capability of the active system to absorb reflected sound.

f [Hz]	Comsol (FEM)	Matlab
75	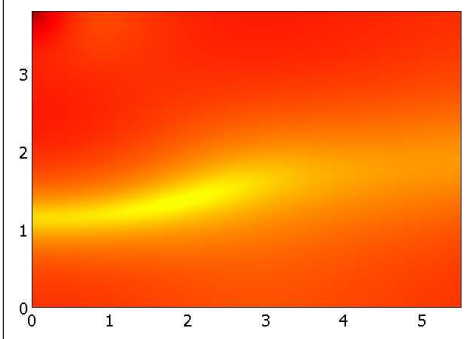	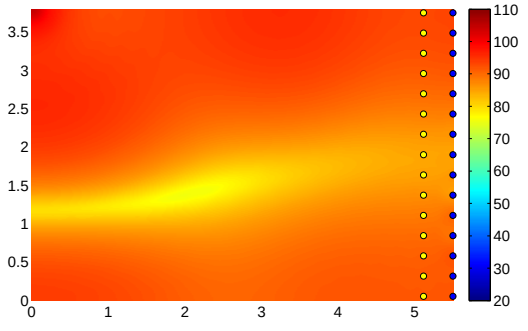
100	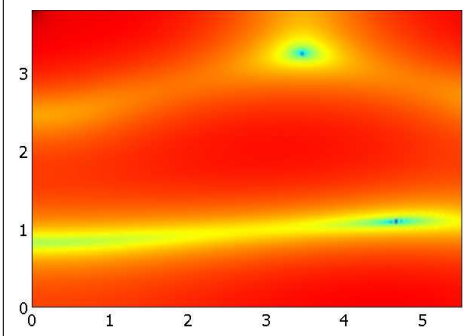	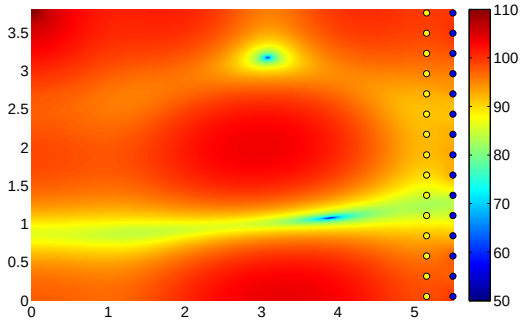
200	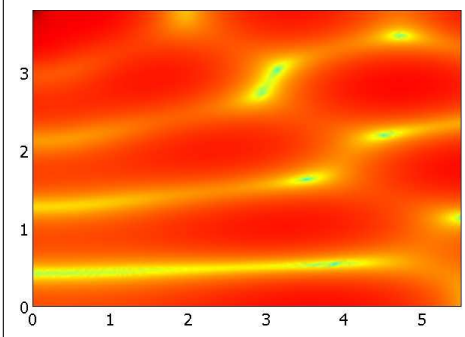	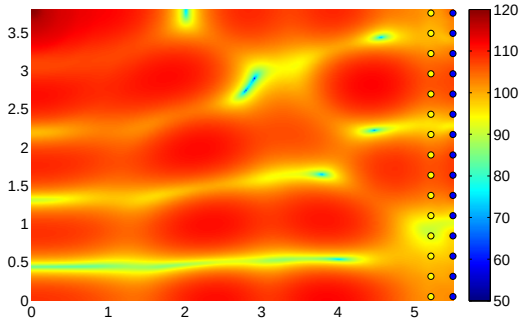
300	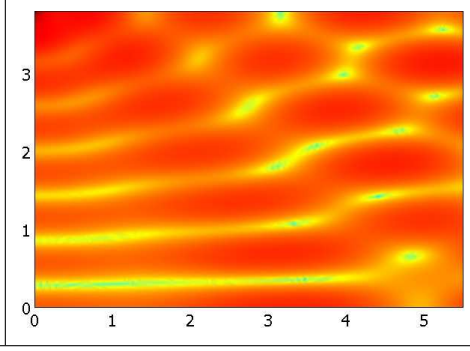	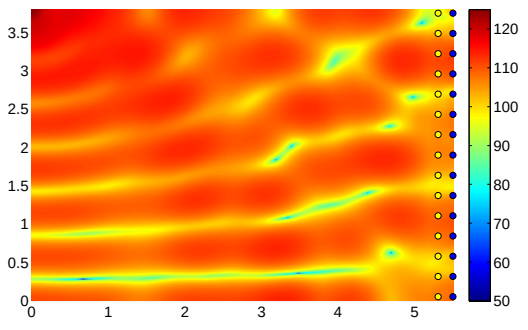

Table 2.1: Simulations comparison of sound pressure field in a two-dimensional enclosure. Primary source located in the upper left corner, right side boundary defined as completely absorbent.

2.2 Sound pressure field within a two-dimensional enclosure

The latter section showed the most simple implementation case, where just only one of the boundaries of the enclosure was set with the active absorption system. This section will expand the simulations, presenting a variety of new cases such as comparisons between control on and off, different excitation frequencies, primary and secondary sources distribution within the enclosure, etc. As mentioned before, a number of L sensor points is required for the minimization of the cost function. For modeling purposes, the number of secondary sources and sensors chosen is the same, i.e. $L = I$. For simplicity, all these initial simulations use a rather large number of secondary sources, however in Section 2.4 a criterion is defined to choose the smallest number of I sources that produce an optimal absorption coefficient.

Below there is a comparison of different secondary sources distribution where the boundaries of the enclosure were covered one by one with secondary sources. The comparison is made for three different low frequencies: 75, 150 and 400 Hz. This set of cases allows to observe the change in the pressure field as the number of sources increases around the enclosure. As stated before, the small blue and yellow circles represent the secondary sources and the sensor points of the active system respectively while the primary source is represented by the red circle. The generation of the active absorption requires to use a cost function J that minimizes the reflection of every boundary of the enclosure, this should be achieved by the combination of the four independent cost functions that minimize p_r for every direction of propagation

$$J = J_{x_p} + J_{x_n} + J_{y_p} + J_{y_n}. \tag{2.1}$$

Results are summarized in Table 2.2.

These first simulations provide important information about the capabilities of the active absorption system, in the sense that proves that the system is able to absorb the reflected waves in every direction of propagation. This demonstrates that the combination of $J_{x_p}, J_{x_n}, J_{y_p}$ and J_{y_n} produces an effective global result. As expected, the active absorption directly influences the distributions of the sound field. This can be noticed by the significant change between the condition OFF and the last case, where 4 walls are used. In this latter case, it is even possible to observe how the pressure decreases with the distance with respect to the primary source, a phenomenon that only takes place in free field.

The second important result that it is worth to point out, are the simulations using 3 walls covered. These, specially at 400 Hz, present a similar result to the one expected when a single source is simulated in front of an infinite rigid plane, cf. the figures in the section *Sound field of two sources* [30]. This is particularly interesting since, once again, it shows that all the reflections from the three walls are cancelled and only one surface is reflecting sound.

2.2.1 Distance between secondary source and control point

Any of the cost functions J described up to this point, define that the active system tries to minimize the sum of the reflected pressure at a number of $\ell = 1, 2, ..., L$ sensor points $\vec{\mathbf{r}}_\ell$.

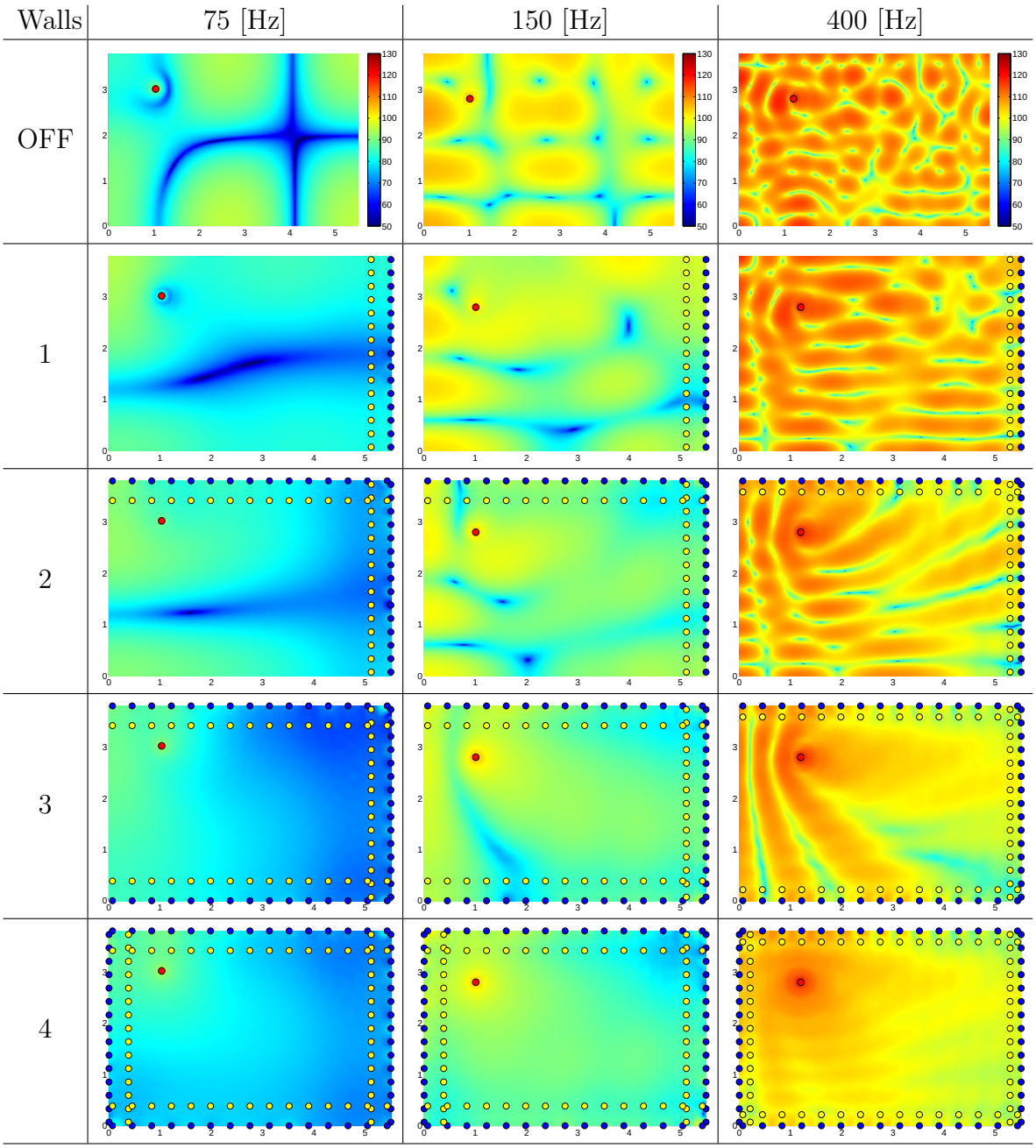

Table 2.2: Simulations comparison of sound pressure field in a two-dimensional enclosure. Active absorption system over different walls for three example frequencies.

Likewise to the latter section, the same number of sensors and secondary sources is used, i.e. $L = I$. In this way, each source has associated one sensor. In general, the positions of these sensors can be arbitrarily defined anywhere within the enclosure. However, it is practical to define each sensor position regarding to its secondary source associated, separated by a distance d. Since the secondary sources are able to minimize the reflections in the perpendicular direction to its cone, it is reasonable to define the sensor position right in front of the source but separated by d. The following simulations compare the resulting sound pressure fields with different separations d. Table 2.3 summarizes the results.

As seen in the fourth row of Table 2.2, every case should ideally tend to look similar to a point source radiating in free field since the absorption system is placed on each

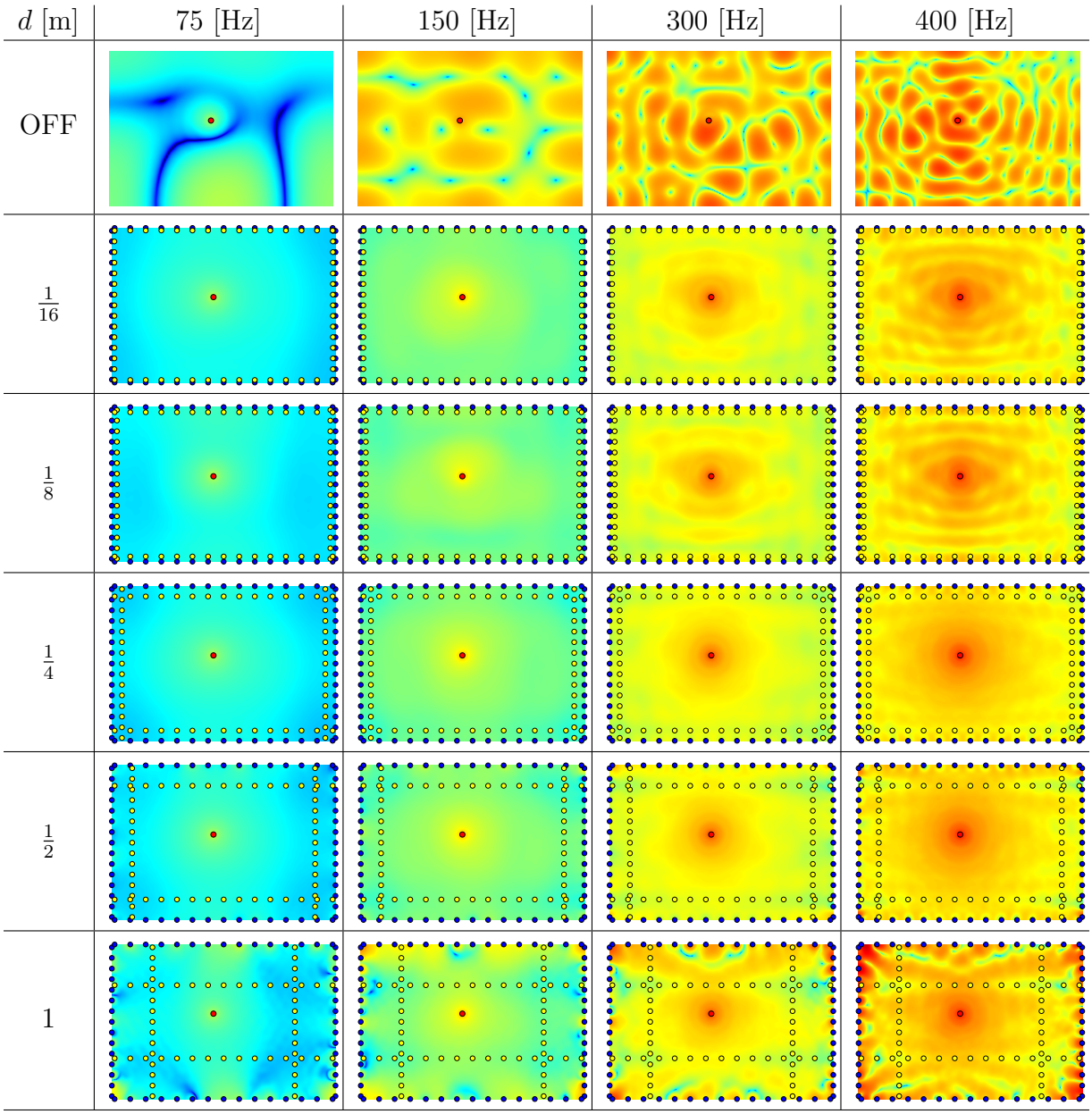

Table 2.3: Comparison of sound pressure field in a two-dimensional enclosure with different separation distances between sensor and secondary source.

boundary. Hence, the resulting sound pressure fields must be compared with this ideal pressure distribution.

In general, it appears that in every case the system is able to generate an efficient absorption response, but it seems that the optimal results are obtained around $d = \frac{1}{4}$ m. In addition, at lower frequencies, smaller values of d generate also similar good results.

If a similar analysis is made converting d into wavelength terms, there is no characteristic value where a superior result is obtained. This means, at lower frequencies the values of d near to $\frac{\lambda}{12}$ or $\frac{\lambda}{10}$ generate the best results, meanwhile at middle frequencies the optimal d moves to $\frac{\lambda}{4}$ or $\frac{\lambda}{2}$. Therefore, there is no clear relationship between the distance d and the wavelength of the excitation signal.

As an special extreme case, it is worth to mention the result obtained when a large $d = 1$ m is used. Although the sound pressure in the whole enclosure looks inhomogeneous

and with clear patterns of maxima and minima specially near to the boundaries, the center area enclosed by the sensor points presents itself as a perfectly controlled region. These inner regions, can be directly compared with any of the best cases of absorption seen so far. Hence, irrespective of the distance between sensors and sources it is possible to assume that the active system will always try to control the reflections inside the region defined by the sensors position.

2.2.2 Comparison against ANC system

It is important to establish how the active absorption system (AAS) differs from other active control systems, specially the widely used active noise control (ANC) system. The fundamental difference was already mentioned throughout the first chapter, but particularly in Section 1.4.3. As defined there, the cost function J of the AAS tries to minimize only the reflected part of the sound pressure p_r, the selective cancelation of this component of the sound field allows to achieve the absorption, moreover, the incident part p_i keeps intact. Meanwhile an ANC system is only capable to cancel the total sound pressure p and consequently reduce only the mean sound pressure within the enclosure. As ANC takes place, the sound pressure reaches a local minimum at every sensor point. This whole process presents none influence or benefit from the absorption point of view. Evidence of this can be observed in Figure 2.1 where AAS and ANC are contrasted. The inability of the ANC system to work as an absorber can be seen by the presence of remaining modes with a noticeable distribution of maxima and minima of pressure. For this simulation a frequency of 150 Hz is used. Figure 2.1 presents also for reference the sound field computed without any control (OFF).

This comparison allows to extend the analysis even further about the efficiency of the absorption and its dependency of the spatial distribution of the sensor points, as already presented in Table 2.3. For this analysis two distributions are defined, *Regular* and *Random*. Where *Regular* follows the same distribution used so far in every simulation up to this point, i.e. each sensor is located in front of its paired secondary source, the *Random* distribution puts the sensors randomly within the enclosure. It is important to notice here that each sensor has an associated direction to quantify the incident and reflected components of the pressure. In the *Regular* distribution, for each sensor, it is evident that the sensing direction points opposite to the associated loudspeaker. On the other hand, the *Random* distribution defines an arbitrary position for each sensor however the sensing direction does not change regarding the *Regular* distribution. Figure 2.2 clarify the difference between both cases.

In both distributions, the ANC system is able to minimize the sound pressure at each sensor without problems while the AAS generates two completely different results. In the *Regular* distribution, the simulation fulfills the expectations generating a result comparable with the best cases of any of the past sections, even though a small number of secondary sources is used. Whereas the *Random* distribution generates a sound field with no distinctive pattern that allows to establish that the system is actively absorbing sound. These two last cases, together with the simulations presented in the Table 2.3 where $d = 1$, allow to conclude that a certain predefined sensor distribution must be used to achieve at least some degree of absorption.

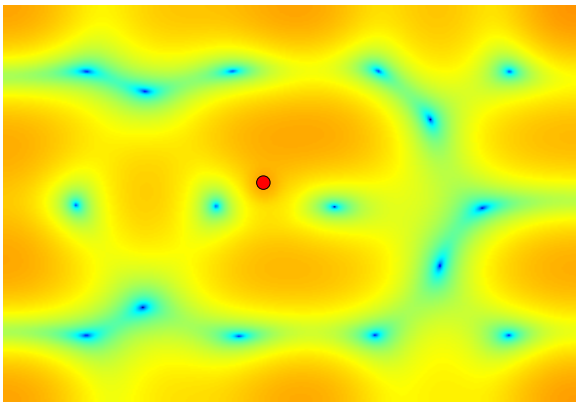

(a) OFF

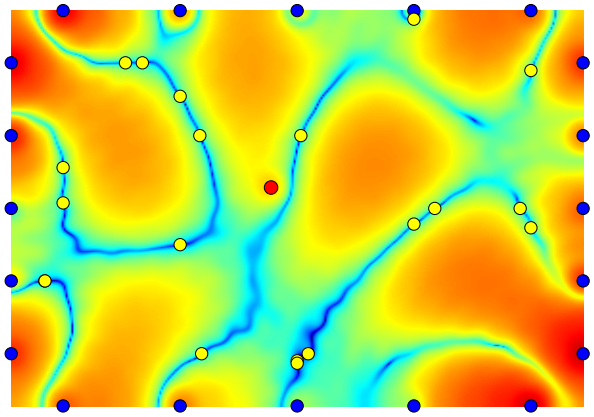

(b) ANC - Random sensors distribution

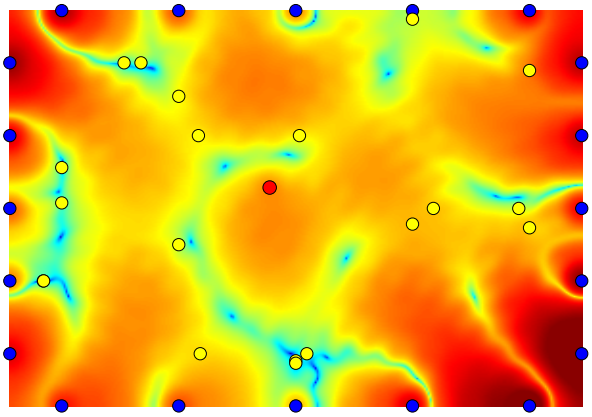

(c) AAS - Random sensors distribution

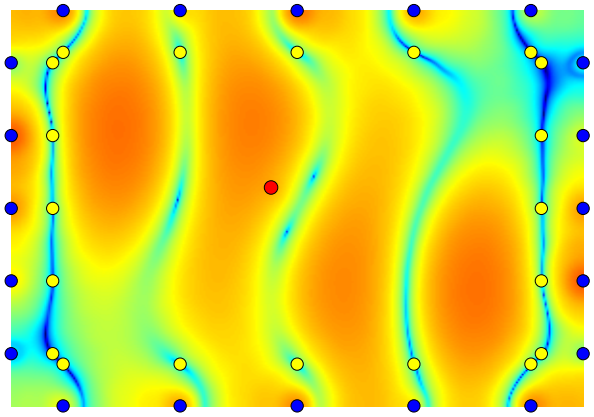

(d) ANC - Regular sensors distribution

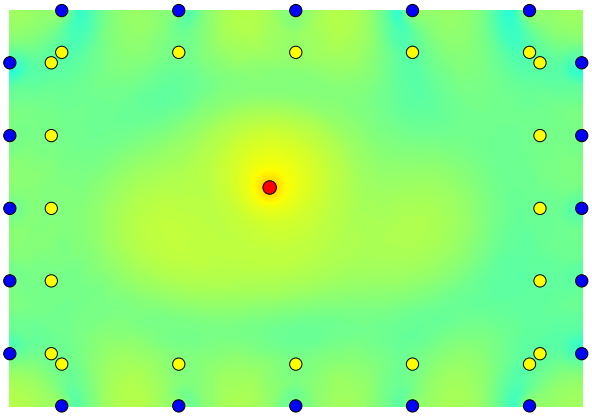

(e) AAS - Regular sensors distribution

Figure 2.1: Sound pressure field comparison between ANC and AAS control strategies. Also two distributions of sensor points are presented. Primary source is represented by the red dot. Blue and yellow dots are secondary sources and sensors respectively.

2.2.3 Different distribution of primary sources

Up to now, the simulations presented consider only one primary source inside the enclosure. This is, of course, a very idealized scenario. Hence, it is important to analyze the behavior of the active absorption system when additional primary sources are included. As before, a rectangular enclosure of dimensions $l_x = 5.5$ and $l_y = 3.8$ is used. A number of I secondary sources that ensures good absorption at these frequencies is used. The

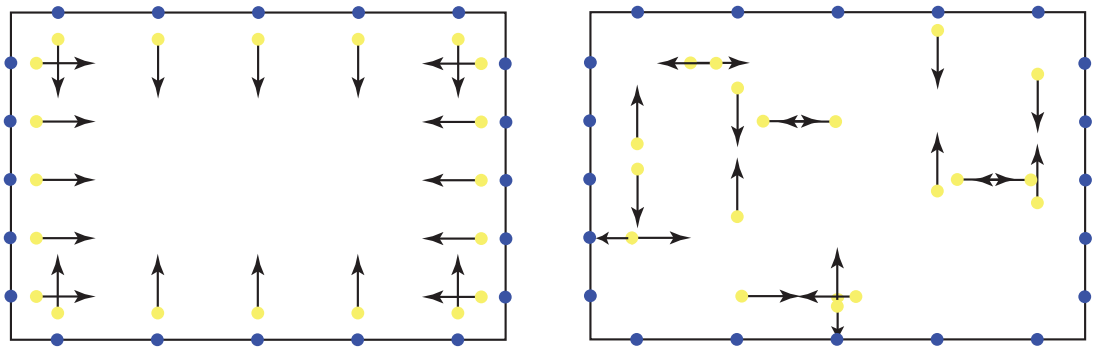

Figure 2.2: Comparison of the sensing direction between *Regular* and *Random* distribution used in the previous AAS simulation (Figure 2.1).

exact criterion to obtain I will be described later on in Section 2.4. Thus, four cases are chosen to simulate

- 2 primary sources at 75 Hz,
- 2 primary sources at 300 Hz,
- 3 primary sources at 300 Hz and
- 28 primary sources at 300 Hz.

In the latter case, the 28 sources are distributed in a squared shape to try to emulate a larger sound source. Figure 2.3 shows the results obtained.

From all the AAS cases, the most important information that can be extracted is that the resulting sound field is the solely product of the interaction of the primary sources with almost no contribution from the reflections of the enclosure. This can be derived by observing for instance the Figure 2.3.d, where the pressure field has the typical distribution of a dipole in phase radiating in free field [30]. This pressure distribution is possible only if the boundaries of the enclosure are highly damped. Figure 2.3.f presents an extension of this same analysis but including an additional source.

As seen, having more than one primary source does not play any role in the efficiency of the active absorption system. But it would be interesting to realize how the system will behave if a larger size source were present in the enclosure, as would be the case with any kind of machinery for instance. A squared shape is chosen since any other distribution will generate an uneven directional pattern and the two latter case already considered that. Figure 2.3.h shows this case. As depicted there, the absorption system is able to successfully damp almost completely all the modes in the enclosure and generate an homogenous pressure distribution. Therefore, it is possible to establish that the efficiency of the active absorption system is completely independent of the primary excitation, and is able to react over it irrespective of the number and shape of sources.

2.3 Sound pressure field within a three-dimensional enclosure

The simplicity of the simulations in two dimensions shown in the previous sections helps to visualize and understand the interaction between the active absorption system and the

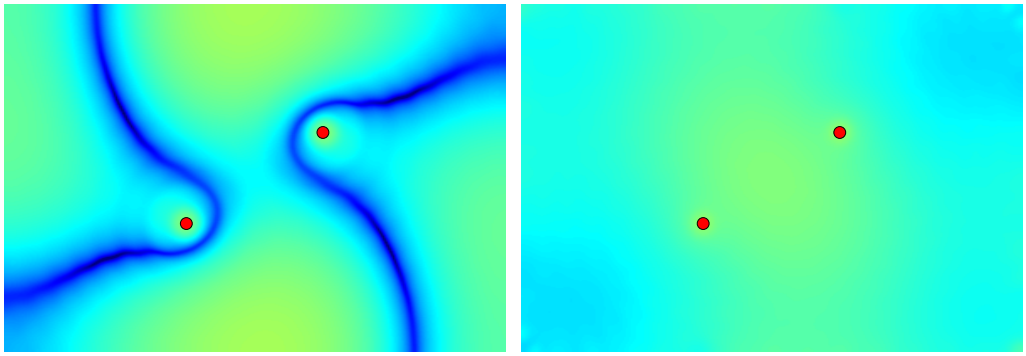

(a) OFF - 2 prim. sources - 75 Hz **(b)** AAS - 2 prim. sources - 75 Hz

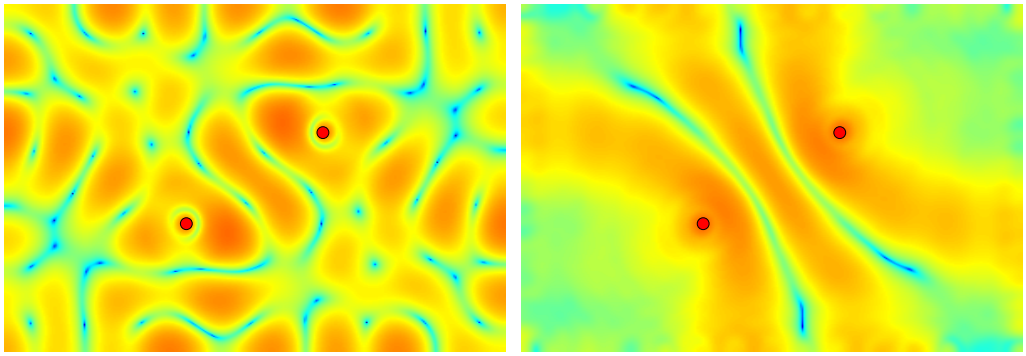

(c) OFF - 2 prim. sources - 300 Hz **(d)** AAS - 2 prim. sources - 300 Hz

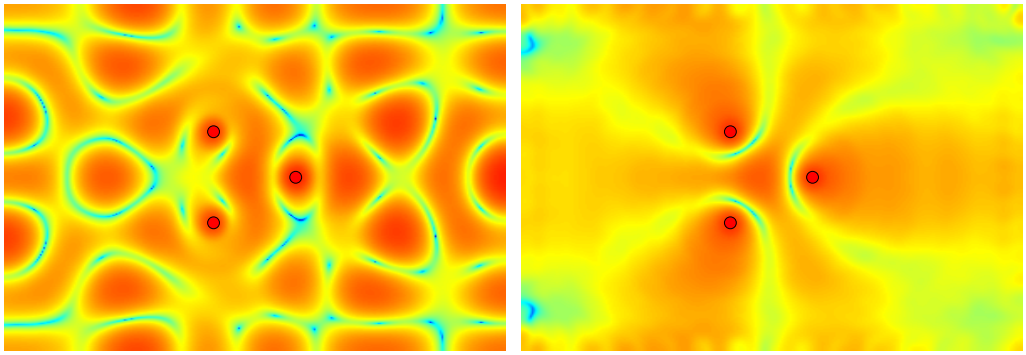

(e) OFF - 3 prim. sources - 300 Hz **(f)** AAS - 3 prim. sources - 300 Hz

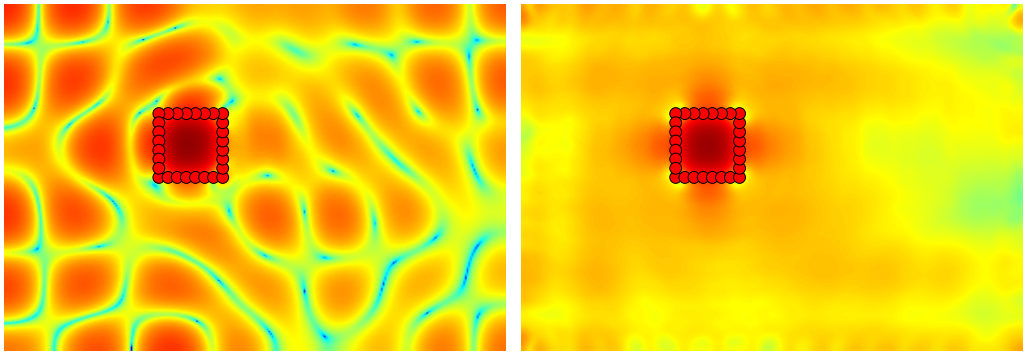

(g) OFF - 28 prim. sources - 300 Hz **(h)** AAS - 28 prim. sources - 300 Hz

Figure 2.3: Sound pressure field comparison between OFF and AAS control methods using different numbers and distributions of primary sources.

resulting sound field, however these two-dimensional fields are far from a real physical

scenario. Therefore it becomes essential to extend these simulations to three-dimensional sound fields.

2.3.1 Control sources over six walls of the enclosure

In these simulations the secondary sources are placed over the walls of a rectangular enclosure in a similar way as shown in Figure 1.10, except that now all of the six walls are covered. In a practical application it does not make much sense to place loudspeakers over the floor, but here it would be interesting to evaluate this particular case since it represents the best possible scenario. For this same reason a large number of secondary sources is used. The following cases use the same number of secondary sources and sensors, i.e. $I = L$. The total number of secondary sources is given by $I = 6\,n^2$, where n is the number of sources per direction of wall, e.g. a wall parallel to the x and z axis with $n = 2$ will have 2 sources in the x direction and 2 sources in the z direction, therefore that wall will have $n^2 = 2^2$ sources and since the enclosure possesses 6 walls $I = 6 \cdot 2^2 = 24$. For the moment an $n = 18$ is used. Later on, in Section 2.4 a criterion is defined to choose a smaller n. In front of each secondary source a sensor is located, both are separated by a small distanc

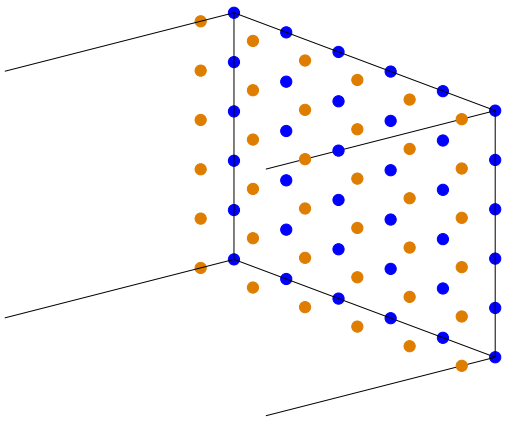

Figure 2.4: Position of a secondary sources array over one wall of the enclosure and its corresponding array of sensors. Sources and sensors correspond to the blue and brown circles respectively. The same configuration is used in every wall.

The primary source is located inside the enclosure, its exact position has no significant importance. Four discrete frequencies are selected for this simulation, 50, 100, 350 and 700 Hz, since they cover the low and middle range of the spectrum. For each of these frequencies, two different conditions are shown, OFF and AAS. Table 2.4 shows the simulated sound pressure field for these cases. Initially, a small room with dimensions $l_x = 5.5$ m, $l_y = 3.8$ m, $l_z = 2.4$ m and 50 m^3 approx. is used. The precise position of the primary source is given by the intersections of the three center planes with black borders.

As expected, the condition OFF in Table 2.4 shows the modes distribution within the enclosure with well defined maxima and minima of pressure. While in the condition AAS, the maxima and minima of pressure appear to be almost entirely damped. But the more important characteristic, as it was already seen in the two-dimensional simulations, is that the pressure decreases with the distance with respect to the primary source in the same way as it would happen with a source radiating in free field. This behavior is the

most clear evidence that the active system is effectively absorbing sound and it is able to cancel almost completely the reflections coming from the walls.

Now, the same calculations are repeated but this time a bigger room of approximately 100 m^3 is used, with dimensions $l_x = 5.5$ m, $l_y = 5.8$ m and $l_z = 3.2$ m. Table 2.5 shows the sound pressure field obtained for this second room. Both conditions, OFF and AAS, present similar behavior respectively with the case depicted in Table 2.4. Condition OFF shows marked differences between maxima and minima of pressure due to the spatial modes distribution, whereas this characteristic changes completely in AAS. Here once again, the sound field tends to become more homogeneous, vanishing the maxima and minima of pressure and only showing a pressure decay with the distance with respect to the source. The comparison between Table 2.4 and 2.5 indicates that a change in the volume, or the modes number, of the room does not affect the efficiency of the active absorption system.

f Hz	OFF	AAS
50	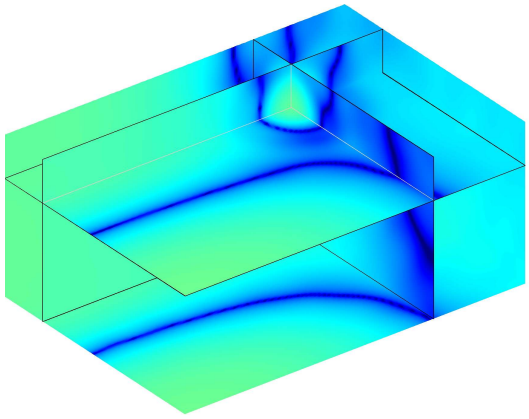	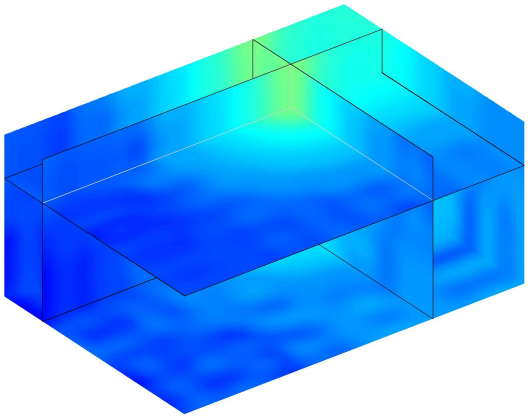
100	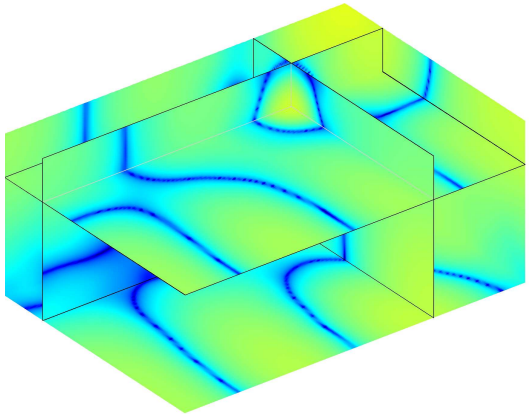	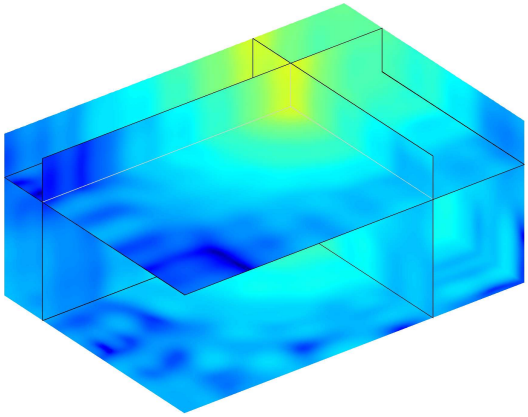
350	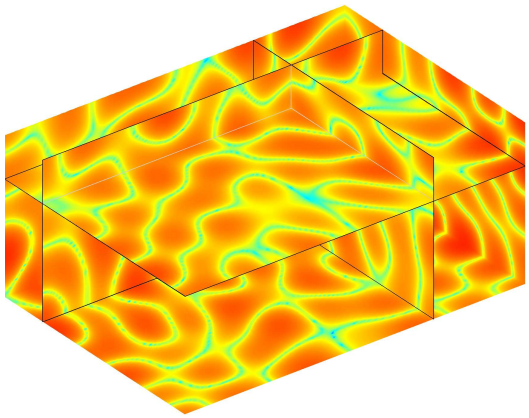	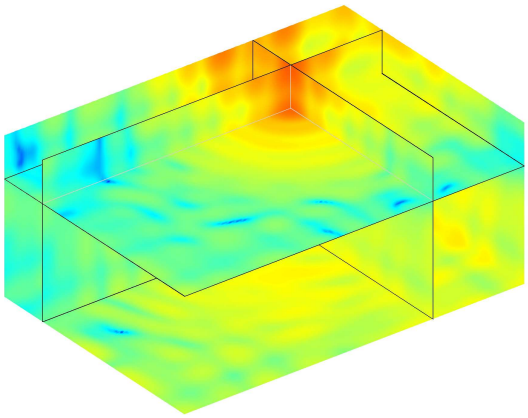
700	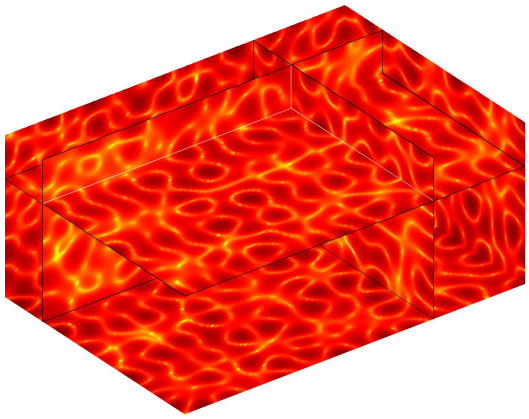	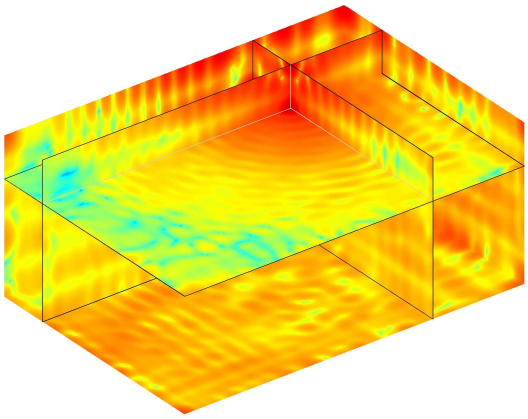

Table 2.4: Simulated sound pressure field using two different conditions: control off (OFF) and active absorption on (AAS). Simulations made for the 'small' room of dimensions $l_x = 5.5$ m, $l_y = 3.8$ m and $l_z = 2.4$ m.

f Hz	OFF	AAS
50	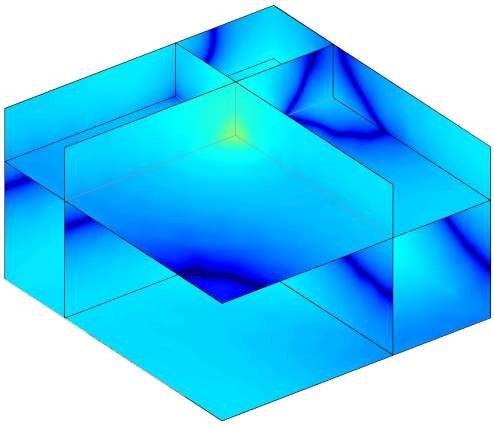	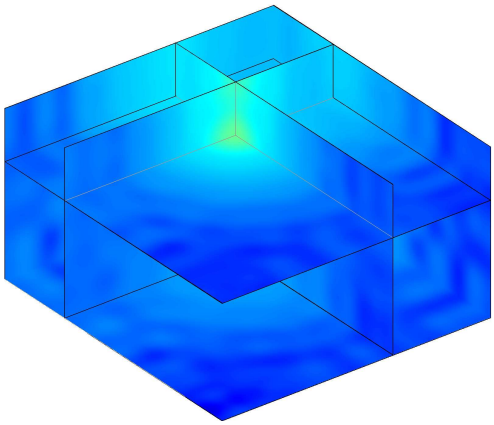
100	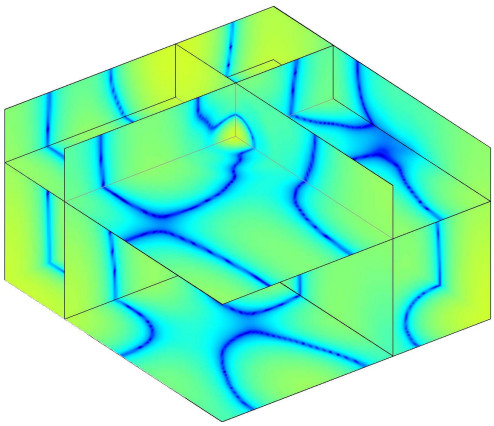	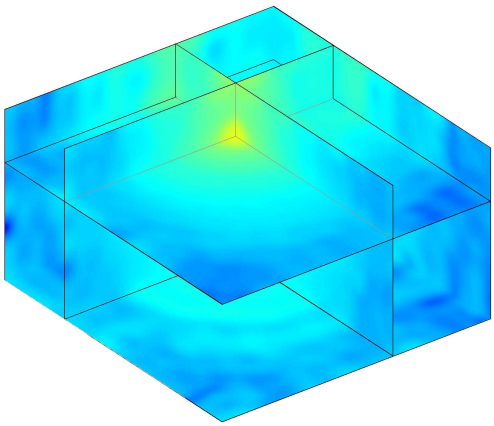
350	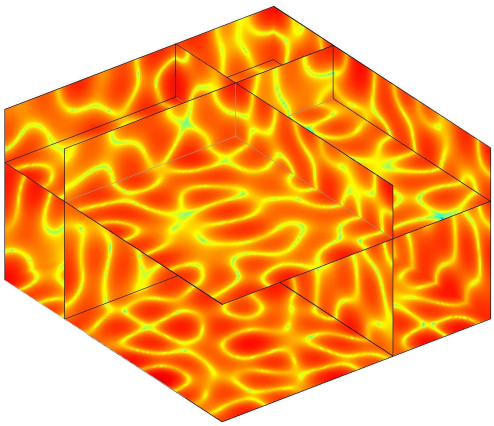	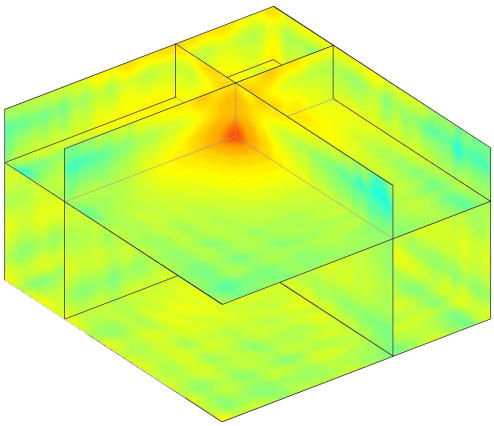
700	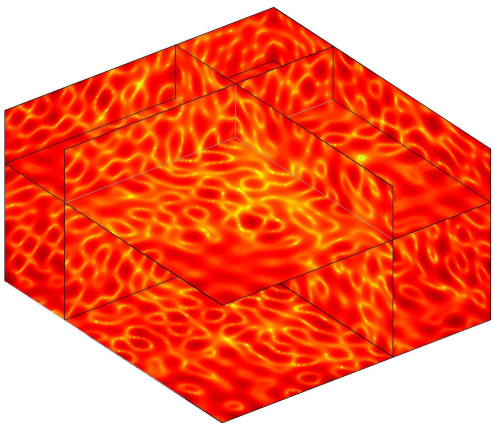	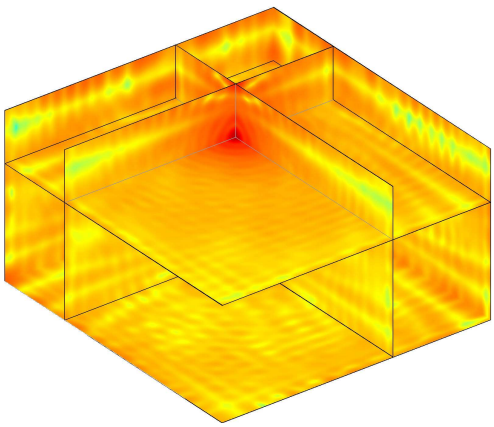

Table 2.5: Simulated sound pressure field using two different conditions: control off and active absorption on. Simulations made for the 'large' room of dimensions $l_x = 5.5$ m, $l_y = 5.8$ m and $l_z = 3.2$ m.

2.3.2 Control sources over only selected walls of the enclosure

In the pressure field simulations presented before, the arrays of secondary sources have been applied over the six walls of the room. The following cases consider different numbers of walls covered with sources. To clarify which walls are covered, each of them is numbered according to Figure 2.5.

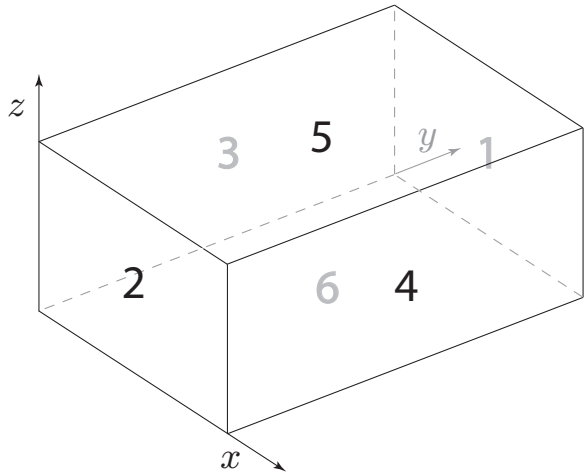

Figure 2.5: Wall numbering.

Hence, three different configurations of AAS are simulated:

- (a) Reflecting floor 6 and the rest of the five walls absorbing,
- (b) Walls 1 - 3 - 6 reflecting and the rest absorbing and
- (c) Parallel walls 3 - 4 absorbing and the rest reflecting.

Table 2.6 summarizes the results. In configuration (a), the sound pressure fields for 50 and 100 Hz are similar to the simulation obtained using six absorbing walls, cf. Table 2.4 condition AAS. A more interesting result arises at 350 and 700 Hz where a pattern of maxima and minima of pressure appears between the primary source and the floor. This pattern is the result of the standing wave generated by the incident wave coming from the primary source and the reflected wave from the rigid floor. The same phenomenon is not easily visible at 50 and 100 Hz due to the large wavelength and the proximity between the source and the floor. Configuration (b) presents the sound field generated by the superposition of the sound coming from the primary source and the reflections from walls 1 - 3 - 6. Although it could seem like a completely random pressure distribution, a slight pattern can be observed at the bottom of the simulation at 700 Hz. The experienced reader will recognize this pattern as a result of the interaction between the primary source and the reflection from the walls 1 and 3. Configuration (c) shows, for all frequencies, a sound field that is composed by modes propagating only in y and z direction. This is expected since the absorption is applied over the walls 3 - 4, i.e. x direction, hence the majority of the modes in this direction are vanished. This effect can be seen specially at 700 Hz where several nodal pressure lines appear parallel to the x axis.

f Hz	a	b	c
50	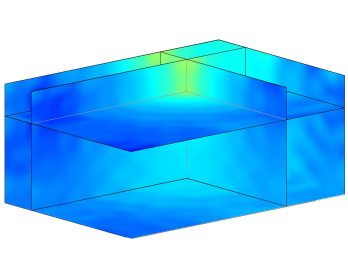	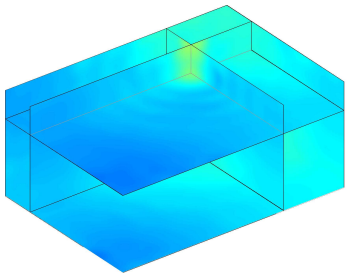	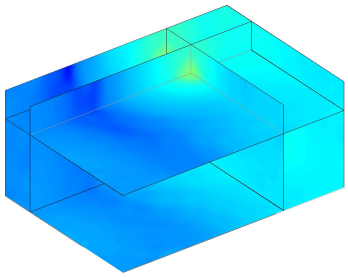
100	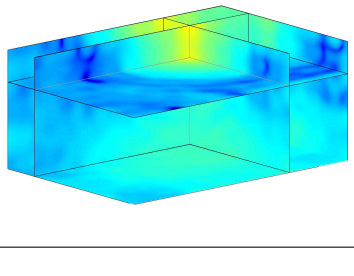	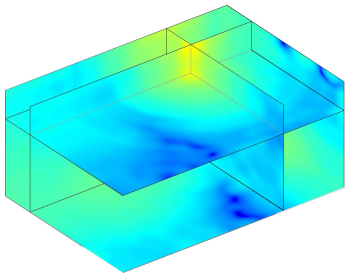	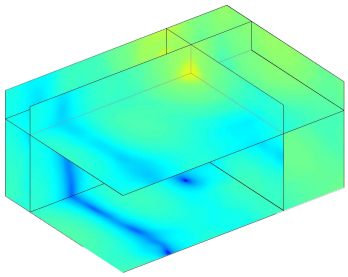
350	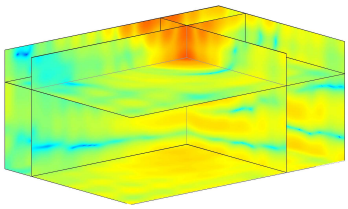	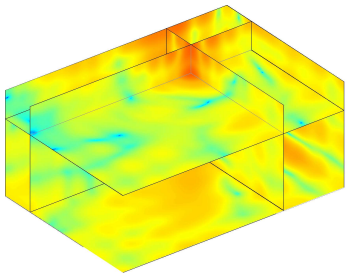	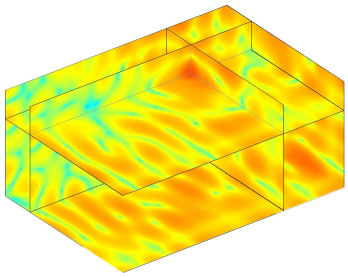
700	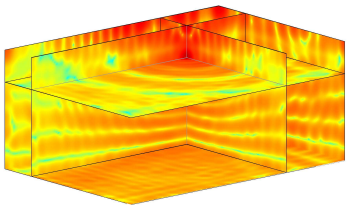	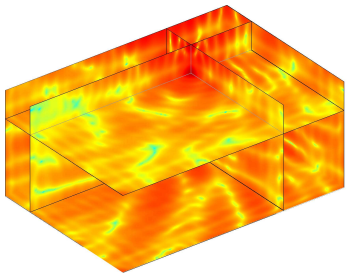	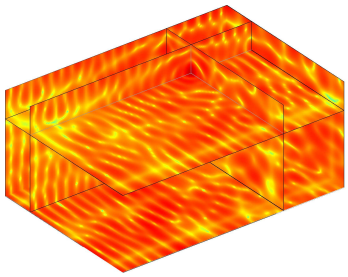

Table 2.6: Simulated sound pressure field using three different configurations of walls with and without secondary sources. Simulations made for the 'small' room of dimensions $l_x = 5.5$ m, $l_y = 3.8$ m and $l_z = 2.4$ m.

2.3.3 Absorption behavior at resonant frequencies

At resonant frequencies, the amount of potential energy present in a room is much larger than in other frequencies. This is true, of course, only if the same excitation level is used for all frequencies. This excess of energy presents no additional effort over a passive absorber, however this is not necessarily true for a real active system.

It must be considered that as higher the excitation of the primary field, the effort of the active system is equally higher to generate the controlling signal. Likewise, for example, the dynamic rage required of input stage is larger too. All this elements must be considered in a real implementation. However, despite all these practical details it is still interesting to observe how the active system will behave under these circumstances. In the following simulations all these practical considerations are obviated.

A simulation of the sound pressure field is made this time choosing a set of low resonant

frequencies of the *Small* room previously used. In this case, the six walls are acting as absorbers. Table 2.7 shows conditions OFF, AAS, frequency and its corresponding mode number.

The results obtained indicate that the active absorption system is able to work at resonant frequencies of the room. Although the energy in these cases is higher, the sound field is driven by fewer degrees of freedom and therefore the control at these frequencies becomes easier. In AAS, all the resonant modes are completely vanished.

2.3.4 Comparison against ANC systems

Although Section 2.2.2 already presented the comparison between AAS and ANC systems acting over a two-dimensional enclosure, this section completes the analysis extending the sound field to a three-dimensional case. Hence, using the *Small* room already defined in Section 2.3, the sound pressure can be computed using ANC according to the cost function J_{ANC} given in equation (1.131). These new simulations, presented in Figure 2.6, can be directly compared with the figures (OFF and AAS) in Table 2.4 since the exact same geometry and sources distribution are used.

Figure 2.6 shows the sound field obtained when the pressure is locally minimized at every sensor position. Here, as in the OFF figures of Table 2.4, it is possible to observe distinct patterns of maxima and minima of pressure. This means that some modes are damped but other modes are amplified and a shift in the spatial distribution of the sound field has occurred. This behavior of shifting of the sound energy to other modes is usually called *control spillover* [19]. Due to this behavior, it can be stated that the ANC system does not behave as an absorbing system, whereas the AAS system does. Although difficult to observe, specially at low frequencies (compare ANC and AAS for 50 Hz and 100 Hz) reflections are still present, as can be appreciated by the 'ripples' of the pressure whereas the AAS system performs noticeably better as it is visible in the 'smooth' sound field distribution.

Since the arrays of sensors are located parallel to every wall of the room, it is possible to observe several nodal planes of pressure that appear in the ANC case. This is visible thanks to a set of lines of low pressure levels near and parallel to the walls. As expected, the nodal planes coincide with the sensors positions.

Mode	f [Hz]	OFF	AAS
010	45.26	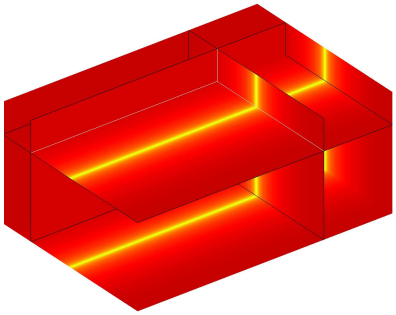	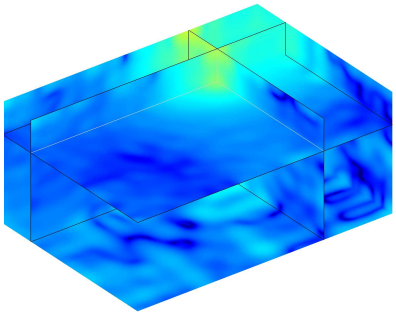
101	78.19	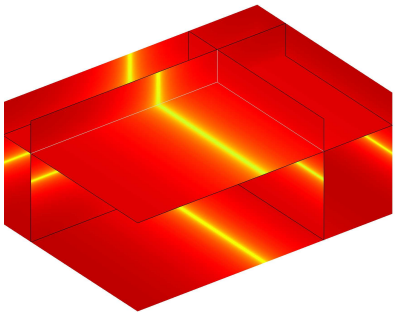	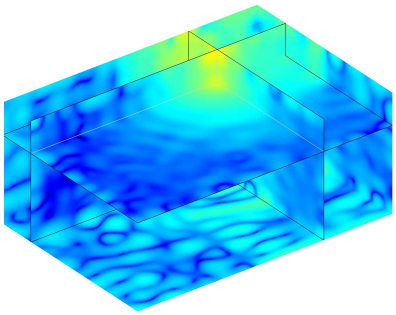
111	90.35	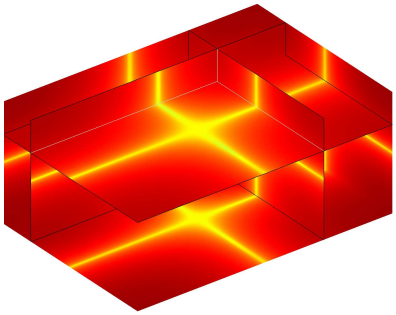	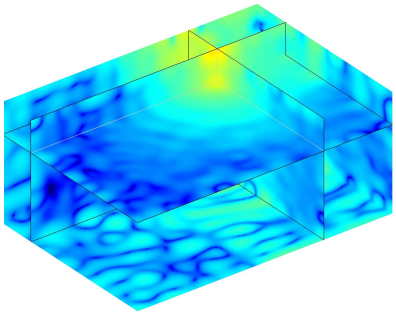
333	271.69	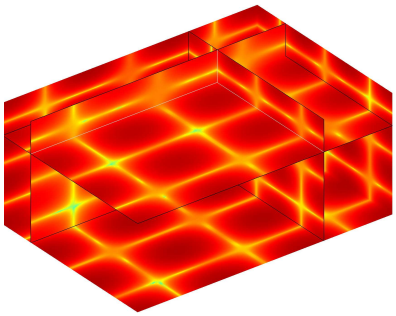	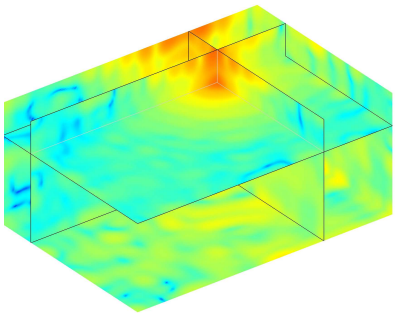
143	282.81	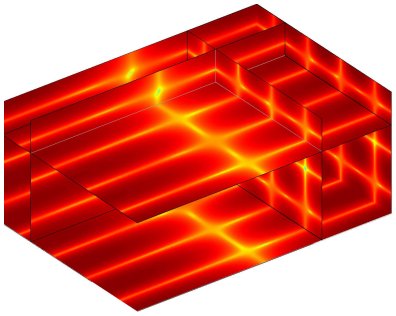	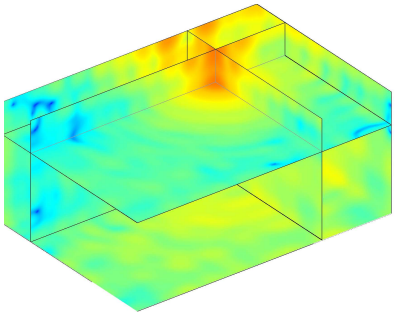

Table 2.7: Comparison of the sound pressure field at resonant frequencies. The precise mode and its frequency are displayed in the left columns.

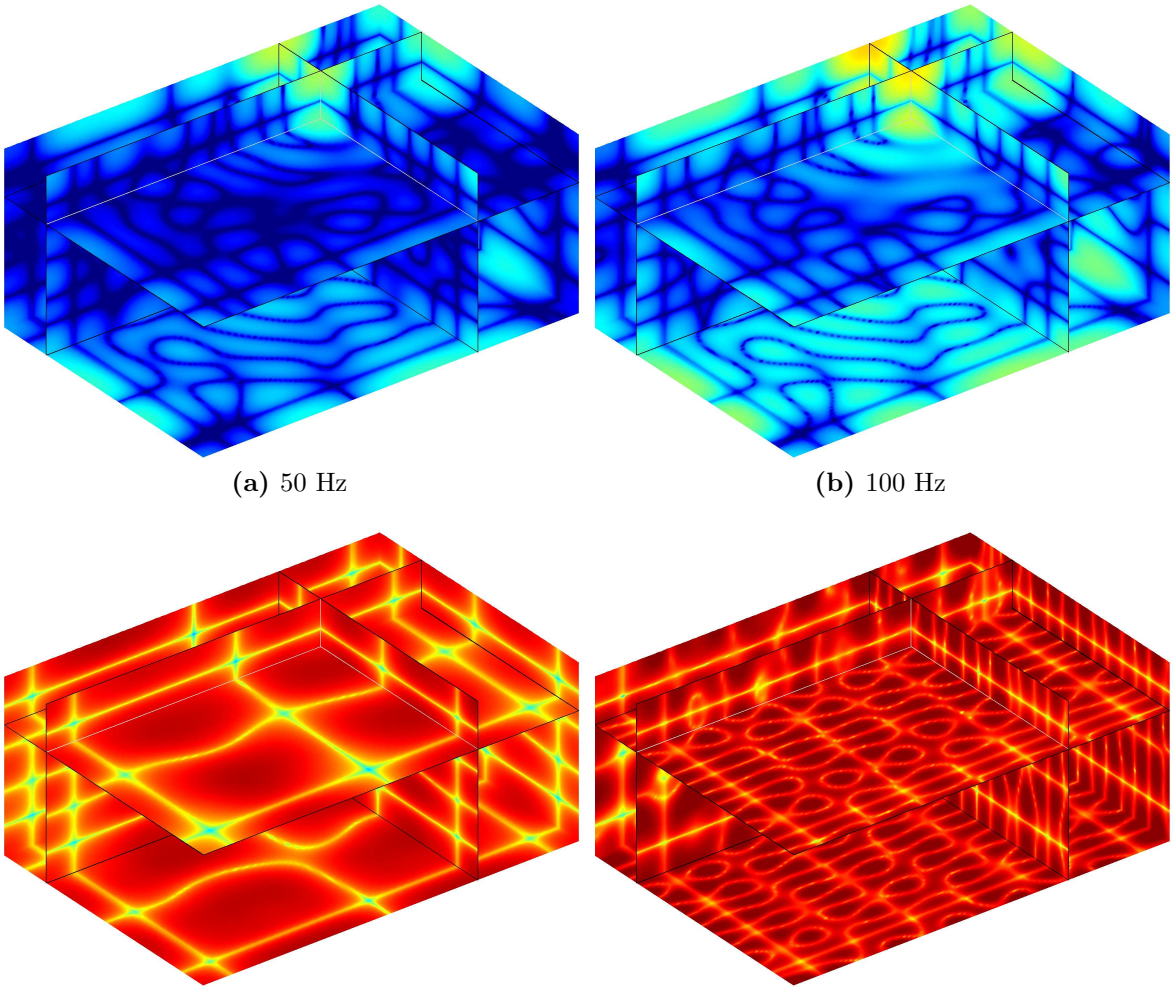

(a) 50 Hz **(b)** 100 Hz

(c) 350 Hz **(d)** 700 Hz

Figure 2.6: Resulting sound pressure field using ANC. Compare against the cases OFF and AAS presented in Table 2.4.

2.4 Absorption coefficient and intensity in front of an array of secondary sources

As described in Section 1.6, an equivalent absorption coefficient α can be associated with an array of secondary sources covering a given area S. Thus, exciting the room with discrete frequencies and increasing the number of sources in the array, several curves of the absorption coefficient can be calculated. The total area S of the array is kept constant while the density of secondary sources is incremented. As explained in Section 1.6, the density of sources in the array can be expressed as a function of the wavelength λ of the excitation signal since it provides more information, additionally, it is equivalent to express this density as *sources per* λ^2 or *sources per* λ for only one direction of the array. As described before in Section 2.3.1, the total number of sources I was defined as $I = 6\,n^2$ for a three-dimensional array, therefore the mentioned density of *sources per* λ can be expressed also as n/λ for a two-dimensional array. As before, it is assumed that the same number of secondary sources and sensors are used, i.e. $I = L$.

Four rooms with volumes of approx. 100, 200, 600 and 1000 m^3 are used in these simulations to also realize the influence of the dimensions of the room over the actively generated absorption coefficient α. Figure 2.8 summarizes all the computed curves. There, it is possible to observe that, for each frequency, as the number of sources per wavelength (n/λ) increases, the absorption coefficient approaches to 1. For low frequencies the density required to achieve an α near 1 is slightly higher than for middle-high frequencies.

An interesting characteristic arises when the density approaches 3 sources per wavelength, all the values of α rapidly increase. This finding gives a valuable rule at design time since it allows to estimate the number of secondary sources required to obtain a high value of the absorption coefficient. Hence, for a given frequency, the election of a source density higher that 3 sources per λ will ensure a high degree of absorption. However, if the density chosen turns to be smaller than 3 sources per λ, it is not possible to predict a precise value of absorption coefficient.

Although at low frequencies the density of sources per wavelength required to obtain a high α seems to be rather large in comparison with the rest of the frequencies, the actual number of sources required is smaller. For an array of sources that covers a constant area S, the number of sources required to satisfy the rule of '3 sources per wavelength' is inversely proportional to the wavelength. To exemplify this consider Figure 2.7.

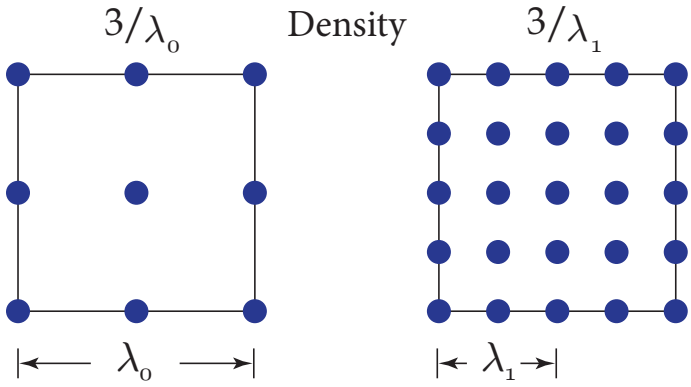

Figure 2.7: Difference in the number of secondary sources required to satisfy the condition of '3 sources per wavelength' as a function of the frequency.

There, both arrays of sources fulfill the condition of 3 sources per wavelength at frequencies f_0 and $f_1 = 2\,f_0$ but they require a completely different number of sources, 9 and 25 respectively. Of course it is possible to reduce the area of the second array to use a smaller number of sources keeping constant the density, however this will have a direct impact over the *total absorption* A (or effective absorbing area [30]) of the room since it is directly proportional to the covering surface S. Recalling that, in a room covered with a number of i absorbing materials, the effective absorbing area A [23] is defined as

$$A = \sum_i \alpha_i \, S_i \,,$$

where for each i-th material, the surface S_i is used as a weighting factor for the absorption coefficient α_i. According to the results presented in Figure 2.8, there are no significant

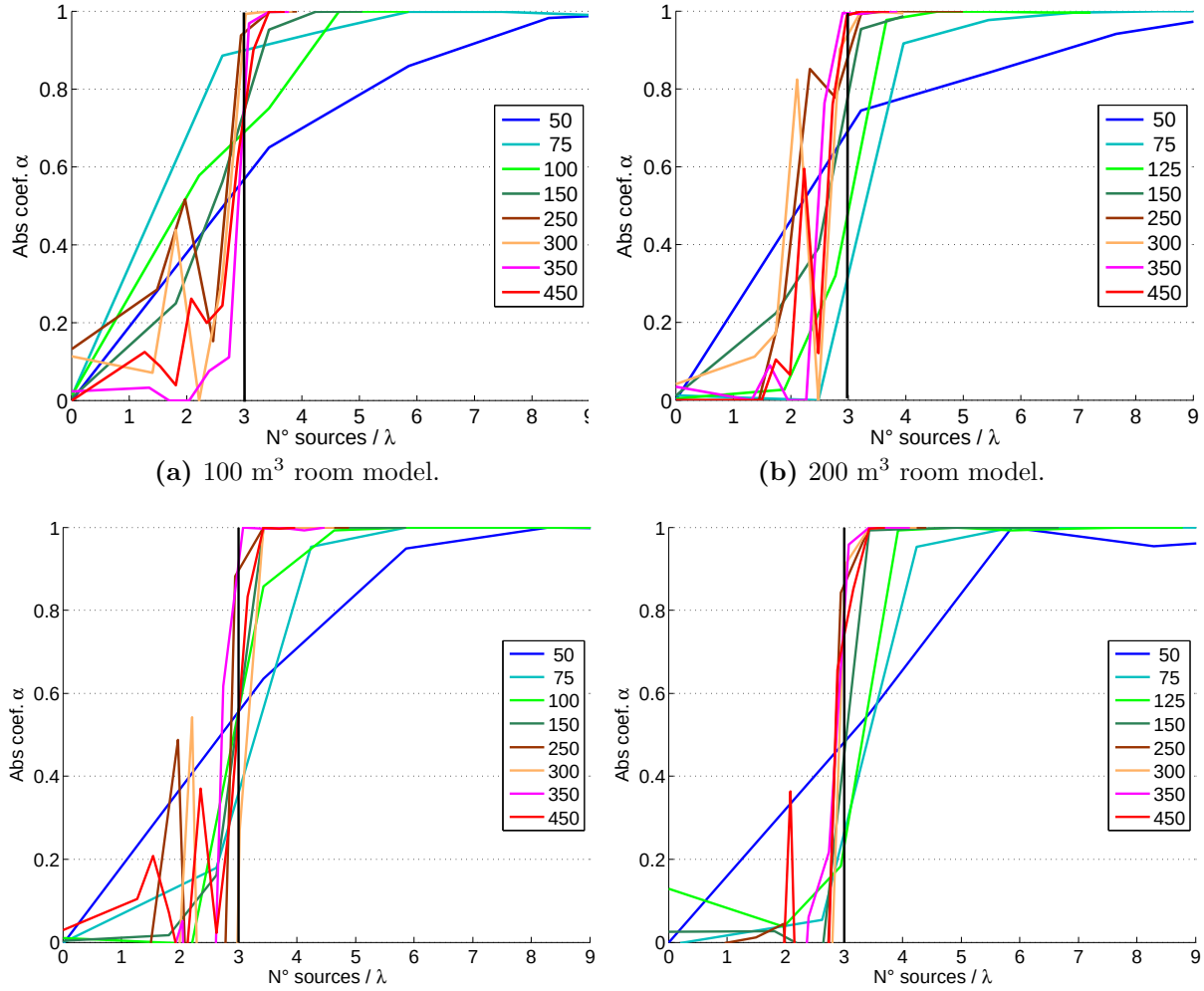

(a) 100 m^3 room model. **(b)** 200 m^3 room model.

(c) 600 m^3 room model. **(d)** 1000 m^3 room model.

Figure 2.8: Absorption coefficient α for different frequencies as a function of the density of secondary sources per wavelength.

differences in the result regarding the room volume. Combining this evidence with the comparison of the sound pressure field within two different rooms presented in Section 2.3.1 it is possible to assume that the volume is not a conditioning parameter for the performance of the active absorption system.

A detailed description on how the density of sources per wavelength is calculated, is given later in Section 2.6.

2.4.1 Different number of secondary sources and sensors

Considering that all the past simulations have been using the same number of secondary sources and sensors in order to analyze the dependency between them and the absorption coefficient, it is necessary to extend the analysis further. This condition of course, $I = L$, isn't rigid and can be freely modified to satisfy implementation requirements. Thus, it is interesting to simulate, for example, a fixed number of sensors L and a variable number of secondary sources I, and vice verse.

The first simulation, shown in Figure 2.9, sets a fixed number of secondary sources $I = n_i^2 = 10^2$. The chosen n_i ensures a density slightly above the criterion of '3 sources per wavelength' introduced in the latter section. n_i fulfills this criterion up to the highest frequency used, i.e. 450 Hz. On the other hand, the number of sensors is defined by $L = n_l^2$ and n_l takes a range from 2 to 10. Thus, the absorption coefficient α is calculated for each frequency. The x-axis is the density of sources per wavelength σ and should not be confused with n_l.

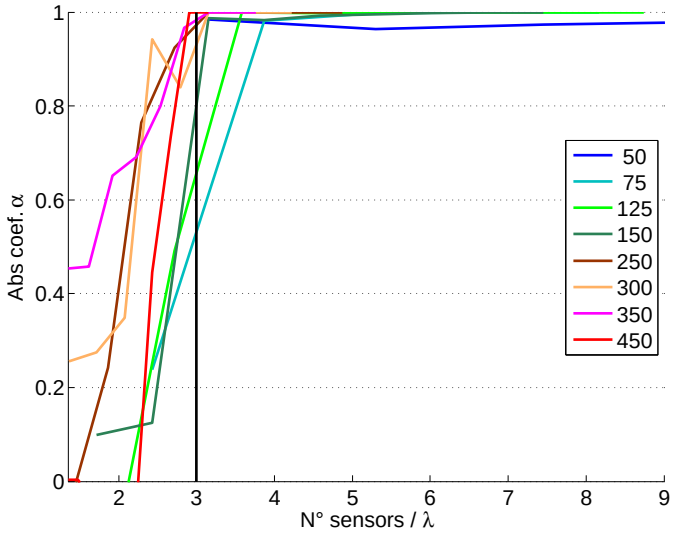

Figure 2.9: Fix number of sources I and a variable density of sensors L per wavelength, where $L \leqslant I$.

In a similar way to the curves depicted in Figure 2.8, the absorption coefficient tends to rapidly increase when the density of sensors reaches the value of 3 sensors per wavelength. At lower frequencies, e.g. 50 or 75 Hz, with just $n_l = 2$ or 3 the density of 3 sensors per wavelength is surpassed.

The opposite case now fixes the number of sensors and increases the number of sources. This time $L = n_l^2 = 10^2$ is chosen for the same reason as before, that ensures a density of at least 3 sensors per wavelength for all the frequencies calculated. Analogously, the number of sources $I = n_i^2$ goes from 2 to 10. Figure 2.10 shows the results.

Once again the absorption coefficient α obtained presents a similar behavior to the previous simulations where α rapidly approaches to 1 when the density of sources reaches 3 sources per wavelength.

These results establish that both elements together, sources and sensors, must satisfy the criterion of 3 elements per wavelength and the fulfillment of only one of them does not necessarily ensure a high value absorption coefficient.

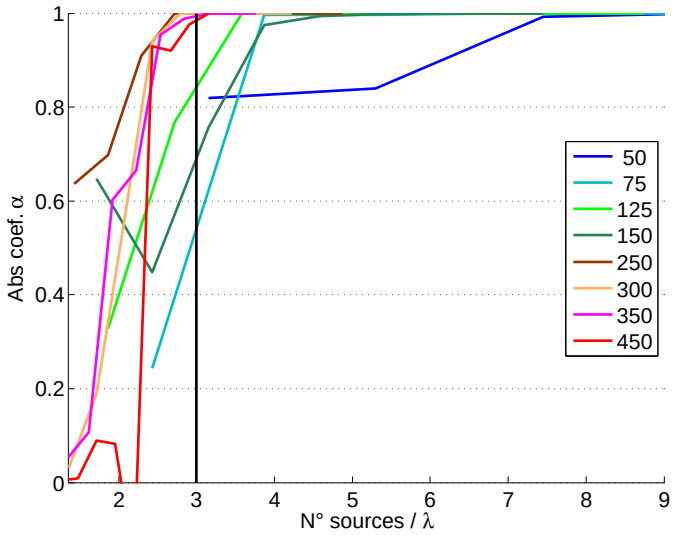

Figure 2.10: Fix number of sensors L and a variable density of sources I per wavelength, where $I \leqslant L$.

2.5 Free field approximation inside a room

It was already proven that the active absorption system is able to generate an absorption coefficient of nearly 1 using an array of secondary sources. As explained in Section 1.6, the absorption coefficient is measured on a plane near the secondary sources that coincide with the sensors position, therefore it can be said that this result is obtain far from the primary source. Thus it will be interesting to evaluate how the active absorption influences the primary source, or in other words, how its radiation is modified by the action of the active absorption.

From the fundamental of acoustics it is known that a point source radiating in free field is defined by

$$p(\vec{\mathbf{r}}) = \frac{p_0}{|\vec{\mathbf{r}} - \vec{\mathbf{r_0}}|}\, e^{-jk|\vec{\mathbf{r}}-\vec{\mathbf{r_0}}|}, \tag{2.2}$$

where the source is located at $\vec{\mathbf{r}} = \vec{\mathbf{r_0}}$ and time dependance is omitted. This equation describes the spherical wave propagation and also the pressure decay of point sources. In more trivial terms it is also the rule used by *acousticians*: "A decay of -6 dB as the distance doubles", which is commonly used to extrapolate the sound pressure level of a source to an arbitrary distance.

In this case, equation (2.2) could be compared with the resulting sound pressure field inside the room, which is the combination of the primary source and the active absorption system. This comparison will provide a clearer view about how the radiation of the primary source is influenced by the active system and will show how close the radiation pattern is to the one described by equation (2.2). However, before making that comparison it is crucial to have a closer look at the sound field generated. For this purpose three planes are taken from the sound pressure field inside the room. These planes are perpendicular to each coordinate axis and they intersect at the source position (x_p, y_p, z_p), which for these simulations was placed slightly off-center of the room. The planes depict contour lines of the sound pressure level. See Figure 2.12, where conditions AAS and OFF are shown together for different frequencies.

When the active absorption system is working, it is possible to notice that the pressure

pattern around the primary source has almost a spherical shape. This is important because it establishes that any direction taken outward the source in terms of sound pressure will have similar behavior.

Thus, this characteristic allows to take an arbitrary direction to plot a pressure profile. A line that results by the intersection between the planes X-Y and X-Z is used since it is one of the longest dimensions of the room. The resulting pressure calculated over this set of points is now compared with the reference sound pressure given by equation (2.2) where it is assumed that $\vec{\mathbf{r_0}} = x_p$. The comparisons are given in Figure 2.11.

The figures show a practically perfect match between both curves. This means that the active absorption system is able to generate almost a free field condition inside the room. These results show the potential of the active absorption system as a tool to generate absorption since it allows to replicate an extremely high absorption condition such as free field but inside a closed and rigid space.

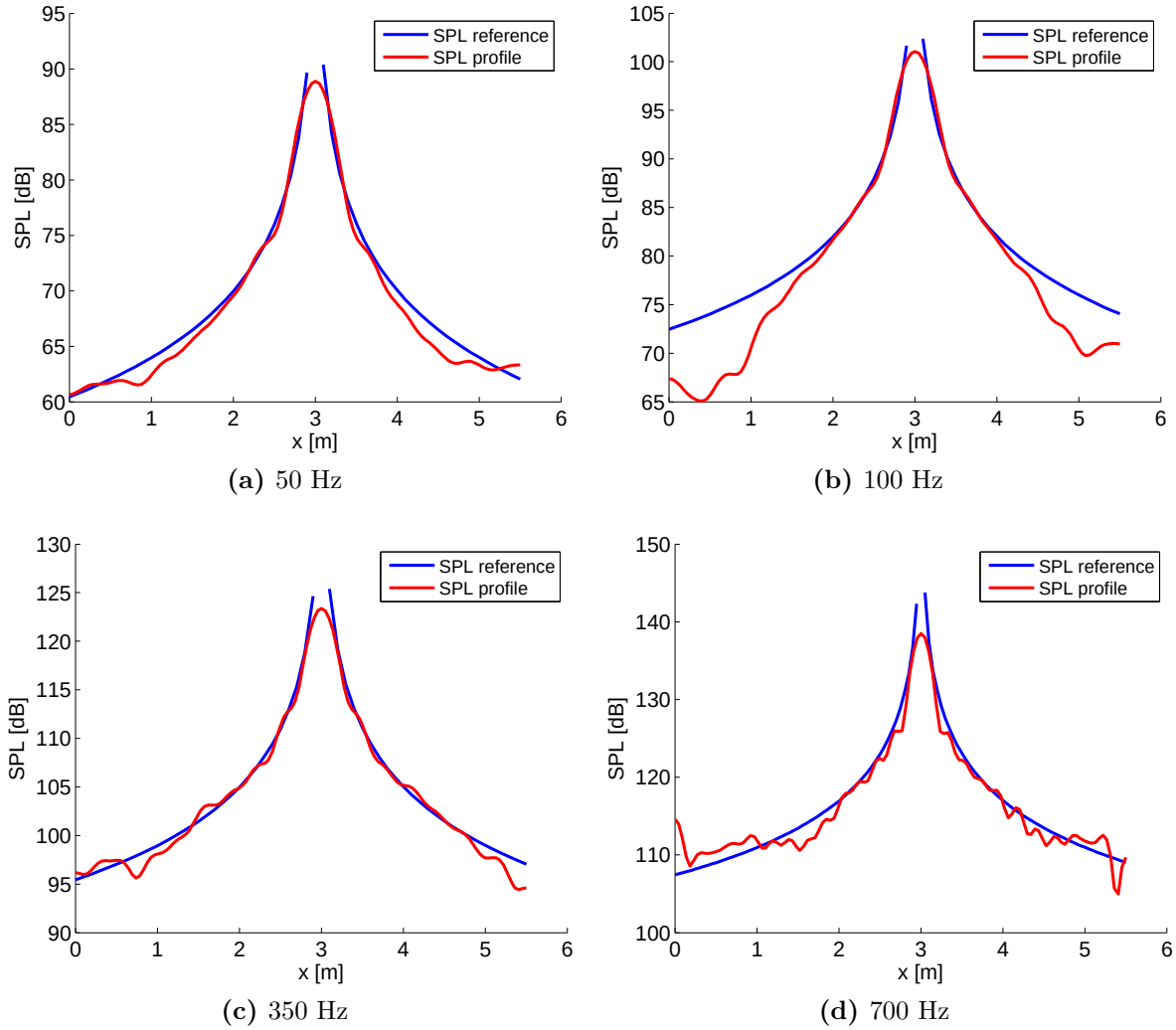

(a) 50 Hz **(b)** 100 Hz

(c) 350 Hz **(d)** 700 Hz

Figure 2.11: Comparison of sound pressure decay between the primary source inside the room and a point source in free field.

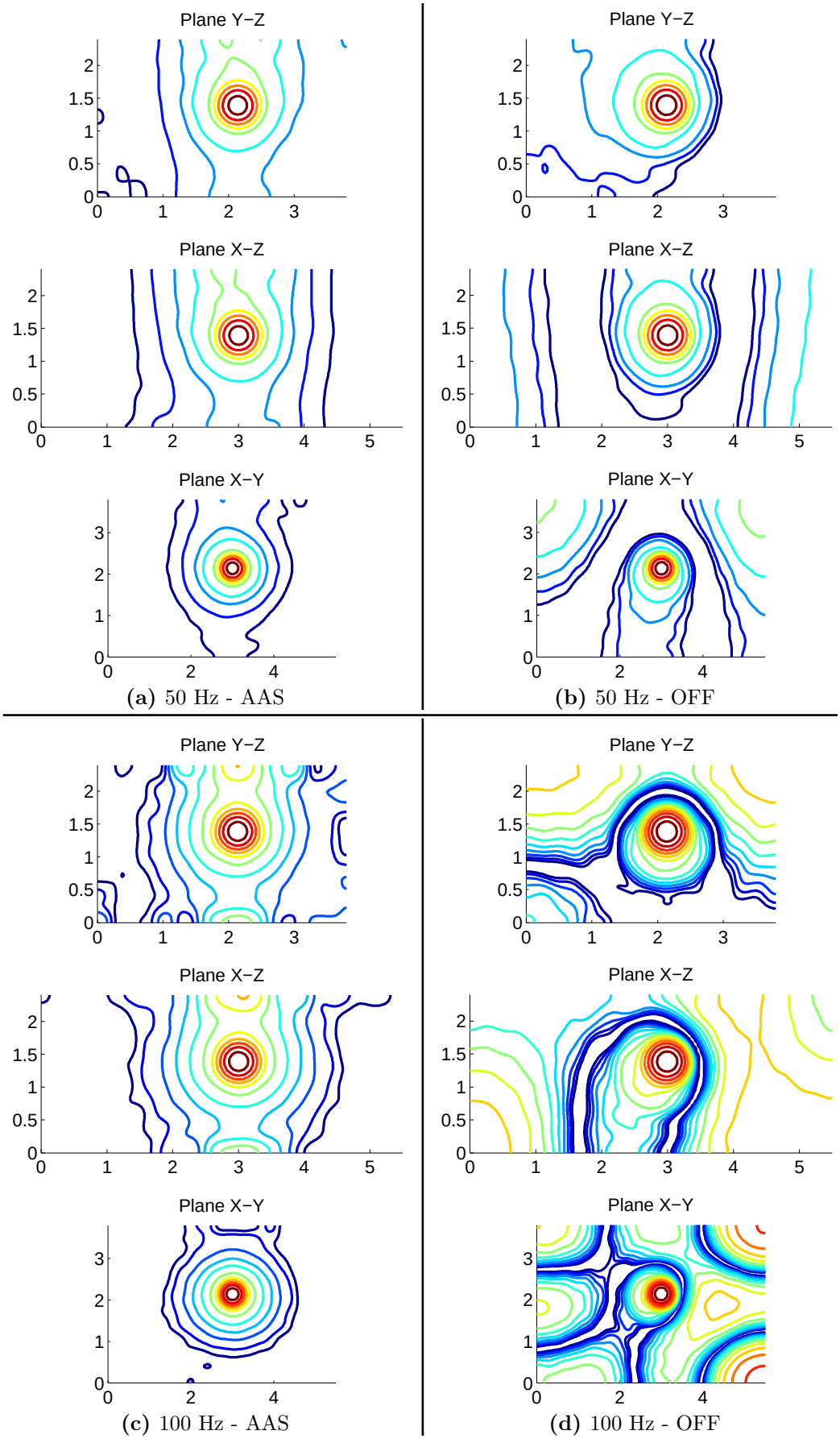

Figure 2.12: Contour lines of sound pressure inside the room at three perpendicular planes intersecting at primary source position.

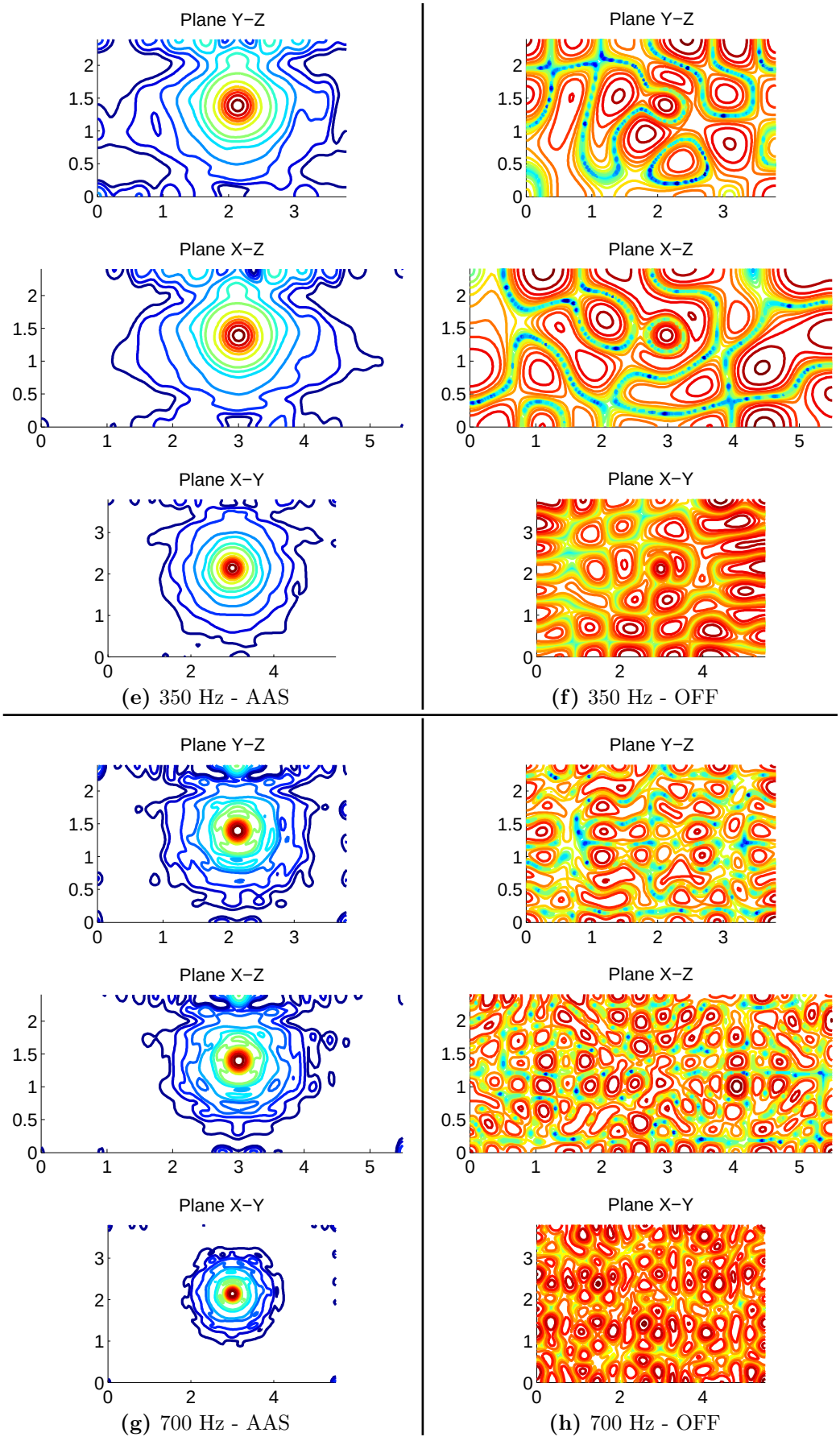

(e) 350 Hz - AAS **(f)** 350 Hz - OFF

(g) 700 Hz - AAS **(h)** 700 Hz - OFF

Figure 2.12: Contour lines of sound pressure inside the room at three perpendicular planes intersecting at primary source position.

2.6 Frequency response within the enclosure

In order to obtain a frequency response, the primary source generates a frequency sweep and the pressure is calculated at one point inside the enclosure. These frequency responses are calculated between two particular positions of source and sensor, and should not be confused with a transfer function. The sound pressure $p(\vec{\mathbf{r}})$ is calculated using the general expression given in equation (1.99).

In these simulations, the frequency response is calculated using different numbers of secondary sources. Two rooms with different volumes are used, a *Small* one with approx. 50 m^3 and a *Large* one with approx. 100 m^3. The exact positions of primary source and sensor are given in Table 2.9. A distribution of secondary sources over each one of the six walls is used in the same way as described at the beginning of Section 2.3. As before, the total number of sources is defined by $I = 6\,n^2$ where n is the number of sources per direction.

Considering the criterion of 3 sources per wavelength as the minimum density of sources to obtain an optimal absorption, this density is not necessarily the same for every wall, in fact as it will be seen next, it is different for each wall. In a room, the length, width and height have different values (l_x, l_y and l_z) although the number of sources per wall n^2 is the same for all walls, this means that for each direction the walls have their own density of sources (σ_x, σ_y and σ_z). Moreover, it is possible to calculate the lowest frequency limit f_{Limit} that ensures a density of 3 sources per wavelength. Certainly each wall has its own f_{Limit} but only the smallest one is considered since it satisfies the criterion for all walls. The distance between two contiguous sources (Δx, Δy and Δz) is given by

$$\Delta x = \frac{l_x}{n-1}, \qquad \Delta y = \frac{l_y}{n-1} \qquad \text{and} \qquad \Delta z = \frac{l_z}{n-1}. \tag{2.3}$$

Thus, the density σ will be defined by

$$\sigma_x = 1 + \frac{\lambda}{\Delta x}, \qquad \sigma_y = 1 + \frac{\lambda}{\Delta y} \qquad \text{and} \qquad \sigma_z = 1 + \frac{\lambda}{\Delta z} \tag{2.4}$$

or

$$\sigma_x = 1 + \frac{c}{f_{\sigma_x}\,\Delta x}, \qquad \sigma_y = 1 + \frac{c}{f_{\sigma_y}\,\Delta y} \qquad \text{and} \qquad \sigma_z = 1 + \frac{c}{f_{\sigma_z}\,\Delta z}, \tag{2.5}$$

where c is the speed of sound. Table 2.8 presents the relationship between n, σ and f_{Limit} for both rooms.

For comparison, the frequency responses are calculated using active absorption (AAS) and active noise control (ANC). Figures 2.13 - 2.14 show the results. Different values of n are presented for both control methods. In both AAS figures (2.13.a and 2.14.a), it is possible to observe that as the number of sources increases, the resonances of the room are more damped, i.e. the spectra tend to become flatter. This effect can be considered as another important evidence to validate the absorption capability of the active system. The modification of the spectrum corroborates that the active absorption system is not only changing the radiation pattern, as seen in the sound pressure field simulated before, but it is generating a real damping of the modes.

Irrespective of the frequency limit f_{Limit}, it is still interesting to observe the frequency response as a function of the number of sources above this point. Comparing f_{Limit} with

Small volume room			*Large* volume room		
$l_x = 5.5,\ l_y = 3.8,\ l_z = 2.4$ [m]			$l_x = 5.5,\ l_y = 5.8,\ l_z = 3.2$ [m]		
n	σ_{xyz}	f_{Limit} [Hz]	n	σ_{xyz}	f_{Limit} [Hz]
2	$\sigma_x = 3.02$ $\sigma_y = 3.92$ $\sigma_z = 5.62$	$f_{\sigma_x} = 31$	2	$\sigma_x = 3.16$ $\sigma_y = 3.05$ $\sigma_z = 4.70$	$f_{\sigma_y} = 29$
4	$\sigma_x = 3.02$ $\sigma_y = 3.92$ $\sigma_z = 5.62$	$f_{\sigma_x} = 93$	4	$\sigma_x = 3.13$ $\sigma_y = 3.02$ $\sigma_z = 4.66$	$f_{\sigma_y} = 88$
6	$\sigma_x = 3.00$ $\sigma_y = 3.90$ $\sigma_z = 5.59$	$f_{\sigma_x} = 156$	6	$\sigma_x = 3.11$ $\sigma_y = 3.00$ $\sigma_z = 4.63$	$f_{\sigma_y} = 148$

Table 2.8: Density of sources per wavelength σ_{xyz} for each dimension and the frequency limit f_{Limit} for the smallest σ, all this as a dependency of the number of sources per direction n.

	Small room	*Large* room
Primary source	(4.5, 1.9, 1.2)	(4.5, 2.9, 1.6)
Sensor	(0.5, 1.9, 1.2)	(0.5, 2.9, 1.6)

Table 2.9: Coordinates (x_0, y_0, z_0) [m] used for positioning.

the Figures 2.13.a and 2.14.a, it is possible to notice a higher damping in the region below each corresponding f_{Limit}. This fact reaffirms that, having a density equal or higher than 3 sources per wavelength of secondary sources, greatly improves the modes damping and consequently the sound absorption. However it must also be noticed that for frequencies above f_{Limit} the responses also present a significant degree of damping. This means that f_{Limit} is not a strict frontier for the absorption.

In contrast to this, the ANC method shown in Figure 2.13.b and 2.14.b generates a completely different frequency response. In these cases, the modes do not present a clear damping, there are still large differences in the pressure levels and there is only a shifting of the minima and maxima of pressure. It is worth to mention that aside of the different shape in the curves of frequency response, a clear further reduction in the sound pressure level occurs at low frequencies as the number of sources increases. This could be considered as an undesired effect if absorption is the objective since also sound cancellation is taking place, and this could negatively affect the perception of the primary source. Moreover, this frequency shift of the resonances could be perceived as a distortion of the primary source.

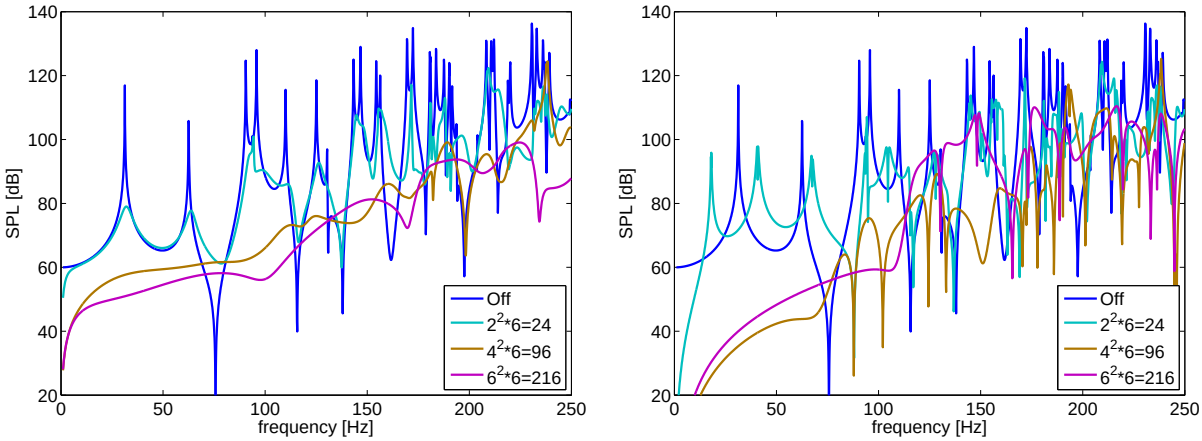

(a) AAS **(b)** ANC

Figure 2.13: Frequency response obtained with two different control criteria using the 'small' room.

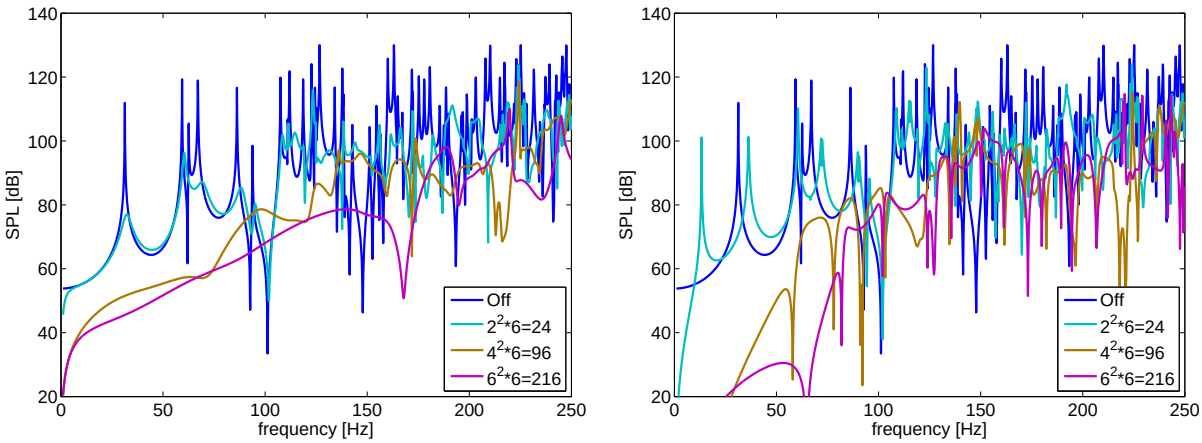

(a) AAS **(b)** ANC

Figure 2.14: Frequency response obtained with two different control criteria using the 'large' room.

2.7 Acoustic potential energy

The analysis of the potential energy provides an insight of the global behavior of the sound field within the enclosure since it integrates the pressure over the whole volume. This global parameter quantifies any change introduced by the active system, whether the energy increases or reduces. This analysis, of course, is valid when a stationary condition has been reached and after any transient variation of the sound field has ended. The potential energy E_p is calculated according to equation (1.143) for different numbers of n. The dimensions of the room used in these simulations are $l_x = 5.1$, $l_y = 4.1$ and $l_z = 3.04$. The primary source is located at $l_x = 1.51$, $l_y = 0.81$ and $l_z = 0.91$. Four different arrays of secondary sources are used, they cover 6, 5, 3 and 2 walls of the enclosure. The latter three configurations (5, 3 and 2) are the same as defined in Section 2.3.2, where cases (a), (b) and (c) are shown in Figures 2.15, 2.17 and 2.18 respectively.

Considering the number of sources used, it is possible to calculate the frequency limit f_{Limit} that defines the lowest frequency where the criterion of 3 sources per wavelength is fulfilled. In this way f_{Limit} serves as reference to compare the performance of E_p below and above this point. Thus, Table 2.10 presents the number of sources per direction n used and its corresponding f_{Limit}.

n	f_{Limit} [Hz]
2	33
4	101
6	168
8	236
10	303
15	472

Table 2.10: Relationship between the number of secondary sources per direction n and the frequency limit where the criterion of 3 sources per wavelength is fulfilled.

It is possible to observe in every simulated case (comparing Table 2.10 and Figures 2.15 - 2.18) that the region near and below f_{Limit} presents significant reduction of E_p. However, far above this point, the E_p shows no clear minimization. These examples emphasize the importance of the density of sources to generate adequate absorption at the desired frequency range.

Among these simulations case (b) (Figure 2.17), where three contiguous walls are absorbing and its three counterparts reflecting, presents an interesting result. Unlike the other cases there is no substantial increment in the E_p above f_{Limit} like the peaks present specially at the highest frequencies. One possible explanation for this phenomenon is that there are no parallel walls with secondary sources. This particular arrangement of sources maybe avoids a face to face interaction of secondary source above f_{Limit} and consequently reduces the peaks in E_p. Although this seems to be a reasonable idea there is not enough evidence to corroborate or dismiss this.

In a similar way as in the simulations of frequency response of the latter section, the energy density tends to reduce its magnitude and become flatter as n increases. Although this is a common pattern for all four simulations, an extreme case of this behavior can

be observed in Figure 2.15 for $n = 15$, where only a smooth line of E_p remains after the action of the absorption system.

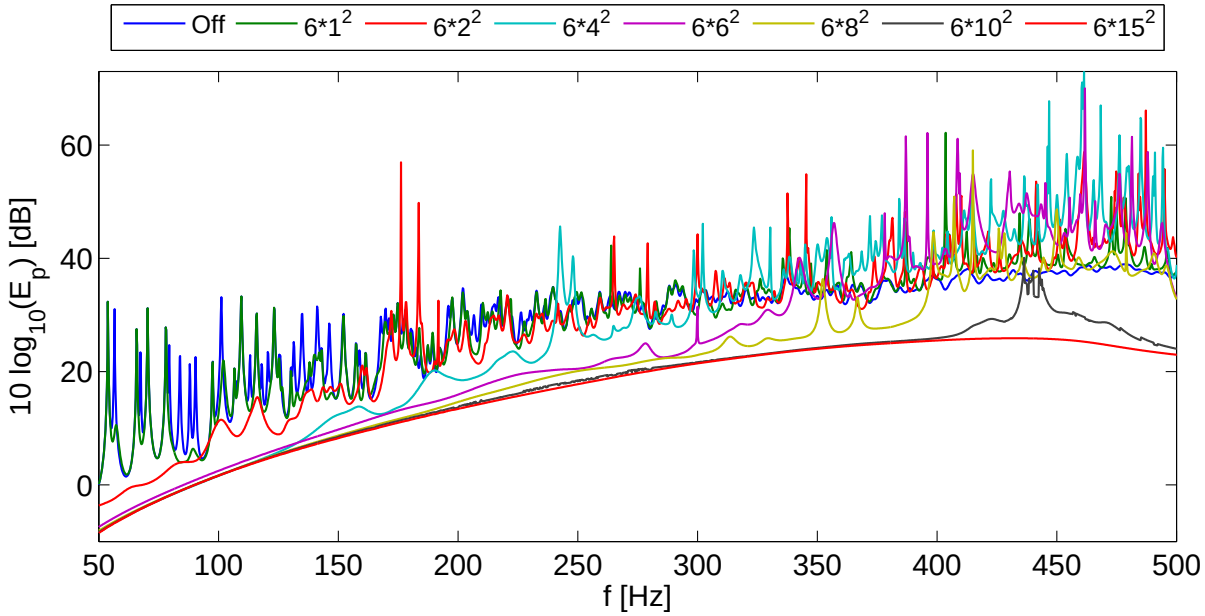

Figure 2.15: Curves of potential energy for a different number of n over 6 walls of the enclosure.

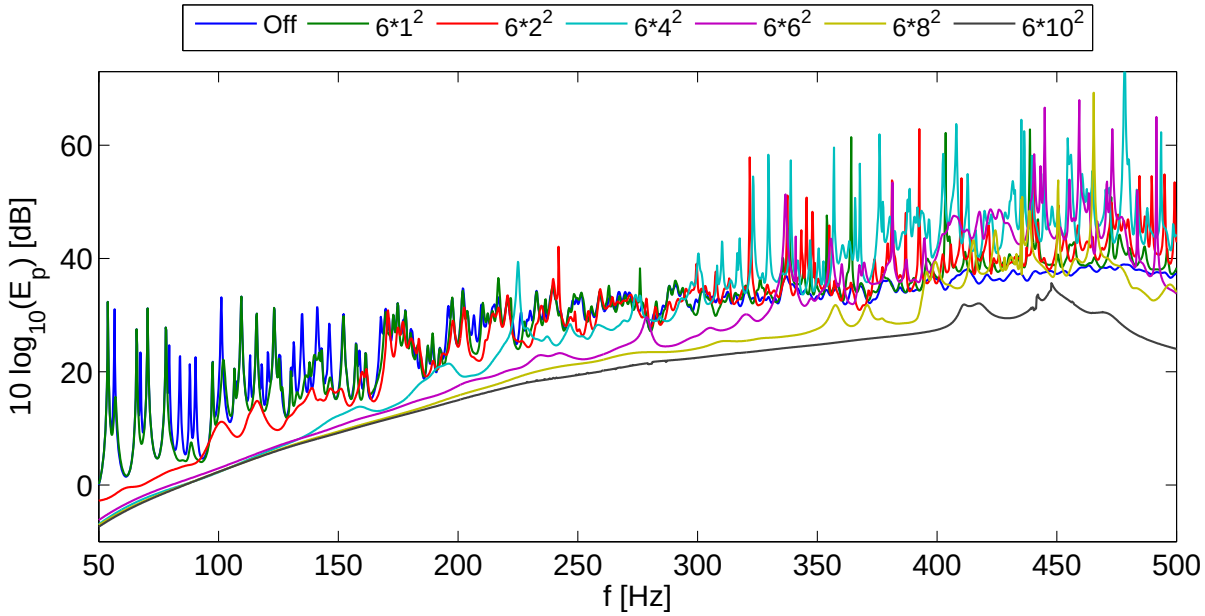

Figure 2.16: Curves of potential energy for a different number of n over 5 walls of the enclosure.

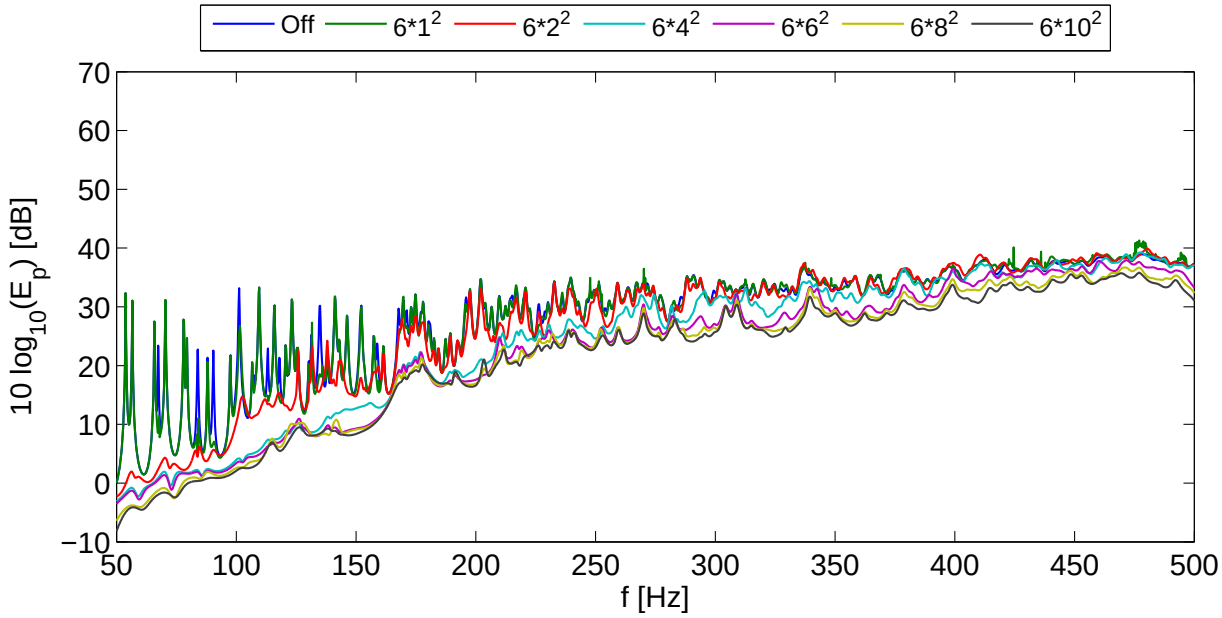

Figure 2.17: Curves of potential energy for a different number of n over 3 walls of the enclosure.

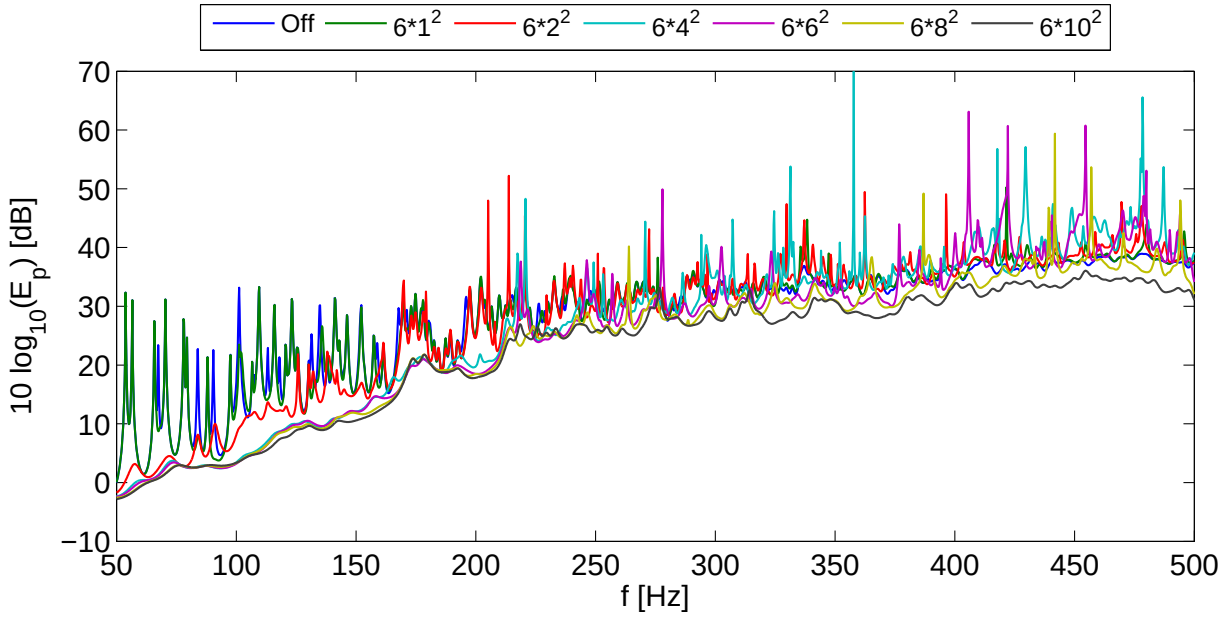

Figure 2.18: Curves of potential energy for a different number of n over 2 walls of the enclosure.

2.8 Direct control of the absorption coefficient α

The general cost function J that controls the active absorption system was already defined in Chapter 1, more specifically J_{x_p} in equation (1.105) for unidirectional control, J_x in (1.129) for one-dimensional control and finally J in (1.130) for three-dimensional control. These equations define the complete minimization of the reflected part of the sound pressure p_r. This minimization, under ideal conditions of enough number of sources and sensors, is always able to generate an absorption condition equivalent to an absorption coefficient of $\alpha \approx 1$, as shown in Section 2.4. This is certainly a remarkable result, however there are some occasions where the objective is to achieve smaller values of α. For those cases the cost function must be extended a step further. To be able to obtain a specific value of absorption coefficient it is now necessary to incorporate the incident part of the sound field p_i and the desired reflection coefficient r that the active system will try to reproduce.

From the control point of view, the active absorption system is able to generate a certain value of α, which is of course proportional to a certain reflection coefficient r. Hence, it is valid to define a new cost function J_α that includes r and p_i. Thus, this new cost function can be written as

$$J_\alpha = \sum_{\ell=1}^{L} \Big| r\, p_i(\vec{\mathbf{r}}_\ell) - p_r(\vec{\mathbf{r}}_\ell) \Big|^2, \tag{2.6}$$

where, as always, $\ell = 1, 2, 3, ..., L$ represents each individual observation point and $\vec{\mathbf{r}}_\ell$ its corresponding position. The new J_α fully agrees with the previously defined cost functions (1.105), (1.129) and (1.130), where $\alpha \approx 1$ was the target and implied $r = 0$. Consequently only p_r remains in the equation producing a minimization only of the reflected part of the sound pressure. However, the inclusion of r into this new cost function J_α allows to arbitrarily define a target value of absorption coefficient. Any value of r different than zero will generate a linear combination of both parts of the pressure (p_i, p_r) and the minimization will act over this quantity.

According to equation (1.7), p_i can be rewritten in matrix form following the same development described in Section 1.4.2 where

$$p_i(\vec{\mathbf{r}}_\ell) = \frac{1}{2}\Big[p(\vec{\mathbf{r}}_\ell) + \varrho\, c\, u_x(\vec{\mathbf{r}}_\ell) \Big], \tag{2.7}$$

thus

$$p_i(\vec{\mathbf{r}}_\ell) = \sum_{i=0}^{I} \beta_i \sum_{pqr}^{\infty} g_{pqr}^{(i)}\ \widetilde{\Phi}_{pqr}(\vec{\mathbf{r}}_\ell), \tag{2.8}$$

and $\widetilde{\Phi}_{pqr}(\vec{\mathbf{r}}_\ell)$ is defined as

$$\widetilde{\Phi}_{pqr}(\vec{\mathbf{r}}_\ell) = \frac{1}{2}\left(\Psi_{pqr}(\vec{\mathbf{r}}_\ell) + \frac{j}{k}\Psi_{pqr}^{S}(\vec{\mathbf{r}}_\ell) \right). \tag{2.9}$$

The only difference between $\widetilde{\Phi}_{pqr}$ and Φ_{pqr} of equation (1.111) is the change in the sign in front of Ψ_{pqr}^{S}. Thus, the matrix version of p_i at the observation point ℓ is given by

$$p_i(\vec{\mathbf{r}}_\ell) = \boldsymbol{\beta}^T \mathbf{G}^T \widetilde{\boldsymbol{\Phi}}_\ell \tag{2.10}$$

where

$$\widetilde{\mathbf{\Phi}}_\ell = \frac{1}{2}\begin{bmatrix} 1 \\ \Psi_{001}(\vec{\mathbf{r}}_\ell) + \frac{j}{k}\Psi^S_{001}(\vec{\mathbf{r}}_\ell) \\ \Psi_{002}(\vec{\mathbf{r}}_\ell) + \frac{j}{k}\Psi^S_{002}(\vec{\mathbf{r}}_\ell) \\ \vdots \\ \Psi_{PQR}(\vec{\mathbf{r}}_\ell) + \frac{j}{k}\Psi^S_{PQR}(\vec{\mathbf{r}}_\ell) \end{bmatrix} \tag{2.11}$$

and $\mathbf{G}$ was already defined in 1.119. For a number of $\ell = L$ observation points p_i becomes

$$\mathbf{p_i} = \begin{bmatrix} p_i(\vec{\mathbf{r}}_1) \\ p_i(\vec{\mathbf{r}}_2) \\ \vdots \\ p_i(\vec{\mathbf{r}}_L) \end{bmatrix} = \begin{bmatrix} \widetilde{\mathbf{\Phi}}_1^T \\ \widetilde{\mathbf{\Phi}}_2^T \\ \vdots \\ \widetilde{\mathbf{\Phi}}_L^T \end{bmatrix} \cdot \mathbf{G}\,\boldsymbol{\beta}. \tag{2.12}$$

As described in (1.120), the matrix form of the reflected component of the sound pressure can be written as

$$\mathbf{p_r} = \begin{bmatrix} p_r(\vec{\mathbf{r}}_1) \\ p_r(\vec{\mathbf{r}}_2) \\ \vdots \\ p_r(\vec{\mathbf{r}}_L) \end{bmatrix} = \begin{bmatrix} \mathbf{\Phi}_1^T \\ \mathbf{\Phi}_2^T \\ \vdots \\ \mathbf{\Phi}_L^T \end{bmatrix} \cdot \mathbf{G}\,\boldsymbol{\beta}.$$

Combining (1.120) and (2.12) it is possible to write the content of J_α as

$$\begin{aligned} r\,\mathbf{p_i} - \mathbf{p_r} &= r \begin{bmatrix} p_i(\vec{\mathbf{r}}_1) \\ p_i(\vec{\mathbf{r}}_2) \\ \vdots \\ p_i(\vec{\mathbf{r}}_L) \end{bmatrix} - \begin{bmatrix} p_r(\vec{\mathbf{r}}_1) \\ p_r(\vec{\mathbf{r}}_2) \\ \vdots \\ p_r(\vec{\mathbf{r}}_L) \end{bmatrix} \\ &= r \begin{bmatrix} \widetilde{\mathbf{\Phi}}_1^T \\ \widetilde{\mathbf{\Phi}}_2^T \\ \vdots \\ \widetilde{\mathbf{\Phi}}_L^T \end{bmatrix} \mathbf{G}\,\boldsymbol{\beta} - \begin{bmatrix} \mathbf{\Phi}_1^T \\ \mathbf{\Phi}_2^T \\ \vdots \\ \mathbf{\Phi}_L^T \end{bmatrix} \mathbf{G}\,\boldsymbol{\beta} \\ &= \mathbf{\Lambda}\,\mathbf{G}\,\boldsymbol{\beta}, \end{aligned} \tag{2.13}$$

where

$$\mathbf{\Lambda} = \begin{bmatrix} \Lambda_1 \\ \Lambda_2 \\ \vdots \\ \Lambda_L \end{bmatrix} = r \begin{bmatrix} \widetilde{\mathbf{\Phi}}_1^T \\ \widetilde{\mathbf{\Phi}}_2^T \\ \vdots \\ \widetilde{\mathbf{\Phi}}_L^T \end{bmatrix} - \begin{bmatrix} \mathbf{\Phi}_1^T \\ \mathbf{\Phi}_2^T \\ \vdots \\ \mathbf{\Phi}_L^T \end{bmatrix}. \tag{2.14}$$

If the auxiliar matrix Υ is constructed as

$$\Upsilon = \mathbf{\Lambda}^H\mathbf{\Lambda} = \begin{bmatrix} \Lambda_1 \\ \Lambda_2 \\ \vdots \\ \Lambda_L \end{bmatrix}^H \cdot \begin{bmatrix} \Lambda_1 \\ \Lambda_2 \\ \vdots \\ \Lambda_L \end{bmatrix}, \tag{2.15}$$

the cost function J_α takes the form

$$\begin{aligned} J_\alpha &= \sum_{\ell=1}^{L} \left| r\, p_i(\vec{\mathbf{r}}_\ell) - p_r(\vec{\mathbf{r}}_\ell) \right|^2 \\ &= (r\,\mathbf{p_i} - \mathbf{p_r})^H\, (r\,\mathbf{p_i} - \mathbf{p_r}) \\ &= (\mathbf{\Lambda}\,\mathbf{G}\,\boldsymbol{\beta})^H\, (\mathbf{\Lambda}\,\mathbf{G}\,\boldsymbol{\beta}) \\ &= (\mathbf{G}\,\boldsymbol{\beta})^H\, \Upsilon\, (\mathbf{G}\,\boldsymbol{\beta}) \\ &= (\mathbf{G}_0\beta_0 + \overline{\mathbf{G}}_I\overline{\boldsymbol{\beta}}_I)^H\, \Upsilon\, (\mathbf{G}_0\beta_0 + \overline{\mathbf{G}}_I\overline{\boldsymbol{\beta}}_I) \\ &= \overline{\boldsymbol{\beta}}_I^H \underbrace{\overline{\mathbf{G}}_I^H\, \Upsilon\, \overline{\mathbf{G}}_I}_{\mathbf{A}} \overline{\boldsymbol{\beta}}_I + \overline{\boldsymbol{\beta}}_I^H \underbrace{\overline{\mathbf{G}}_I^H\, \Upsilon\, \mathbf{G}_0}_{\mathbf{b}} \beta_0 + \beta_0^H \underbrace{\mathbf{G}_0^H\, \Upsilon\, \overline{\mathbf{G}}_I}_{\mathbf{b}^H} \overline{\boldsymbol{\beta}}_I + \beta_0^H \underbrace{\mathbf{G}_0^H\, \Upsilon\, \mathbf{G}_0}_{c_h} \beta_0. \end{aligned} \tag{2.16}$$

As described in Section 2.4 it is possible to calculate the absorption coefficient generated by the active system. The difference right now is that a desired absorption coefficient can be set into J_α through r. This means that for a target α set, a resulting α is obtained.

For the next simulation, a range between 0 and 1 of desired α is defined and the resulting α's are plotted for different frequencies. Figure 2.19 shows the result.

The resulting curves of α present an almost perfect linear behavior. This means that the active system is able to reproduce any target value of absorption coefficient.

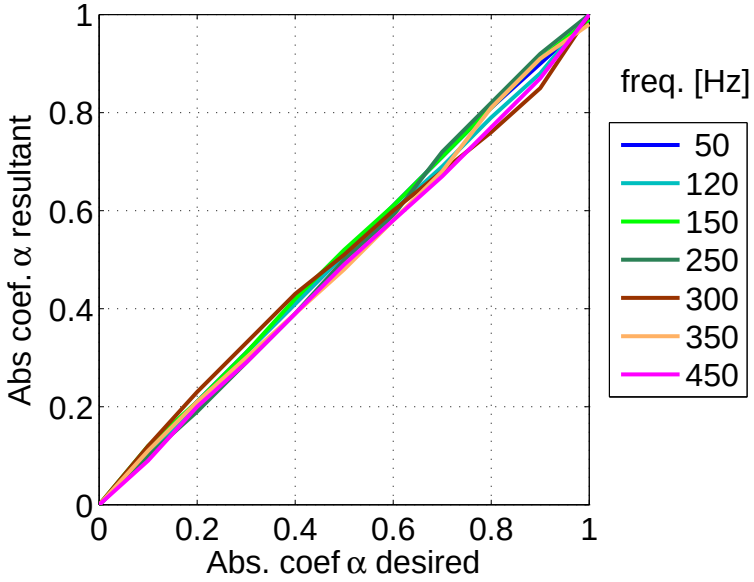

Figure 2.19: Active absorption system set to achieve different values of absorption coefficient α for different frequencies.

Chapter 3

Experimental results

3.1 Control system

As mentioned in the past chapters the minimization of the reflected part p_r of the sound field is used as a control criterion (or cost function) to generate the active absorption. The practical implementation of the active absorption system was developed in two stages. The first part consisted in the minimization of p_r by means of a manual adjustment of the magnitude and phase of the signal that was fed into the secondary source. At the beginning of this stage, extensive measurements were carried out using a Kundt's tube. This simplified sound field provided the first insights behind the active absorption, e.g. relationship between absorption coefficient and phases-gain of sources and sensors, bandwidth of absorption, etc.

In the second stage an adaptive procedure was developed to automatically control the signal sent to the secondary source. Even though the adaptive controller was successfully realized, this implementation should be considered more like a proof of concept since it uses a simple Fx-NLMS algorithm and it does not focus in speed of convergence or tracking capability, as a final product should do.

3.1.1 Manual control

As seen before, the total pressure inside a Kundt's tube can be calculated by superimposing two waves traveling in opposite direction,

$$p(x) = p_0 \left[A\, e^{-jkx} + B\, e^{jkx} \right] \tag{3.1}$$

where A and B correspond to the amplitudes of the traveling waves in positive and negative direction of x respectively. Both, consequently, are the magnitudes of the incident and reflected part of the sound field. The development of the following control strategy requires to acquire the sound pressure at two different points inside the tube (p_1 and p_2). Hence, for example, if the origin of the x axis is defined in front of the microphone 1, it is possible to obtain the next set of equations

$$p_1(0) = A + B, \tag{3.2}$$

$$p_2(\Delta x) = A\, e^{-jk\Delta x} + B\, e^{jk\Delta x}, \tag{3.3}$$

where Δx represents the distance between both microphones. Combining these equations it is possible to calculate the value of the complex constants A and B as

$$A = \frac{p_2 - p_1\, e^{jk\Delta x}}{e^{-jk\Delta x} - e^{jk\Delta x}} \tag{3.4}$$

$$B = -\frac{p_2 - p_1\, e^{-jk\Delta x}}{e^{-jk\Delta x} - e^{jk\Delta x}}. \tag{3.5}$$

Now, driving the same signal into both sources but manually adjusting the amplitude and phase of the secondary source, it is possible to minimize the magnitude of B. A diagram of the control system used is shown in Figure 3.3. If B is made to vanish, only a progressive wave traveling in the positive direction will remain and all the reflected waves will be absorbed by the secondary source acting as an active absorber.

When the system reaches this point of minimum magnitude of B, the absorption coefficient α is calculated. The description of how α is obtained, is given in Section 3.2.

3.1.2 Adaptive control

The automatic control algorithm is mainly composed by two parts, a wave separation process and an adaptive filtering. The fundamentals of the wave separation process were described in Section 1.1. It uses the signal coming from two closely spaced microphones to calculate the sound pressure p and the particle velocity v_x in the middle points between the microphone pair as previously described by equations

$$p(t) = \frac{p_1(t) + p_2(t)}{2} \tag{1.9}$$

and

$$u_x(t) = \frac{1}{\varrho} \int_{-\infty}^{t} \frac{p_1(\tau) - p_2(\tau)}{d_{pp}}\, d\tau. \tag{1.10}$$

As mentioned before (Section 1.1), replacing p and v_x into equations

$$p_i = \frac{1}{2}\,(p + \varrho\, c\, u) \tag{1.7}$$

and

$$p_r = \frac{1}{2}\,(p - \varrho\, c\, u), \tag{1.8}$$

it is possible to obtain the incident and the reflected part of the sound field. All the procedure described above is denominated from now on as wave separation (WS). The second part of the controller consists of an adaptive filter. This types of filters have the ability to self-adjust its transfer function in real-time according to a given criterion or cost function.

In this implementation, a Fx-NLMS adaptive filter [31] was chosen since it provides the necessary compensation for the secondary path and additionally normalizes the updating filter to improve stability and convergence speed. An electro-acoustic block diagram that represents the adaptive system can be seen in Figure 3.1. There, $\mathbf{w}$ represents the filter coefficients responsible to generate the controlling signal y fed into the secondary source, $\widehat{\mathbf{c}}$ is the estimation of the secondary path and r_0 is the desired reflection coefficient of the

controller. In order to obtain full absorption, r_0 must be set to a small value, close or equal to 0.

The complete independence between the controller and the primary source, i.e. the apparent absence of reference signal coming from the primary excitation, helps to confuse this configuration with a feedback system but this certainly is not the case. Assuming that the wave separation procedure WS is working properly, only p_i is used as a reference signal to generate the absorption while the radiation of the secondary source only contributes to the reflected part p_r of the sound field. This means that the reference signal is completely independent of the control signal. The second characteristic that differentiates it from a feedback system is that the error signal is not used to generate the controlling output signal y, it is only used to drive the update of the coefficients $\mathbf{w}$ as part of the adaptation. Therefore the presented system here can be considered as a feed-forward indeed.

At the beginning of this work it was established that the wave separation method used is based on the work of Nishimura [14,15], however there is a fundamental difference that is important to remark. Nishimura uses an additional sensor to acquire the reference signal near the primary source while the absorption system developed here uses a reference coming from the output of the wave decomposition. The reference is the incident pressure p_i of the sound field. In a first approximation p_i can be considered only as the contribution of the direct sound coming from the primary source, although in general p_i also contains reflected components of the sound field coming from the same direction of the primary source wavefront. For the control algorithm these individual reflected components are irrelevant since all of them are grouped into p_i. Therefore, if p_r is completely minimized somehow by the controller, p_i will always be available to serve as reference signal. This approach to obtain the reference signal allows to eliminate the extra microphone used by Nishimura. As consequence, the active absorption system can be eventually build as a compact unit without the need of any sensor near the primary source.

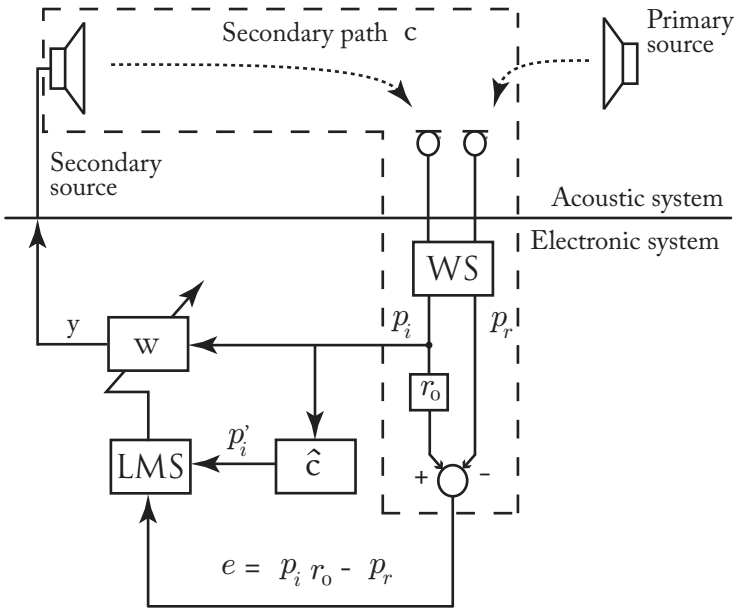

Figure 3.1: Block diagram of the active absorption system.

The numerical integration to calculate eq. (1.10) generates a DC offset in the value of $v_x(t)$, which is then transferred to p_i and p_r, producing p_{iDC} and p_{rDC}, and subsequently

through the whole algorithm making it impossible to generate the right output signal y to perform the absorption. Therefore it becomes necessary to include a DC blocking filter before calculating p_i and p_r. In general, any DC blocking filter will serve for this purpose. As an example, a good option to execute this task is to include a first order high pass IIR filer, such that p_i and p_r are calculated as

$$p_i[n] = p_{iDC}[n] - p_{iDC}[n-1] + 0.8\ p_i[n-1] \tag{3.6}$$

$$p_r[n] = p_{rDC}[n] - p_{rDC}[n-1] + 0.8\ p_r[n-1]. \tag{3.7}$$

Once eq. (3.6) and (3.7) are obtained, it is required to use a Fx-NLMS algorithm to periodically update the output signal y with each new sample. The error signal e of the controller is defined by

$$e[n] = p_i[n]\ r_0 - p_r[n]. \tag{3.8}$$

The input signal $p_i{}'$ of the Fx-NLMS is the reference signal $\mathbf{p_i}$ filtered by the estimated impulse response of the secondary path $\widehat{\mathbf{c}}$. In addition, every new sample computed of p_i' is stored in the delay line $\mathbf{p_i}'$ to update $\mathbf{w}$. The whole control algorithm in discrete time-domain is shown in Table 3.1.

All this adaptive process tries to automatically reduce the reflected part p_r of the sound field by means of the minimization of the error $e[n]$, which represents the excess of reflected sound.

The algorithm was implemented in an Analog Devices ADSP-21161N SHARC 100 MHz ez-kit development board. This DSP possesses a characteristic called Single Instruction - Multiple Data (SIMD) that allows to process one mathematical operation over two sets of data in just one clock cycle. This characteristic duplicates the performance of most algorithm. The code was written directly in Assembler language since provides direct control over the memory registers and arithmetic logic units of the DSP. As a result, a significative reduction of the overhead is obtained. Although the development complexity increases, in comparison compared with other programing languages like C or C++, the performance also increases. The benefit of this is that a higher sampling frequency can be used.

Secondary path $\widehat{\mathbf{c}}$ estimation

The coefficients of the secondary path $\widehat{\mathbf{c}}$ must be estimated previously with an LMS algorithm in an identification procedure. In a classic ANC system the secondary path is defined between the control source and the error microphone used, but in our system the error signal is not physically available, the error is generated inside the DSP as described in (3.8). Hence, in this particular case the secondary path $\mathbf{c}$ goes from the output of the digital-to-analog converters (DAC) to the error signal $e[n]$ inside the controller, passing through the secondary source, the plant, the microphone pair, the analog-to-digital converter (ADC) and the WS until it reaches $e[n]$, as it can be seen in the block diagram of Figure 3.1. Therefore the identification must include all this elements.

Generating a Maximum Length Sequence (MLS) [32, 33] of 2048 coefficients inside of the DSP processor to feed the secondary source and comparing this signal with the error of the controller $e[n]$ sample by sample, a new error $e_c[n]$ to estimate $\widehat{\mathbf{c}}$ can be defined as

$$e_c[n] = e[n] - \widehat{\mathbf{c}}[n]^{\mathrm{T}}\ \mathbf{MLS}[n]$$

Summarized table with the AAS algorithm

Initialization:

$\mathbf{w_0} = 0$

$0 < \mu < 2$

$\delta = 0.06$ (small arbitrary constant)

For each sample [n]:

$$
\begin{aligned}
p[n] &= \frac{1}{2}\Big[p_1[n] + p_2[n]\Big] \\
a[n] &= p_1[n] - p_2[n] \\
I[n] &= \frac{1}{2\,f_s}\Big[a[n] + a[n-1]\Big] + I[n-1] \\
u[n] &= \frac{I[n]}{d_{pp}} \\
p_{iDC}[n] &= \frac{1}{2}\Big[p[n] + c\,u[n]\Big] \\
p_{rDC}[n] &= \frac{1}{2}\Big[p[n] - c\,u[n]\Big] \\
p_i[n] &= p_{iDC}[n] - p_{iDC}[n-1] + 0.8\; p_i[n-1] \\
p_r[n] &= p_{rDC}[n] - p_{rDC}[n-1] + 0.8\; p_r[n-1] \\
e[n] &= p_i[n]\; r_0 - p_r[n] \\
y[n] &= \mathbf{w}[n]^{\mathrm{T}}\, \mathbf{p_i}[n] \\
p_i'[n] &= \widehat{\mathbf{c}}^{\mathrm{T}}\; \mathbf{p_i}[n] \\
\mathbf{w}[n+1] &= \mathbf{w}[n] - \frac{\mu}{\delta + \mathbf{p_i'}[n]^{\mathrm{T}}\, \mathbf{p_i'}[n]}\, e[n]\, \mathbf{p_i'}[n]
\end{aligned}
$$

Table 3.1: Description of the active absorption control algorithm for each sample acquired through the microphones p_1 and p_2. d_{pp} is the distance between the two microphones, f_s is the sampling frequency, c is the speed of sound and μ is the step-size of the algorithm. ($^{\mathrm{T}}$ means vector transpose).

and the update equation as

$$\widehat{\mathbf{c}}[n+1] = \widehat{\mathbf{c}}[n] - \mu\; e_c[n]\; \mathbf{MLS}[n].$$

A schema of the identification algorithm is presented in Figure 3.2. Once $\widehat{\mathbf{c}}$ is estimated, it is incorporated back into the active absorption algorithm already described in Table 3.1.

3.2 Active absorption in a one-dimensional waveguide

The first step in the experimental process is to evaluate the system under the simplest conditions and later increase the complexity. Hence, the first measurements are made using a one-dimensional waveguide. This setup consists of a Kundt's tube with a lateral branch, two loudspeakers and a pair of microphones. A detailed sketch of the setup is shown in Figure 3.3 where manual and adaptive control setups are depicted. A cylindrical

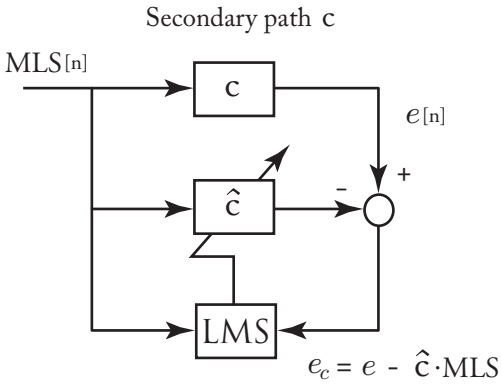

Figure 3.2: Schema of the identification algorithm used to estimate the secondary path $\hat{\mathbf{c}}$ of the active absorption system.

plexiglass tube of 1.7 m length and 14.8 cm diameter was used. The cutoff frequency f_{cutoff} [34] for this tube corresponds to

$$f_{\text{cutoff}} = \frac{0.58 \cdot c}{d_d} = 1348 \text{ [Hz]},$$

where c is the speed of sound and d_d is the inner diameter of the tube. All the measurements were made for the range of 100-1000 Hz.

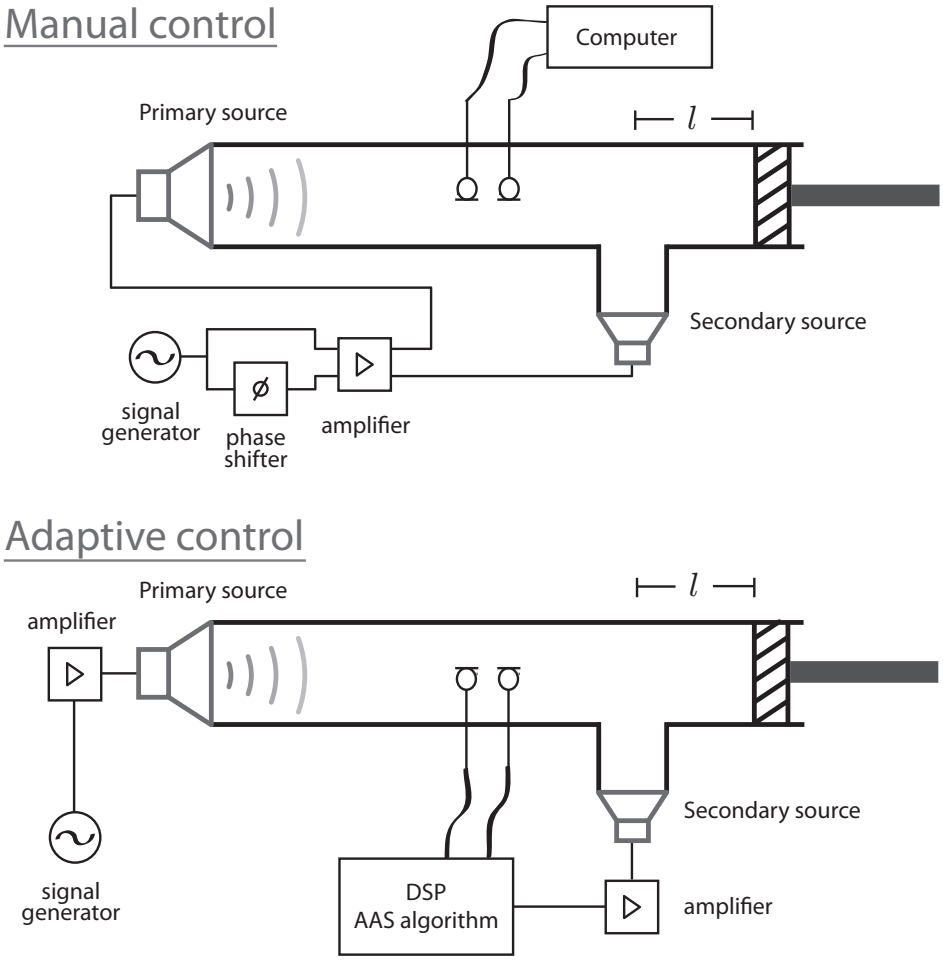

Figure 3.3: Sketch of both control setup used.

With this configuration it was also possible to modify the distance Δx between both microphones and the distance l between the secondary source and the rigid end of the tube, allowing to study the influence of these parameter over the absorption system. Table 3.2 summarizes the evaluated cases.

	Δx [cm]			Excitation signal	
l [cm]	5	10	15	Pure tone	Broadband
40	✓	✓	✓	✓	✓*
27	×	✓	×	✓	✓
18	×	✓	×	✓	×
17	×	✓	×	✓	×
16	×	✓	×	✓	×
15	✓	✓	✓	✓	✓*

Table 3.2: Summary of the measurements performed (✓) and not performed (×). (*) Only measured using $\Delta x = 10$.

The following descriptions of the performed measurements are separated accordingly to the excitation signal used. The measurements of the absorption coefficient α were made using the transfer function method between two microphones as described in ISO-10534-2 [34].

3.2.1 Pure tone excitation

Manual control

The primary and secondary sources were driven with a set of pure tone signals as shown in Table 3.3. Manually adjusting the magnitude and phase of the signal sent through the secondary source, the magnitude of the reflected sound pressure was minimized according to equation (3.5). The absorption coefficient was measured for all the possible combinations of Δx and l, the results are also given in Table 3.3.

The important conclusion that can be extracted from these results is that for all the frequencies used it was possible to obtain a high value of absorption coefficients of $\alpha \approx 1$. The combination of Δx and l used did not play any particular role in the maxima of values of α reached. However there are some exceptions to this statement. For instance the value of $\alpha = 0.565$ which corresponds to the case $l = 17$ cm and $f = 550$ Hz, if we calculate l/λ and compare it with Figure 1.6.a, it is possible to observe the closeness of l/λ with a peak in the curve. Since the phase shifter used had only a limited amplification gain, this was not enough to generate the required output signal and therefore it was not possible to achieve a higher value of α. The value

$$\frac{l}{\lambda} = 0.2718$$

differs from the theoretical 0.25 where the indetermination occurs. This deviation is subject to the intrinsic differences between an idealized and a real system, which for example uses real sources and not point sources, or even the Kundt's tube which has a lateral branch. Therefore it is reasonable to assume that in this case l/λ was quite near to the discontinuity. A similar case but less evident occurs at $l = 16$ cm and $f = 550$ Hz.

		Absorption Coefficient α							
		$f$requency [Hz]							
l [cm]	Δx	100	250	400	550	700	850	1000	1250
15	5	1	0.99943	1	0.99996	1	1	0.99999	–
	10	1	0.99975	1	0.99999	1	0.99999	0.99999	0.99997
	15	1	0.99995	0.99999	1	1	0.99995	0.99997	–
16	10	1	1	1	0.96946	1	1	1	0.99999
17		1	0.99996	1	0.56522	1	1	1	1
18		1	0.99999	1	1	0.99994	0.99999	0.99996	0.99998
27		1	0.99997	1	1**	0.99471**	1**	1	–
40	5	1	1	1	0.99999	1	1	1	–
	10	1	1	1	1	1	0.99999	1	–
	15	1	1	0.99997	1	1	1	1	–

Table 3.3: Maximum absorption coefficient reached for each case and frequency. (**) For these values the frequencies of the excitation signals used were 500, 710 and 800 [Hz] respectively.

The efficiency of the system is defined by the capability to reduce the reflected part of the sound field, therefore it is important to measure the change between the initial state of the system, i.e. the secondary source switched off, and the optimal state (when B is minimum). Equation (3.9) offers a quantification parameter that describes this change in the reflected wave. Figure 3.4 shows the reduction of the magnitude $|B|$ between both states for different frequencies. From this data set a reduction average for each frequency can be calculated, these averages are shown in Table 3.4.

$$Reduction = 10 \log \frac{|B_{\text{optimal}}|}{|B_{\text{initial}}|} \text{ [dB]} \tag{3.9}$$

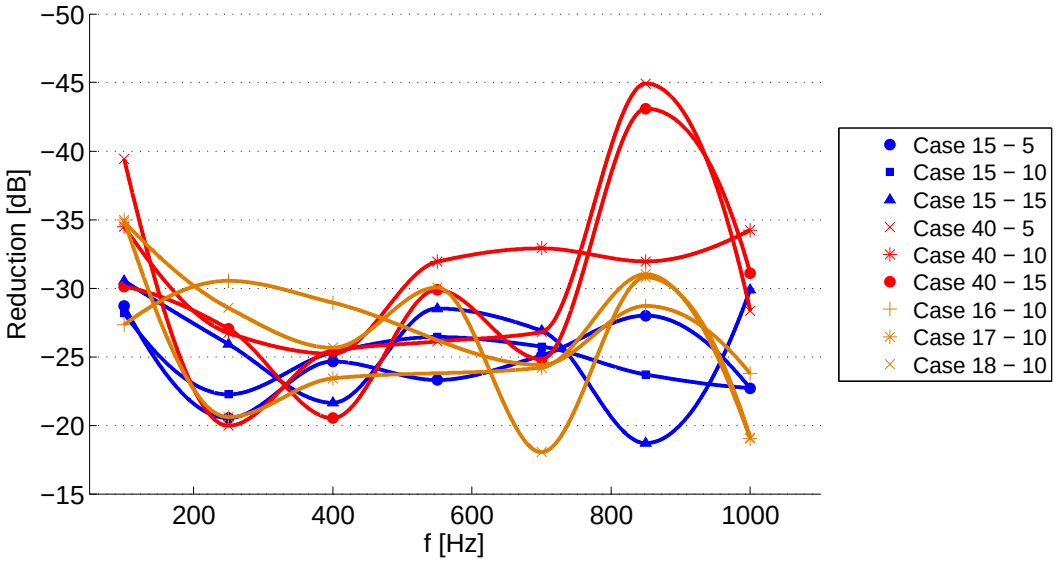

Figure 3.4: Reduction of the magnitude of the reflected wave B, between the initial and optimal absorption state. Different cases of l and Δx.

These results show that the active system is able to generate a significant reduction level in the amplitude of the reflected wave. The reduction achieved is rather similar for

	f [Hz]						
	100	250	400	550	700	850	1000
Reduction average [dB]	-32.07	-24.69	-24.54	-28.04	-25.44	-31.21	-25.66

Table 3.4: Reduction average of the magnitude B between the initial and optimal absorption state.

all frequencies and, more importantly, completely independent of the parameters studied, i.e. l and Δx.

Absorption coefficient and Gain-Phase relationship

It has been seen that the maximal absorption point of the active system is reached by means of adjusting the right magnitude and phase of the signal sent to the secondary source. In this relationship between magnitude and phase it can be shown that if one of this parameters is kept fix, there is only a single value of the other parameter that allows to reach the maximum absorption point. For example, if the maximum absorption point is reached at gain g_0 and phase ϕ_0, keeping the gain at g_0 and sweeping the phase between -180° and 180° will show only a unique point of maximum absorption precisely at ϕ_0. The exact same behavior applies if the phase ϕ_0 is kept fix and the gain is swept. This, can be visualized in Figures 3.5 and 3.6 for the case $l = 15$ and $\Delta x = 10$, and Figures 3.7 and 3.8 for the case $l = 40$ and $\Delta x = 10$. These results establish that for each frequency there is a unique pair of gain and phase (g_0, ϕ_0) coefficients that will minimize the reflected part of the sound field and consequently will generate maximal absorption.

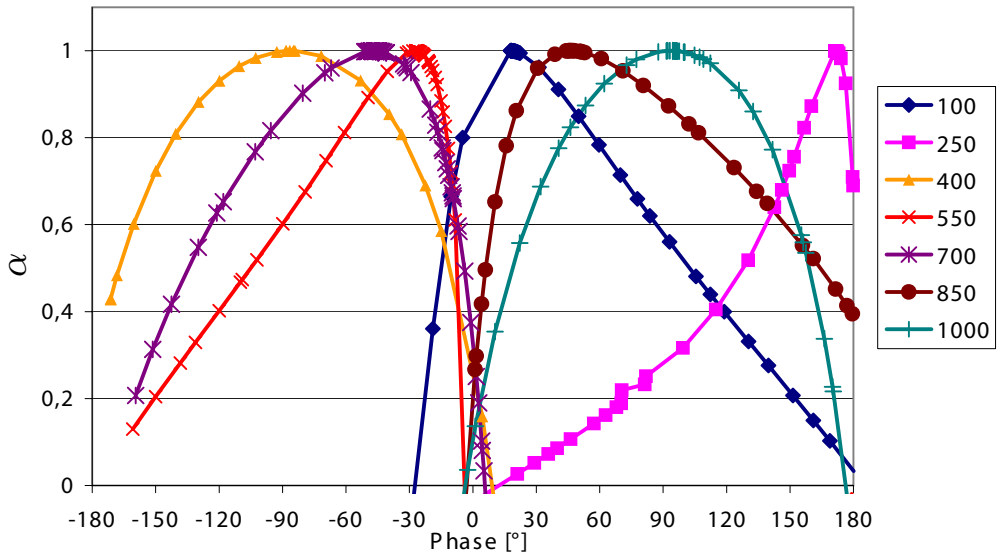

Figure 3.5: Absorption coefficient α as a function of the phase between primary and secondary source. Case $l = 15$ and $\Delta x = 10$.

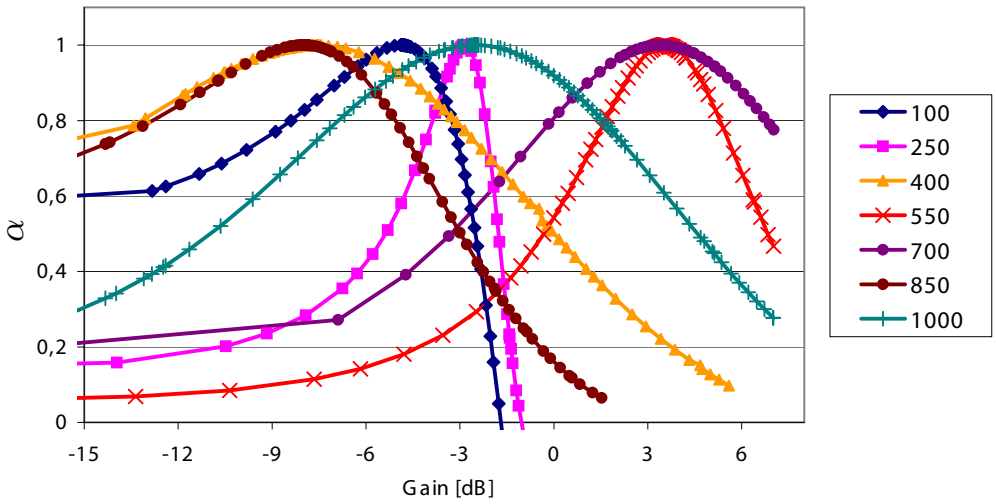

Figure 3.6: Absorption coefficient α as a function of the gain between primary and secondary source. Case $l = 15$ and $\Delta x = 10$.

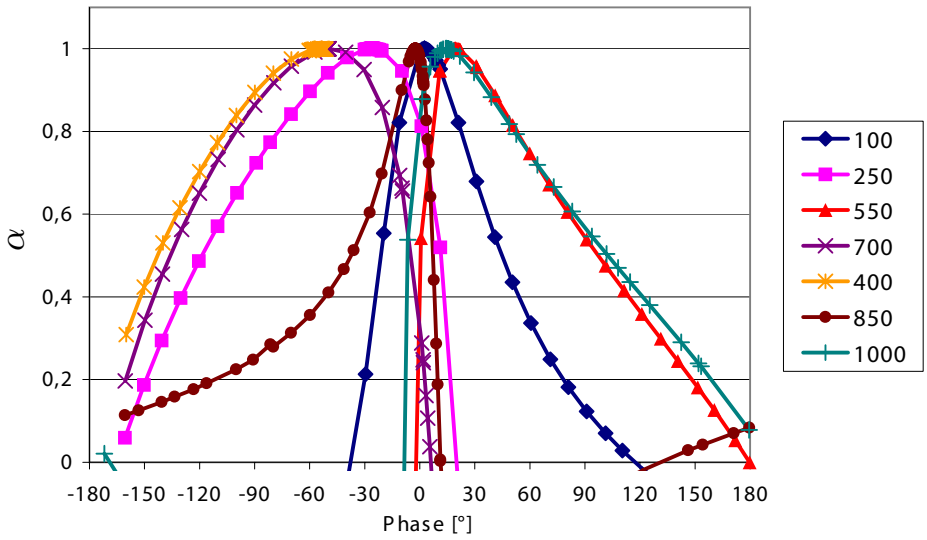

Figure 3.7: Absorption coefficient α as a function of the phase between primary and secondary source. Case $l = 40$ and $\Delta x = 10$.

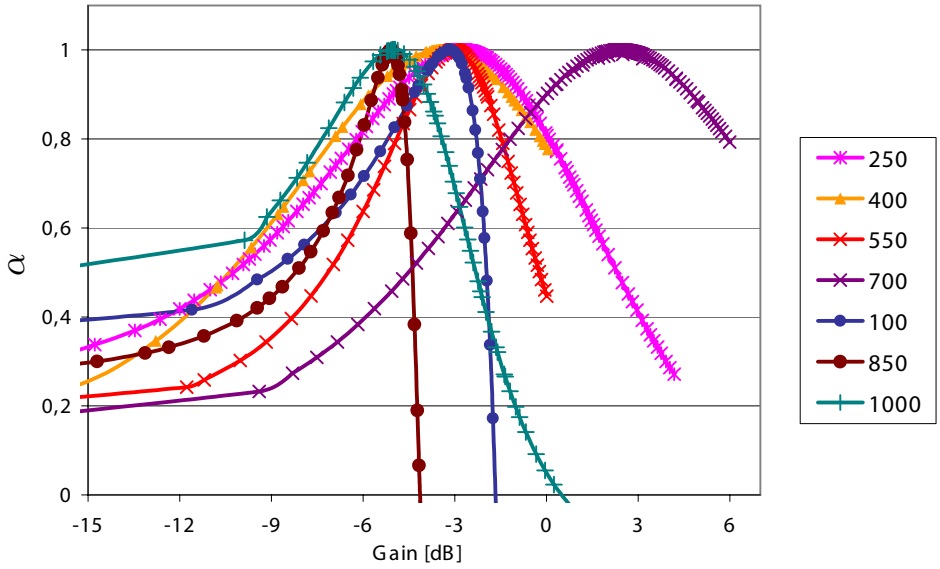

Figure 3.8: Absorption coefficient α as a function of the gain between primary and secondary source. Case $l = 40$ and $\Delta x = 10$.

Adaptive control

In this case, the primary source excites the Kundt's tube with a set of discrete pure tone signals, while the active absorption system acts automatically driven by the sensing signals coming from the microphone pair. Once the minimization process ended, the absorption coefficient α was measured. For comparison, the absorption coefficient was also measured with the controller turned off. Table 3.5 summarizes the results.

f [Hz]	Absorption coefficient α	
	System off	System on
100	0.9990	0.9993
200	0.8665	0.9994
300	0.6867	0.9994
400	0.6626	0.9994
500	0.6430	0.9995
600	0.6285	0.9995
700	0.6039	0.9996
800	0.6347	0.9996
900	0.6104	0.9997
1000	0.6290	0.9997

Table 3.5: Absorption coefficients obtained with the active system on and off using pure tones as excitation signal inside a Kundt's tube.

These results show for the first time that the adaptive system is able to efficiently generate absorption, irrespective of the frequency used. A uniform behavior is obtained across all the excitation frequencies.

Especially around 100 Hz, the high values of α (when the system is off) are explained due to the passive absorption of the secondary source produced by the movement of the membrane of the loudspeaker and the losses of the tube.

3.2.2 Broadband excitation

In the latter section the absorption coefficient α was calculated for a discrete number of frequencies. Now instead, band-passed noise is used as a primary signal, this wide range of frequencies makes it possible to obtain not only a single value of α but a whole curve of absorption coefficients for the frequencies of the band selected.

Manual control

To obtain these curves of α, a similar procedure as described in the latter section is used, i.e. a pure tone is driven through the primary and secondary source, and the magnitude-phase of the secondary signal is adjusted to minimize B. When the point of minimum B is reached, the signal sent to both loudspeakers is switched from this pure tone to band-passed noise, keeping fix the previous magnitude-phase. For instance, a pure tone of 200 Hz is used first to minimize B, the system is adjusted until the maximum absorption coefficient α is reached, then the input signal is switched to a band-passed 1/3 octave noise with their center band at 200 Hz, and excites the range between 178-224 Hz. Then,

the absorption coefficient is measured for this band-pass signal. Hence, for this case it is said that 200 Hz is the tunning frequency of the system.

The noise generator used was able to deliver noise through a 1/1 or 1/3 octave band pass filter network. The output of the noise generator was adjusted in such a way to ensure a sufficient level in order to avoid external disturbances like background noise. Table 3.6 summarize the measurements and the corresponding figures show the results. The distance $\Delta x = 10$ was kept constant for all measurements.

	l [cm]	Octave bandwidth	Figure
Cases	15	1/3	3.9
	27	1/3	3.10
	40	1/3	3.11
	40	1/1	3.12

Table 3.6: Summary of parameters evaluated: l, Δx and bandwidth excitation.

For each case, two conditions were measured to compare the performance of the system, the optimal absorption point (on) and the system without control (off).

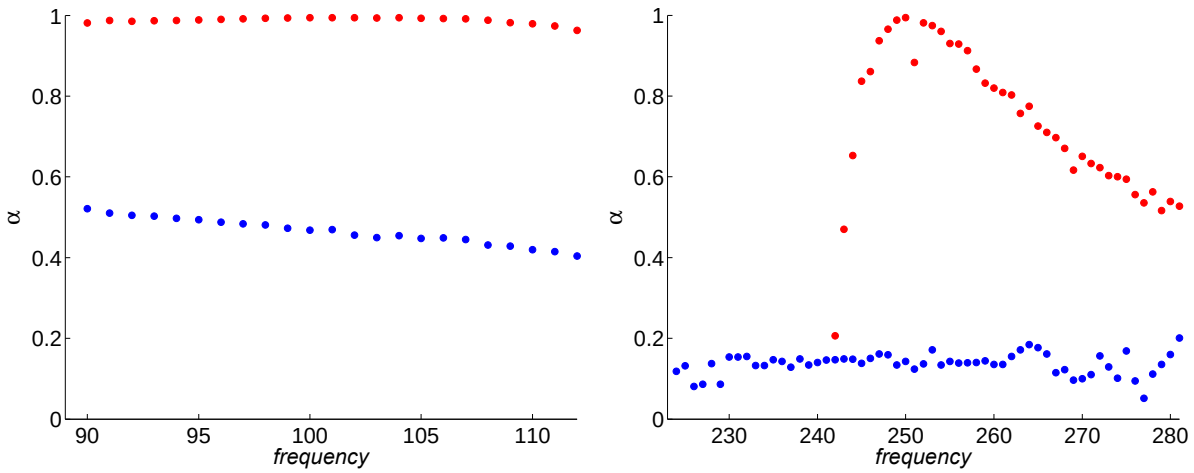

(a) 100 [Hz]

(b) 250 [Hz]

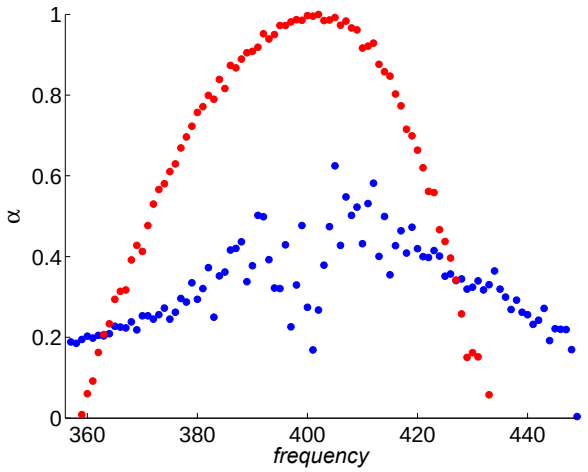

(c) 400 [Hz]

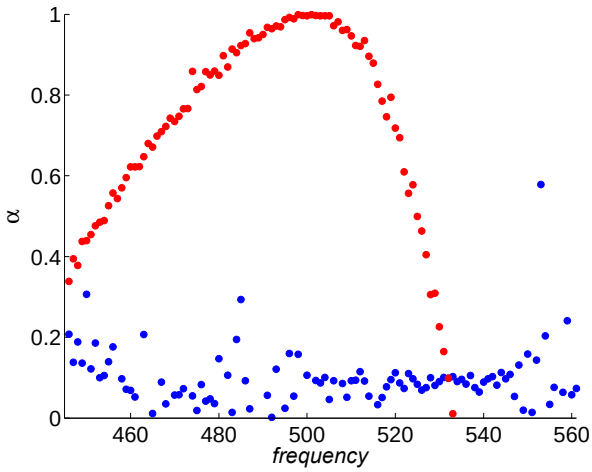

(d) 500 [Hz]

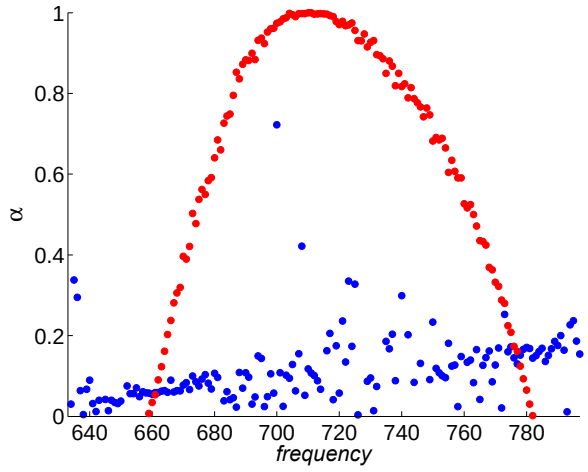

(e) 710 [Hz]

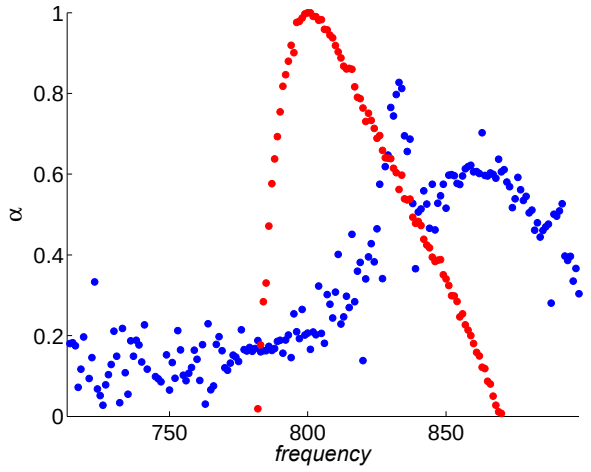

(f) 800 [Hz]

Figure 3.9: Curves of absorption coefficients α for each tunning frequency indicated, system on (red) and system off (blue). Case (l = 15, Δx = 10). 1/3 octave band noise as excitation signal.

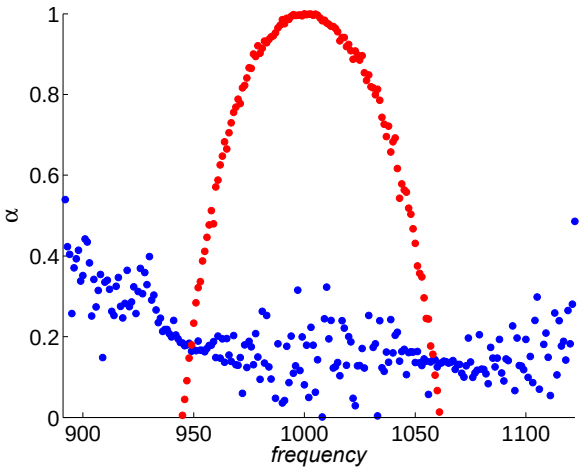

(g) 1000 [Hz]

Figure 3.9: Curves of absorption coefficients α for each tunning frequency indicated, system on (red) and system off (blue). Case (l = 15, Δx = 10). 1/3 octave band noise as excitation signal.

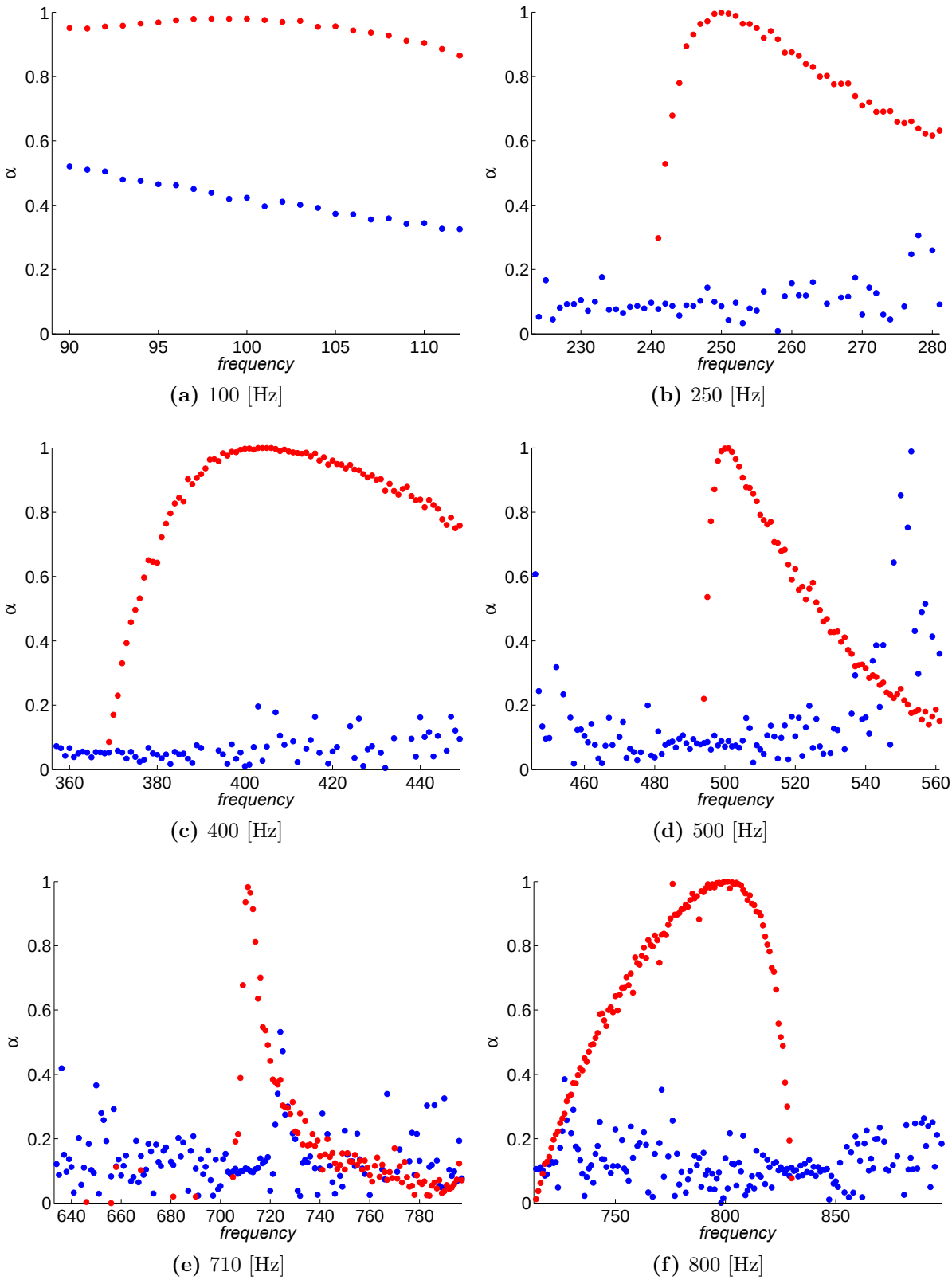

(a) 100 [Hz] **(b)** 250 [Hz]

(c) 400 [Hz] **(d)** 500 [Hz]

(e) 710 [Hz] **(f)** 800 [Hz]

Figure 3.10: Curves of absorption coefficients α for each tunning frequency indicated, system on (red) and system off (blue). Case (l = 27, Δx = 10). 1/3 octave band noise as excitation signal.

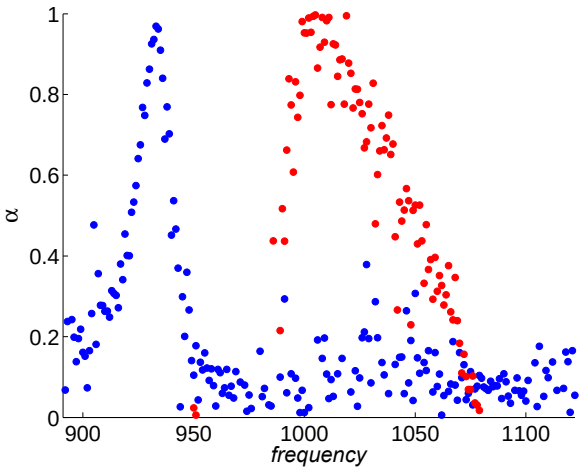

(g) 1000 [Hz]

Figure 3.10: Curves of absorption coefficients α for each tunning frequency indicated, system on (red) and system off (blue). Case (l = 27, Δx = 10). 1/3 octave band noise as excitation signal.

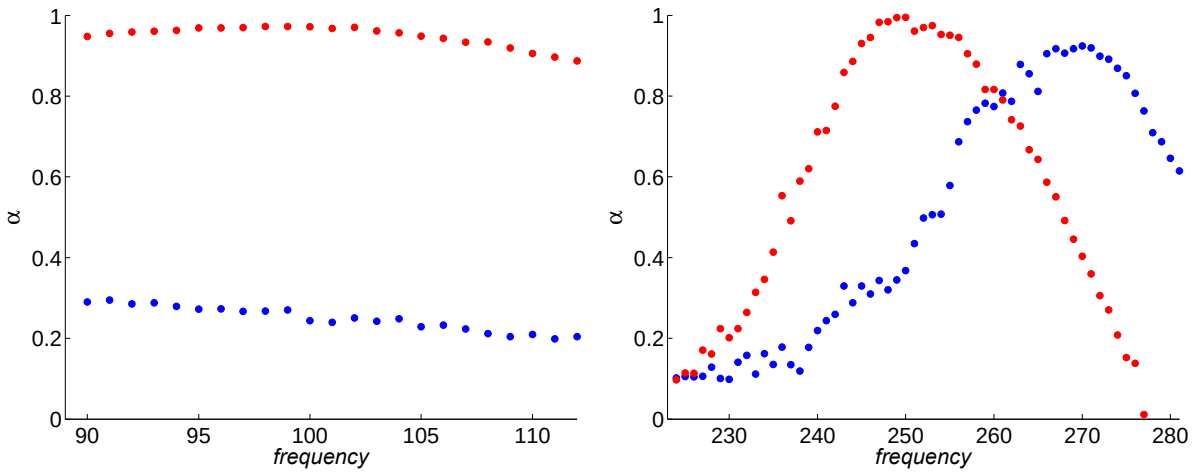

(a) 100 [Hz]

(b) 250 [Hz]

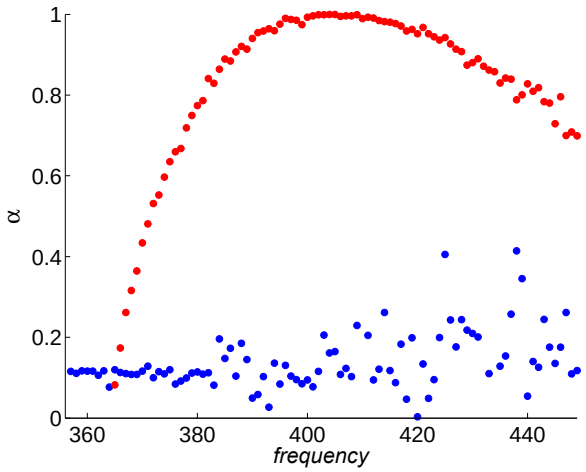

(c) 400 [Hz]

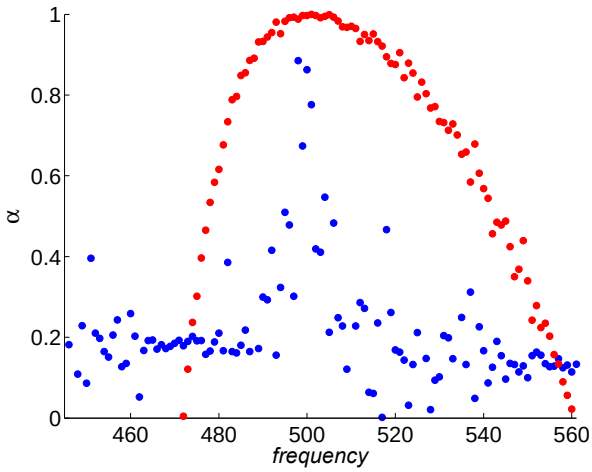

(d) 500 [Hz]

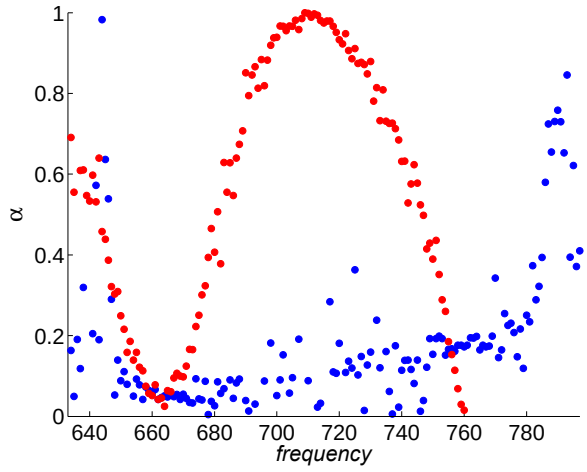

(e) 710 [Hz]

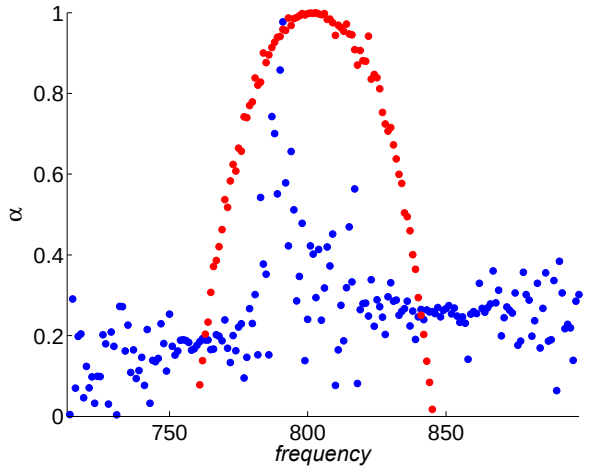

(f) 800 [Hz]

Figure 3.11: Curves of absorption coefficients α for each tunning frequency indicated, system on (red) and system off (blue). Case (l = 40, Δx = 10). 1/3 octave band noise as excitation signal.

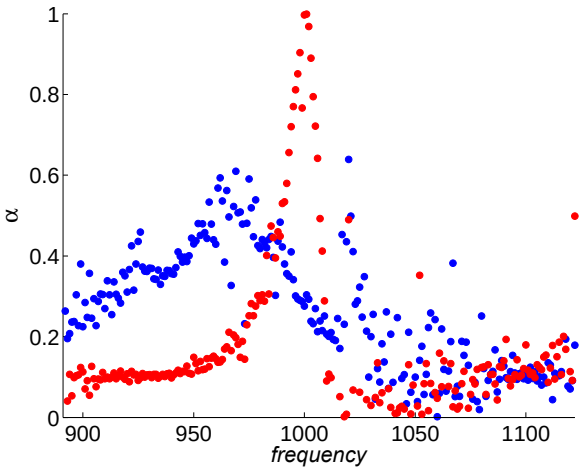

(g) 1000 [Hz]

Figure 3.11: Curves of absorption coefficients α for each tunning frequency indicated, system on (red) and system off (blue). Case (l = 40, Δx = 10). 1/3 octave band noise as excitation signal.

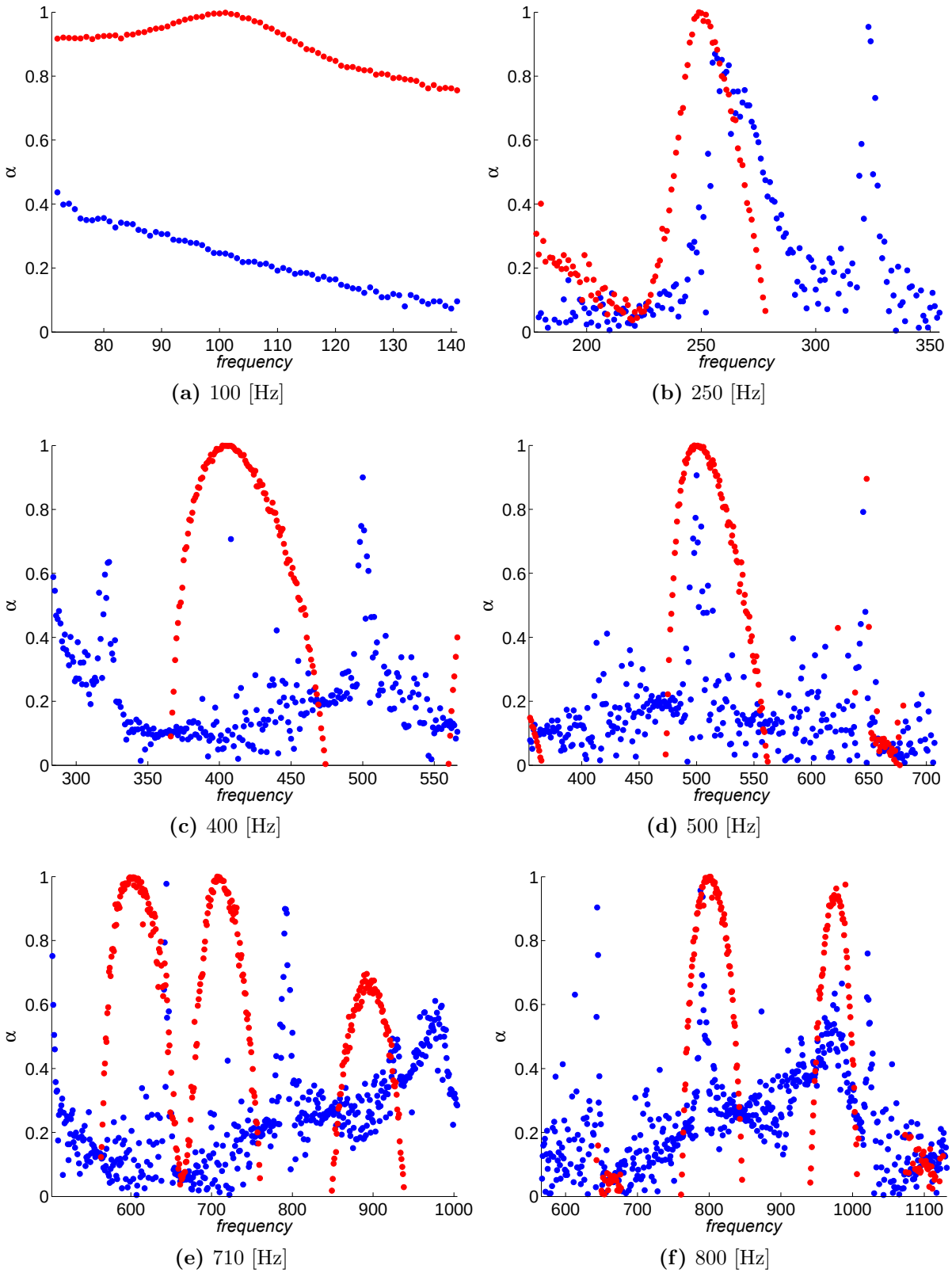

(a) 100 [Hz] **(b)** 250 [Hz]

(c) 400 [Hz] **(d)** 500 [Hz]

(e) 710 [Hz] **(f)** 800 [Hz]

Figure 3.12: Curves of absorption coefficients α for each tunning frequency indicated, system on (red) and system off (blue). Case (l = 40, Δx = 10). 1/1 octave band noise as excitation signal.

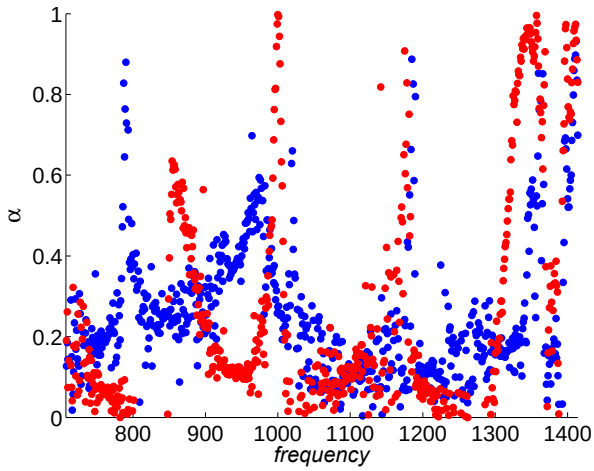

(g) 1000 [Hz]

Figure 3.12: Curves of absorption coefficients α for each tunning frequency indicated, system on (red) and system off (blue). Case (l = 40, Δx = 10). 1/1 octave band noise as excitation signal.

It is possible to notice that in each case presented (Figures 3.9 - 3.12) high values of absorption coefficients were reached around the tunning frequency. These results prove that it is possible to actively absorb sound not only for pure tone excitation but for a broader band around a defined tunning frequency.

In the first three cases where a 1/3 octave band excitation was used (Figures 3.9 - 3.11), there is a single peak in the absorption coefficient curve that, as expected, coincides with the tunning frequency. But this changes in the last case (Figure 3.12), for instance, Figure 3.12e displays three peaks of high values of absorption coefficients around 600, 710 and 895 Hz. This behavior is explained due to the influence of the phase-shifter over the control signal sent to the secondary source. To visualize this, the phase of the microphone pair is compared under four circumstances: broad band excitation with a tunning frequency of 710 Hz and pure tone excitation at 600, 710 and 895 Hz. The phase measured under broadband excitation with tunning at 710 Hz is shown in Figure 3.13, meanwhile Table 3.7 shows the three pure tones mentioned. There it is possible to observe the coincidence between the phases under pure tones and broadband excitation. This means simply that although the broadband signal is tunned to absorb only at 710 Hz, the phase response of the phase-shifter generates points of coincidence at other frequencies where the system is also able to absorb. A more detailed discussion of this matter is presented in Section 3.3.

f [Hz]	Abs. coeff. α	phase [°]
600	0.98	-62.12
710	1	-73.97
895	0.64	-89.47

Table 3.7: Values of α and phase measured using pure tone excitation.

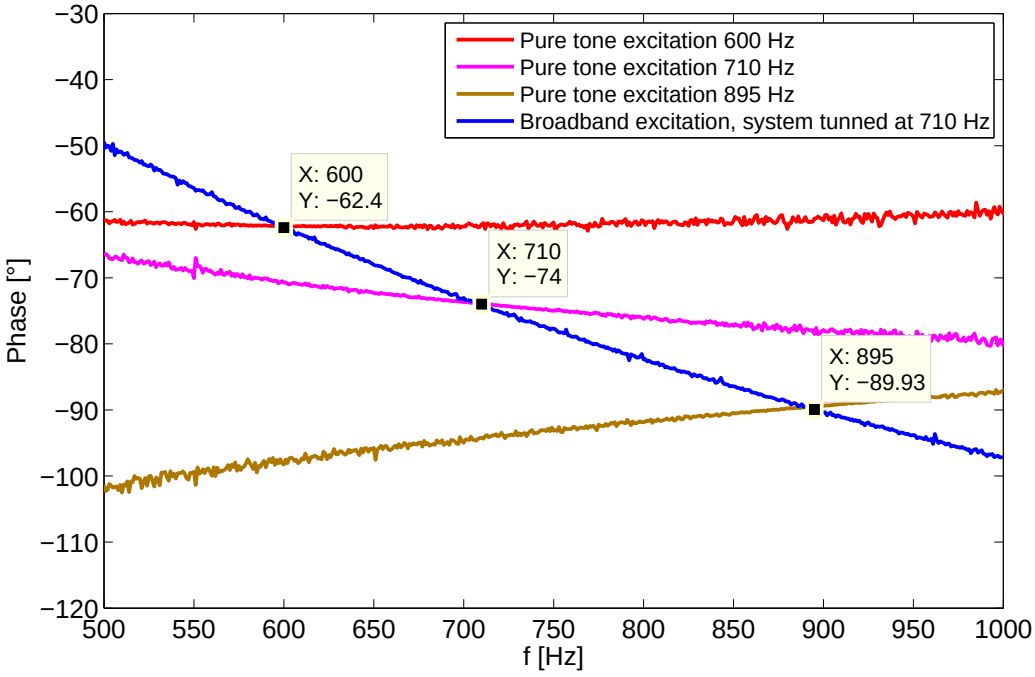

Figure 3.13: Phase response coincidence between broadband and pure tone excitation as a result of the phase-shifter in the system. The points highlighted are the values of phase under broadband excitation.

Adaptive control

Once again the absorption coefficient was measured to show the performance of the system, but this time using the adaptive control procedure already described. In these measurements, 1/3 octave band-passed noise was fed through the primary source. Figure 3.14 shows the absorption coefficient curves obtained, a few selected bands are plotted 160, 250, 500 and 800 Hz. An extra case is shown in Figure 3.14b where also a signal of 1/1 octave band was used to excite the system and compare the results with a wider band excitation. Additionally the last plot, i.e Figure 3.14e shows the response of the system using the full range of interest as excitation signal, 100-1000 Hz.

Although the active absorption system presents a clear improvement in the absorption coefficient under 1/3 octave excitation, or even in the curve of 1/1 octave, this is not the case when the full range of excitation is used. This result is somewhat expected since typically adaptive systems using FIR filters with limited number of coefficients are not able to operate efficiently over large bandwidths. Moreover, as seen in the previous section, the active system presents a limited bandwidth response around the tunning frequency where the absorption coefficient shows a significant enhancement.

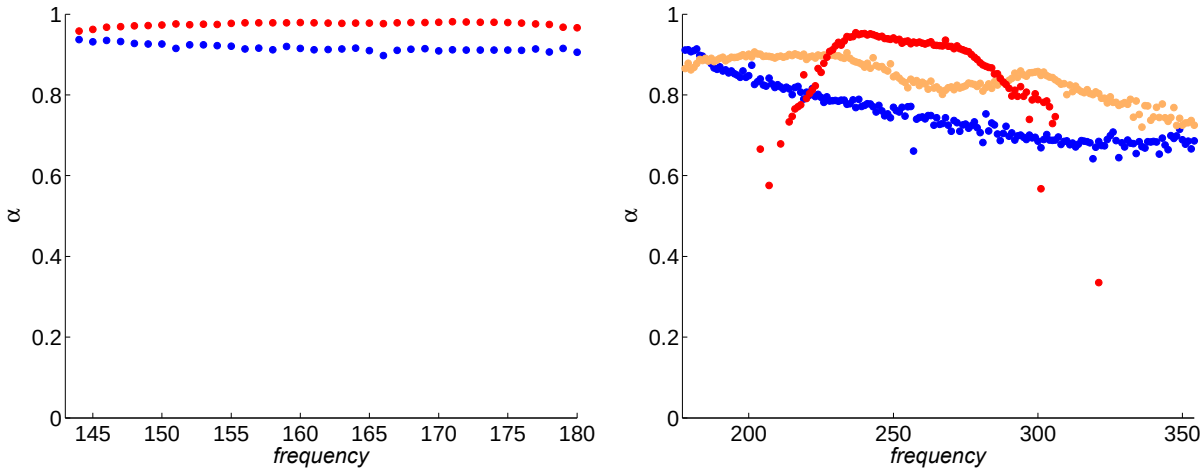

(a) 160 [Hz] **(b)** 250 [Hz]

Figure 3.14: Curves of absorption coefficients α for each tunning frequency mentioned, system on (red) and system off (blue). 1/3 octave bands (except (b) with additional 1/1 octave band (orange)).

Although all the measurements shown up to this point describe the behavior and the positive performance of the active absorption system, it possesses limited applicability due to the one-dimensional nature of the setup used, i.e. Kundt's tube. Hence, a second set of evaluations was implemented to bring the system closer to real working conditions. Section 3.4 addresses this matter.

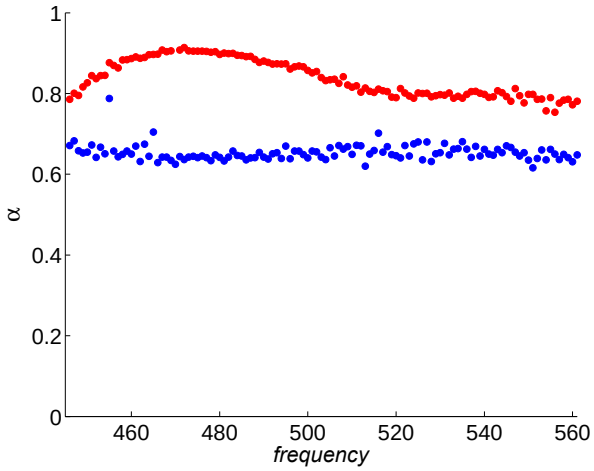

(c) 500 [Hz]

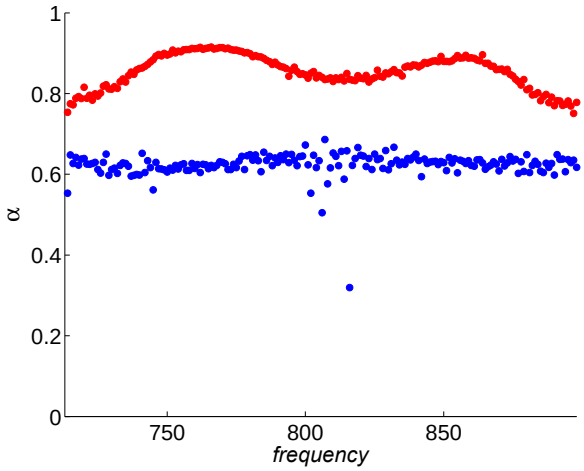

(d) 800 [Hz]

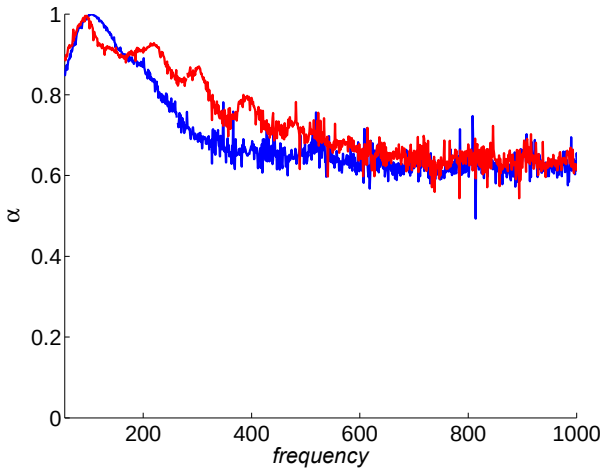

(e) Linear [Hz]

Figure 3.14: Curves of absorption coefficients α for each tunning frequency mentioned, system on (red) and system off (blue).

3.3 Microphone pair transfer function

If we think for a moment in only a propagating wave in an infinite tube and we measure the sound pressure at two different points along the tube, two distinctive characteristics will be observed.

- The magnitudes of the signals of the two microphones will be equal.
- The phase between both signals will be only a time delay τ given by

$$\tau = \omega_0 \, t_0 = 2\pi f_0 \frac{\Delta x}{c} \tag{3.10}$$

where Δx is the distance between the microphones, f_0 is the frequency of the propagating wave and c the speed of sound. Both characteristics are extremely useful to provide further evidence of the active absorption of the system. Making the assumption that a system is able to completely absorb all the reflected waves, a similar situation as described above should take place.

In all the measurements made, when the optimal absorption point was reached through the minimization of B, the magnitudes of the signals of the microphone pair were almost identical. Moreover, a later analysis of the phase shift between these two signals showed the exact delay τ mentioned. This is another way to prove that the system is efficiently absorbing the reflected wave.

The transfer function of the microphone pair H_{21} can be defined simply as

$$H_{21}(\omega) = \frac{p_1(\omega)}{p_2(\omega)}, \tag{3.11}$$

where p_1 and p_2 are the signals coming from each microphone. Thus, $H_{21}(\omega)$ can be used to illustrate both characteristics. If we assume that the magnitude of B is minimized, i.e. the maximum absorption point is reached, the above characteristics should take the form of

- $|H_{21}(\omega)| = 1$
- $\angle H_{21}(\omega) = \tau$.

Table 3.8 shows the magnitude of $H_{21}(\omega)$ for some of the cases evaluated. In almost every case the magnitude measured is nearly 1. These results confirm the first characteristic mentioned.

	$\lvert H_{21} \rvert$		
f [Hz]	Case $l = 40$	Case $l = 27$	Case $l = 15$
100	0.9998	0.9996	0.9995
250	0.9997	0.9955	0.9866
400	1.0002	0.9978	1.0017
550	1.0004	0.9986*	1.0017
700	1.0006	1.1504* **	0.9979
850	1.0049	1.0032*	0.9968
1000	0.9994	0.9989	0.9947

Table 3.8: Magnitude of the transfer function for different cases of l and $\Delta x = 10$. (*) For these values the frequencies of the excitation signals used were 500, 710 and 800 Hz respectively. (**) In this case the maximal absorption point was not reached.

Now, the evaluation of $\angle H_{21}$ is shown in Figure 3.15, where each phase measured is divided by its corresponding theoretical τ, i.e. $\angle H_{21}/\tau$. Once again, the results shown there indicate that the second characteristic takes place when the system is actively absorbing.

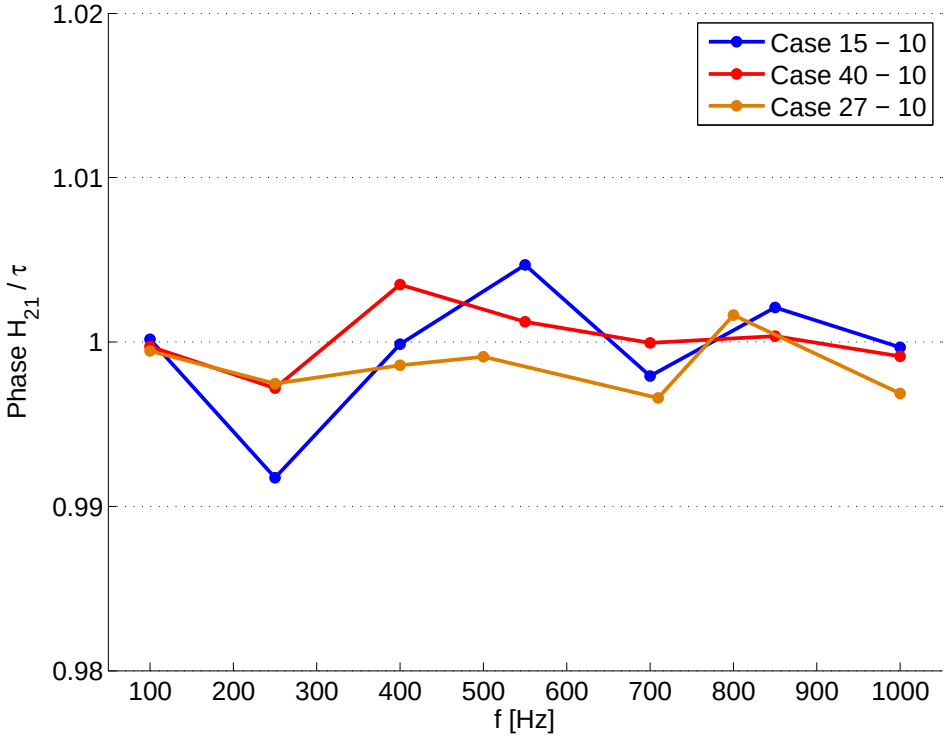

Figure 3.15: Ratio $\angle H_{21}(\omega)/\tau$ for different cases (l) measured using pure tone signals and $\Delta x = 10$.

An extension of this same analysis can be made now for broadband noise excitation too. As explained in Section 3.2.2, sometimes a broad excitation of the system generates a couple of additional points aside of the tunning frequency where the absorption coefficients reach high values. These frequency points are created when both characteristics, magnitude equals 1 and phase equals τ, occur simultaneously.

Taking for example the case where $\Delta x = 10$ and the system is tunned at 500 Hz for maximal absorption. Figure 3.18 shows the absorption coefficient curve obtained where two additional peaks appear. An analysis of the magnitude and the phase of H_{21} reveals

the occurrence of these coincidence points. $|H_{21}|$ and $\angle H_{21}$ are plotted and compared with the aforementioned characteristics where a straight line represents the unitary amplitude and τ in each plot respectively. See 3.16 and 3.17. The points highlighted correspond precisely to the state where the system is able to generate an absorption coefficient of approximately 1 as shown in Figure 3.18.

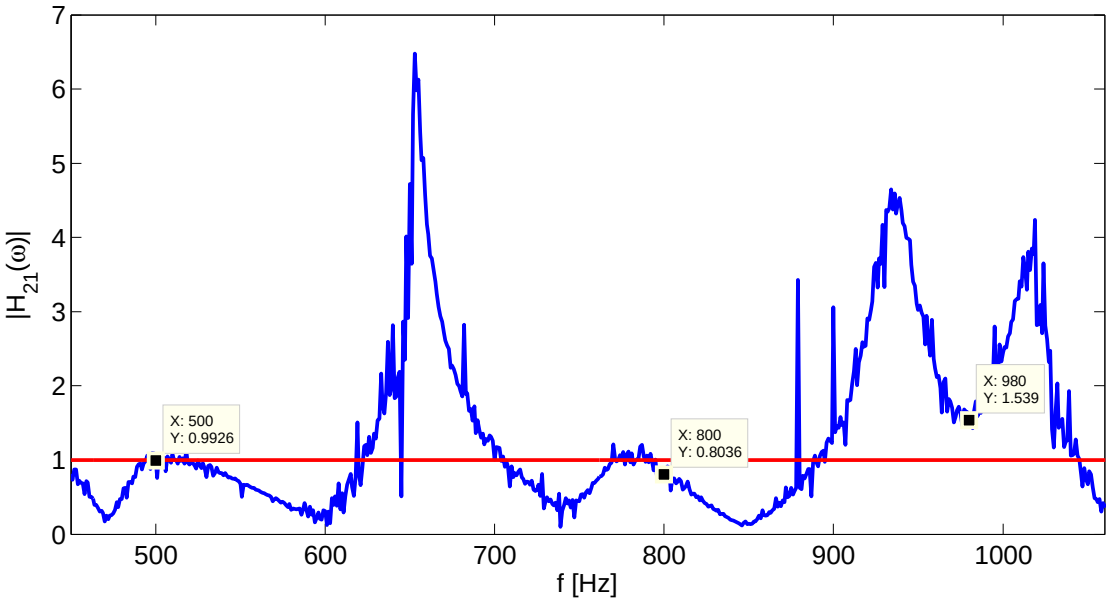

Figure 3.16: Magnitude of the frequency response H_{21} between microphones.

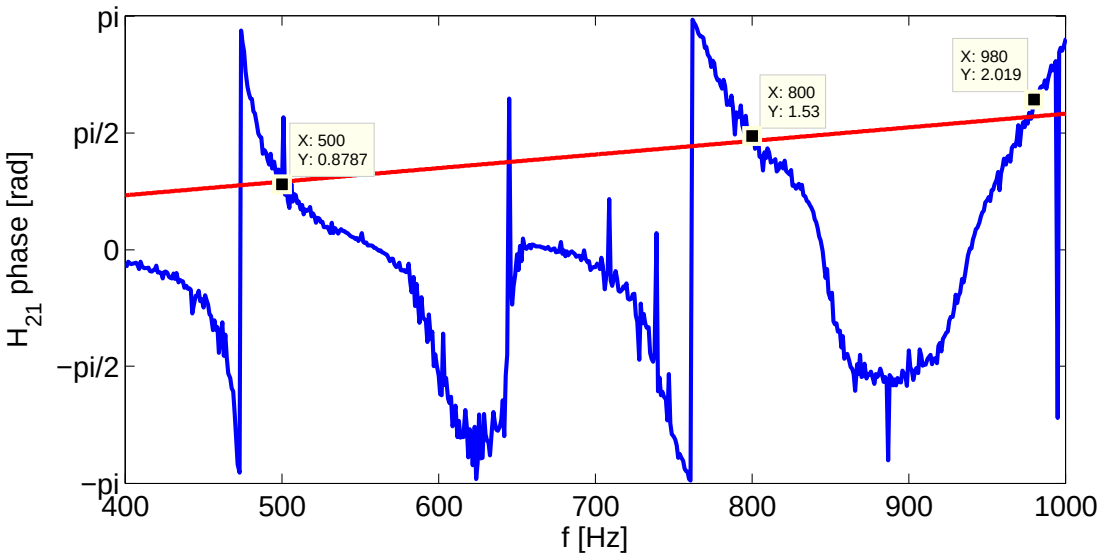

Figure 3.17: Phase response between the microphones.

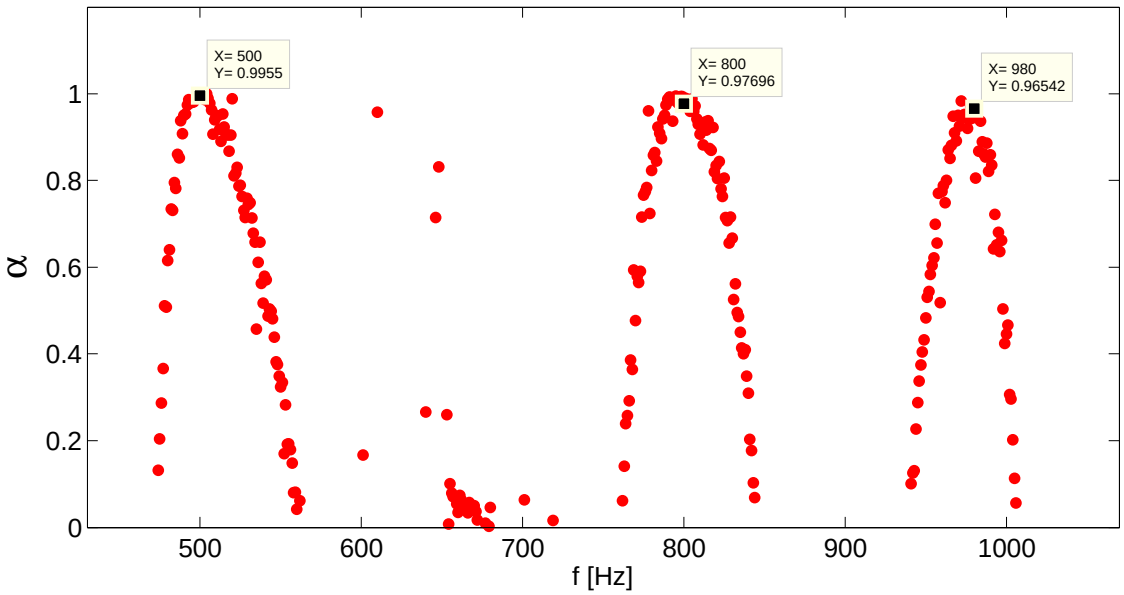

Figure 3.18: Absorption coefficients α for broadband excitation. The active absorption system is tunned at 500 Hz.

3.4 Active absorption of a single source mounted over a panel

This experiment was designed to observe the behavior of the active absorption system in a more realistic, but still simplified, condition. In this case, the secondary source was mounted over the surface of a panel and the primary source was placed a couple of meters apart from the panel. To avoid any external disturbance the setup was placed inside an anechoic chamber. Under these conditions, the active absorption system is exposed to a simplified three-dimensional wave propagation condition. This configuration allows to obtain two important results, once again the absorption coefficient but more importantly a pressure map of the sound field in front of the secondary source. As shown in the simulations depicted in Sections 2.2 and 2.3, this sound pressure map gives a close view of the effect of the active absorber over the sound field, specifically regarding to the minimization of the reflected part of the sound field and consequently the real absorption generated.

Before starting the development of this section it is necessary to remark an important detail about the absorption coefficients measured here. In the past sections the absorption coefficient was measured with the active system in a Kundt's tube and therefore under plane wave propagation conditions. This of course complies with the conditions and methods descried in ISO 10534-2 [34], but now that is not the case since the microphone pair is subject to a three-dimensional sound field. The problematic of the measurement of the absorption coefficient under random and spherical incidence has been studied by several authors, like Rudnick [35], Ingard [36], Cramond [37] and Nocke [38] among others. None of them is completely conclusive about a method to estimate the absorption coefficient. But they agree, specially Ingard, that under some restrictions it is valid to approximate the result of absorption coefficient from plane wave to spherical incidence. The restrictions require that, first, the reflecting surface is acoustically hard enough (i.e. $Z_{\text{panel}} >> \varrho c$), and second, primary source, secondary source and microphone pair are placed over the same axis perpendicular to the panel. According to Ingard, assuming a conservative impedance of the panel of $Z_{\text{panel}} = 10\,\varrho c$, allows to place the primary source at least $1.4\,\lambda$ apart from the panel to have an approximation error of 1 %. If the impedance Z_{panel} increases, the approximation error decreases even more.

Although this criterion is clear about the approximation made for the primary source, it doesn't give much information about how to consider the secondary source. Nevertheless, we estimate that the measurements of the absorption coefficient are still valid. This is based on the fact that the secondary source is used to control the sound reflection in only one direction, perpendicular to the panel, and the absorption coefficient is measured only for this exact same direction.

Normally, in every measurement of absorption coefficients, two conditions (system on and off) are presented. Therefore, even if a small error or bias is introduced in the measurement, this error will be present in both results. Consequently, the comparison between them will still give useful and valid data.

Since the comparison of the performance between manual and adaptive control was already made in the previous sections, and the results showed that there were almost identical performances, this section will simply use the adaptive control system and focus on other important matters.

3.4.1 Absorption coefficient

Pure tone excitation

For these measurements, the secondary source was mounted on a small wood panel of 1 x 1.2 m^2. The primary source was fed with pure tones and the absorption coefficient α was measured. For comparison, α was measured with the control system on and off. Table 3.9 summarizes the results obtained. It is clear to notice that the *System on* condition gives an $\alpha \approx 1$ in every single frequency. The higher values of α at 100-200 Hz when the system is off can be explained by the small dimensions of the panel used and the large wavelengths involved.

f [Hz]	Absorption coefficient α	
	System off	System on
100	0.94952	0.99972
200	0.87513	0.99992
300	0.55602	0.99997
400	0	0.99998
500	0	0.99998
600	0.10163	0.99998
700	0.31450	0.99997
800	0.28528	0.99995
900	0.35285	0.99991

Table 3.9: Absorption coefficients obtained with the active system on and off using pure tones as excitation signal inside the anechoic chamber.

Broadband excitation

In these measurements, the secondary source was mounted on a larger panel of 2.08 x 2.6 m^2. This time the secondary source was fed with band-passed noise signals to obtain a curve of absorption coefficients α. Figure 3.19 shows the results. As one could expect, the results of these measurements show a similar behavior of the α curves obtained in Section 3.2.2 where the measurements were made in a Kundt's tube using broad band noise excitation. In both cases the active system is able to generate reasonably good levels of α, not only for the tunning frequency of the system but also in the surrounding frequencies.

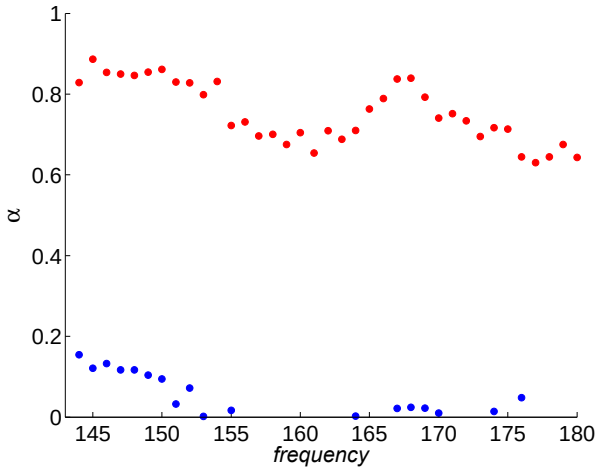

(a) 160 [Hz]

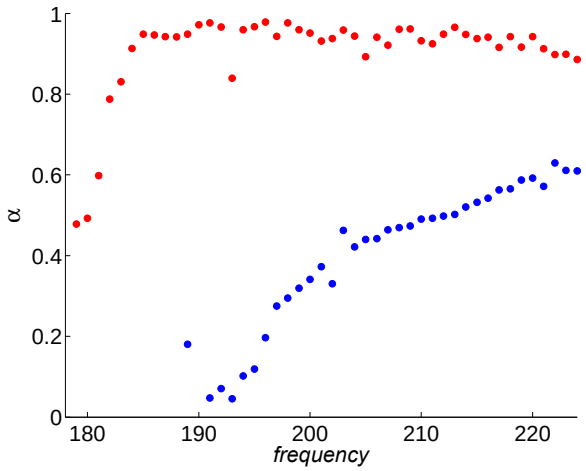

(b) 200 [Hz]

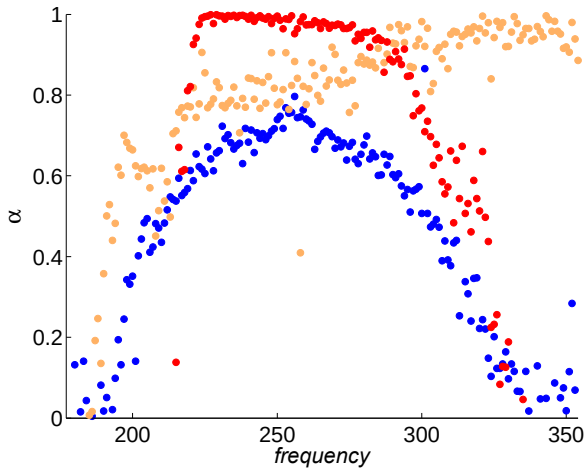

(c) 250 [Hz]

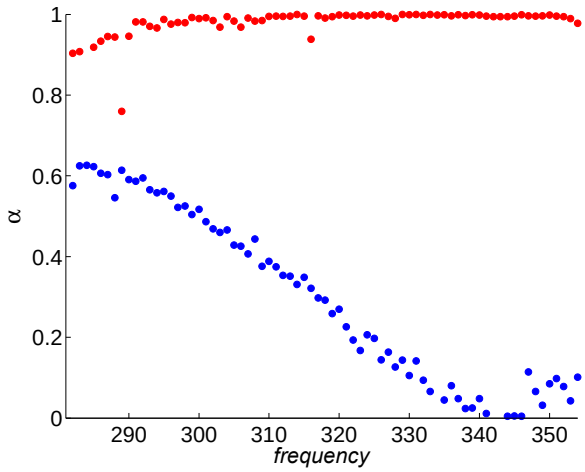

(d) 315 [Hz]

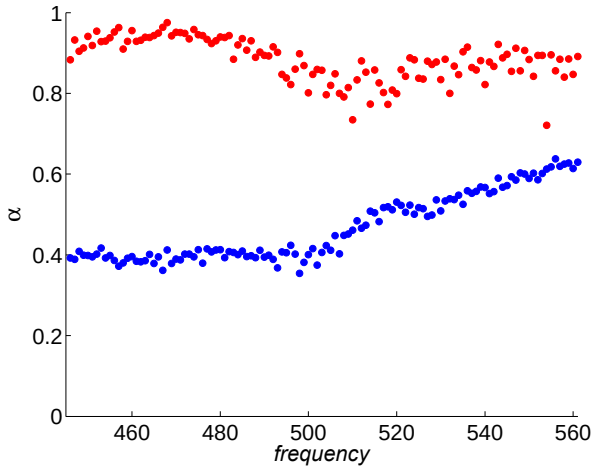

(e) 500 [Hz]

Figure 3.19: Curves of absorption coefficients α for each tunning frequency mentioned, system on (red) and system off (blue). 1/3 octave band noise excitation used. Figure (c) also shows system on using 1/1 octave band excitation, in orange.

3.4.2 Sound pressure map in front of the secondary source

The simulations made in Section 2.3 provided key information about the effect of the active absorption system over the sound pressure field within an enclosure. The data obtained there showed that, as part of the absorption process, the active system damps the normal modes of the enclosure. This, of course, is something that can be expected from any absorbent material. Thus, this characteristic can be used to visualize the active absorption generated by a more realistic implementation of the system.

In the simple case where a primary source radiates in front of a rigid infinite plane, a stationary field will be generated between the source and the plane. Now, if an absorber is placed over the surface of the plane, it is expected that the stationary field will be damped. This condition can be replicated in an experiment that will allow to put the real effectiveness of the active system under test. Of course, in this case the secondary source will replace the passive absorbent material over the panel.

Hence, this experiment will measure the sound pressure in front of the secondary source, specifically over a plane perpendicular to the membrane of the loudspeaker. Figure 3.20 shows a diagram of the experiment.

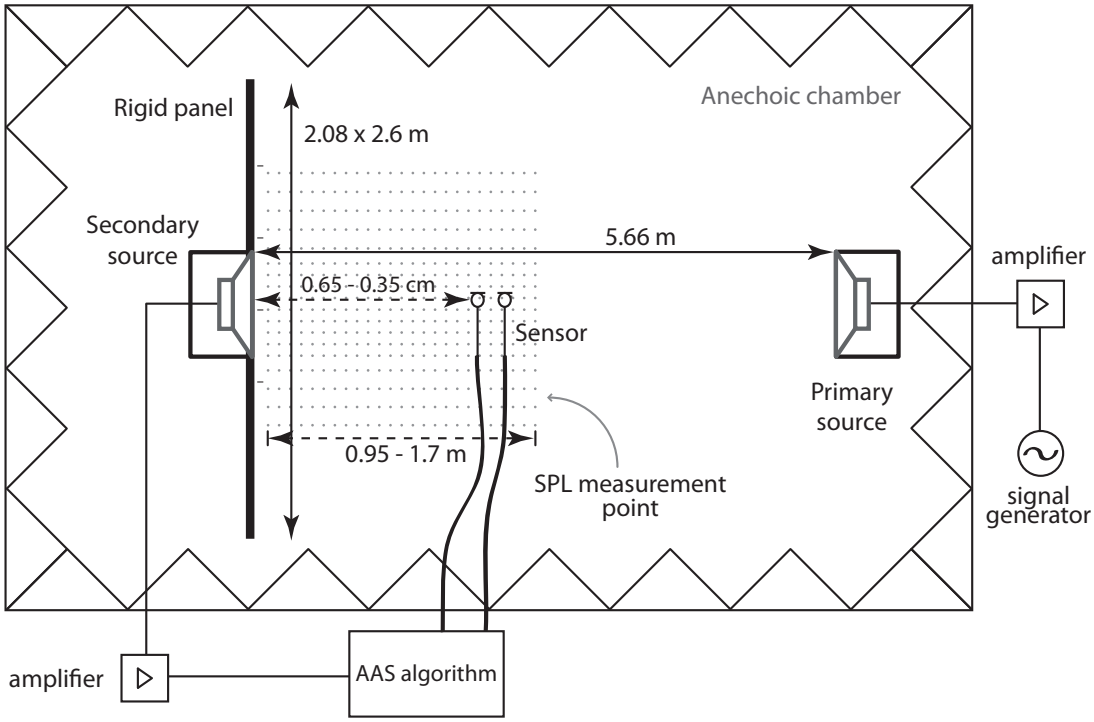

Figure 3.20: Schema of the experiment mounted inside the anechoic chamber. Distribution of the points where the SPL was measured is shown in Figure 3.21.

In practice, to simplify the measurement procedure, an array of 18 microphones was used to sweep the measurement plane. As a result, matrices with 810 - 990 points of sound pressure were obtained. Since our focus is the absorption at low and mid frequencies, the range considered was 75 - 500 Hz.

In the range of 200 - 500 Hz, the microphone array was swept between 0.03 and 0.95 m apart from the secondary source with 45 points equally distributed along the way, recalling that the array had 18 microphones, this gives a total of 810 points of measurements. On the other hand, given the larger wavelength at 75 and 100 Hz, the microphone array was

swept between 0.03 and 1.7 m with 55 points, this results in 990 points of measurements. Depicted in Figure 3.21 is the latter case where 990 points are used, the position of the secondary source is also shown . The mesh of points defined was intentionally denser in front of the loudspeaker. Figure 3.22 presents a set of pictures of the actual setup and the microphone array.

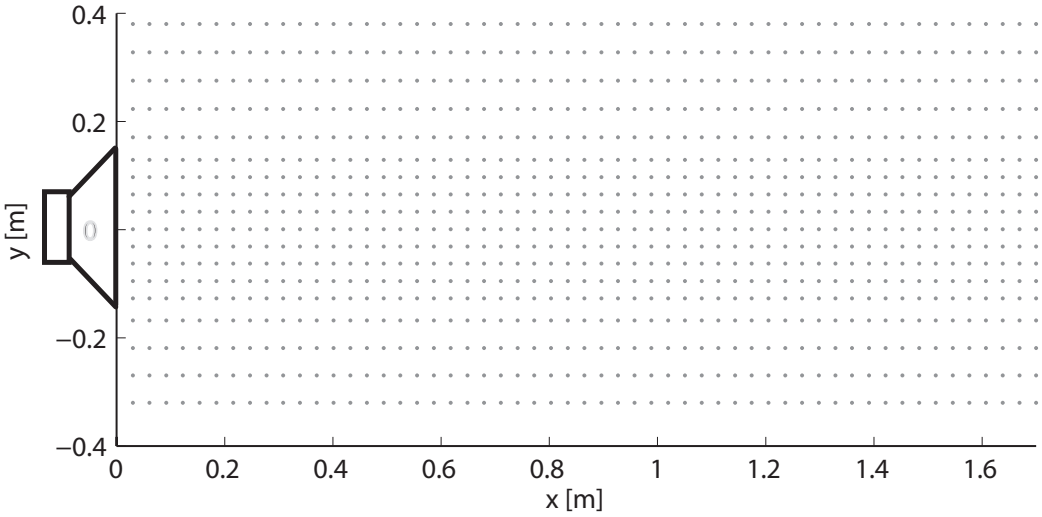

Figure 3.21: Schema of the 990 measurement points and the position of the secondary source.

As seen in the simulations, there is a certain distance between the secondary source and the sensor where the resulting sound pressure field generated by the active absorption appears to be smother, i.e. the pressure decay of the primary source is more homogenous for certain cases. Table 2.3 depict this behavior. Considering this, several distances were tested in these measurements. The distances chosen correspond with the cases were the sound pressure presents a more uniform decay. In the measurements, these distances are easier to visualize in the ANC figures.

f [Hz]	d [cm]
75	65
100	55
200	45
300	35
400	35
500	35

Table 3.10: Distance between secondary source and sensor used in the measurements.

Although the results of these measurements are significants on its own merit, it is important to compare them with simulations of similar conditions. The modeled system considers a primary source simulated as a point source radiating in front of an infinite plane and the secondary source placed on the plane is simulated as a radiating piston.

As mentioned throughout this work, the active absorption system differs entirely with a classical, and widely used, active noise control system. This experiment allows also a direct comparison of these methods since the electronics can be easily adjusted to achieve both control schemes.

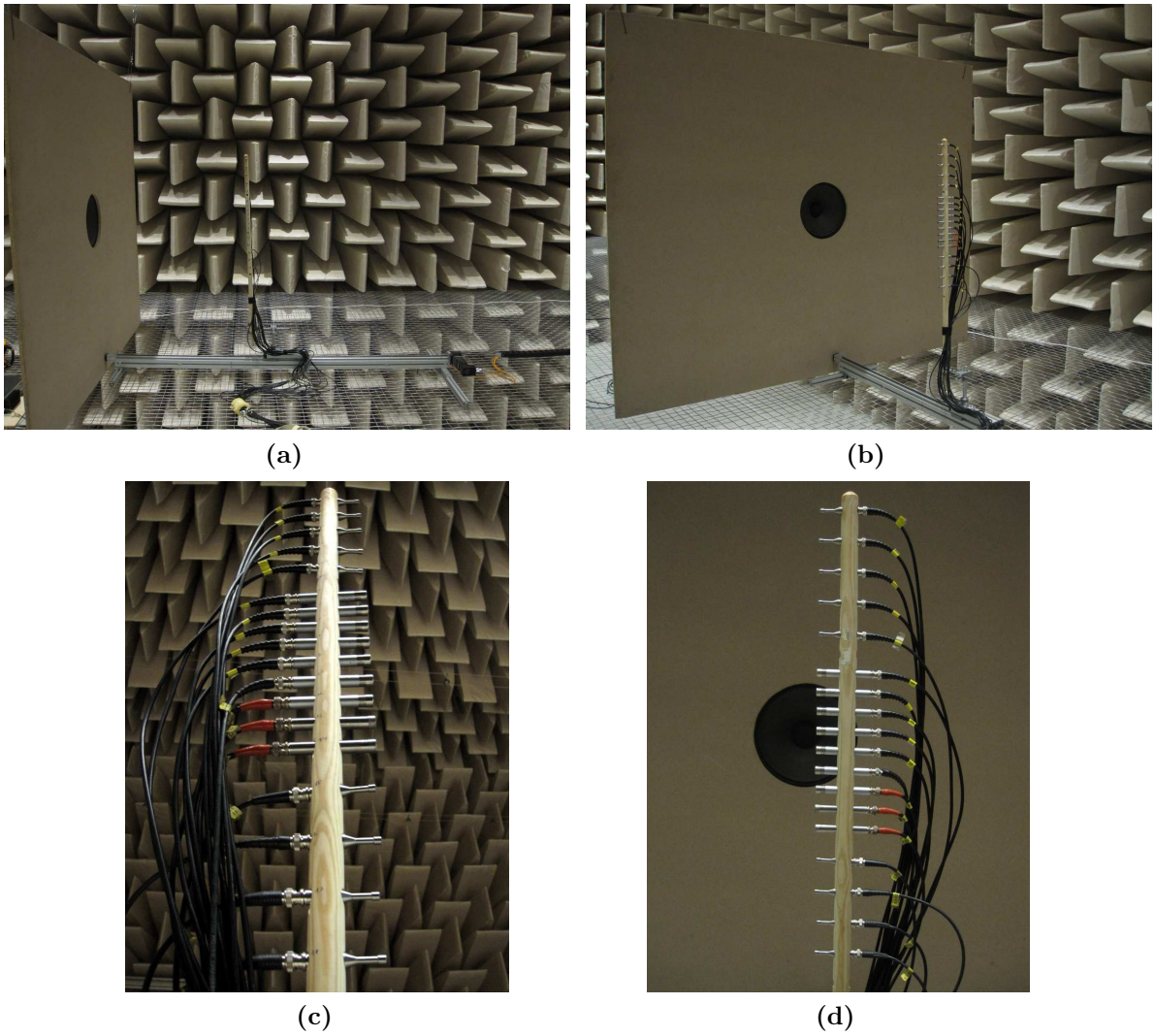

Figure 3.22: Pictures of the experiment setup. (a) and (b) depict the secondary source mounted in the panel and the microphone array in front of it. (c) and (d) show the array with 18 microphones.

Hence for each frequency, three conditions (OFF, AAS and ANC) are measured and presented. Additionally the simulated condition AAS is also included in the figures. Tables 3.11 - 3.16 summarize the results for each frequency.

As expected, the condition OFF in every measurement shows the stationary field generated in front of the panel with its maxima and minima of pressure, these patterns are easier to distinguish at higher frequencies. In the condition AAS it is possible to observe that now the maxima and the minima of pressure present themselves clearly damped, i.e. the lower levels of pressure increase and the higher values decrease. This effect generates a rather homogenous sound field. The results of the measurement agree precisely with simulations, showing that a single control source is able to damp the stationary field in front of it. The area covered by this effect seems to be not so large, but it is necessary to remember that only one secondary source is used. Therefore it is valid to assume that increasing the number of sources over the wall will generate a larger controlled area. On the other hand, the condition ANC shows a common pattern for each frequency measured, where a minimum of pressure is found at the position of the error microphone. As seen, AAS and ANC, present distinctive differences in the resulting sound field.

	75 Hz
OFF	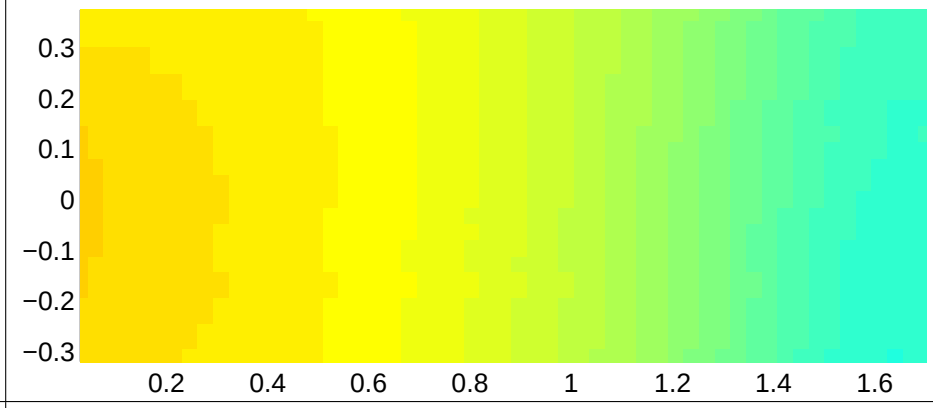
AAS	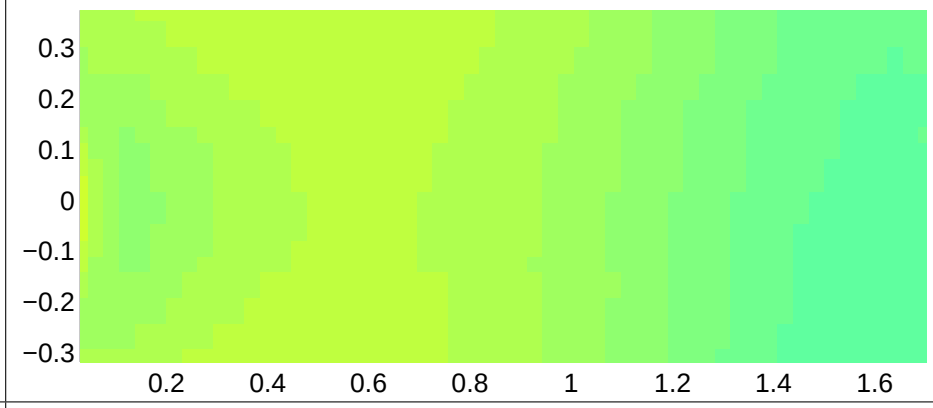
AAS Simulated	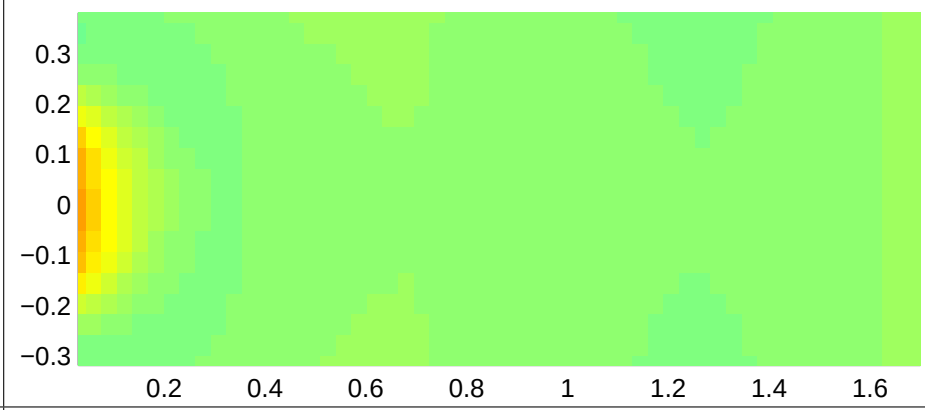
ANC	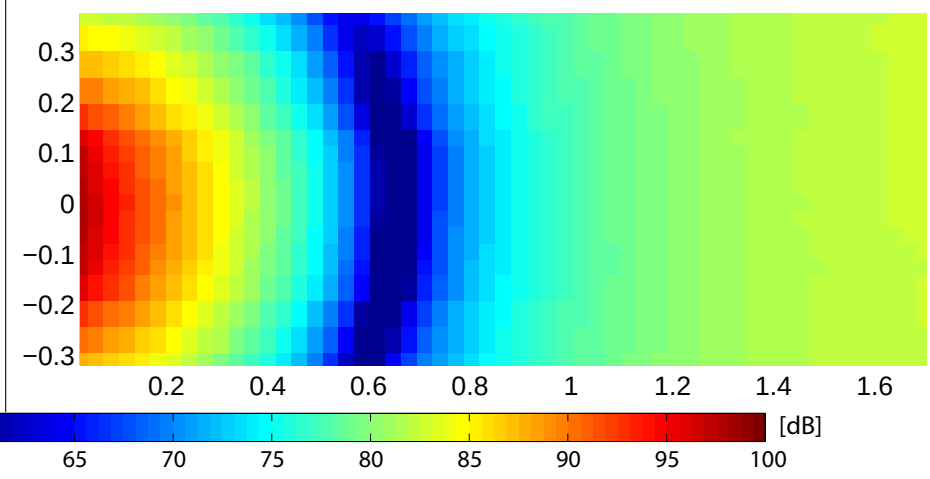

Table 3.11: Measured sound pressure map at 75 Hz: OFF, AAS and ANC. Sound pressure simulation: AAS Simulated. Sensor is located 65 cm away from the secondary source.

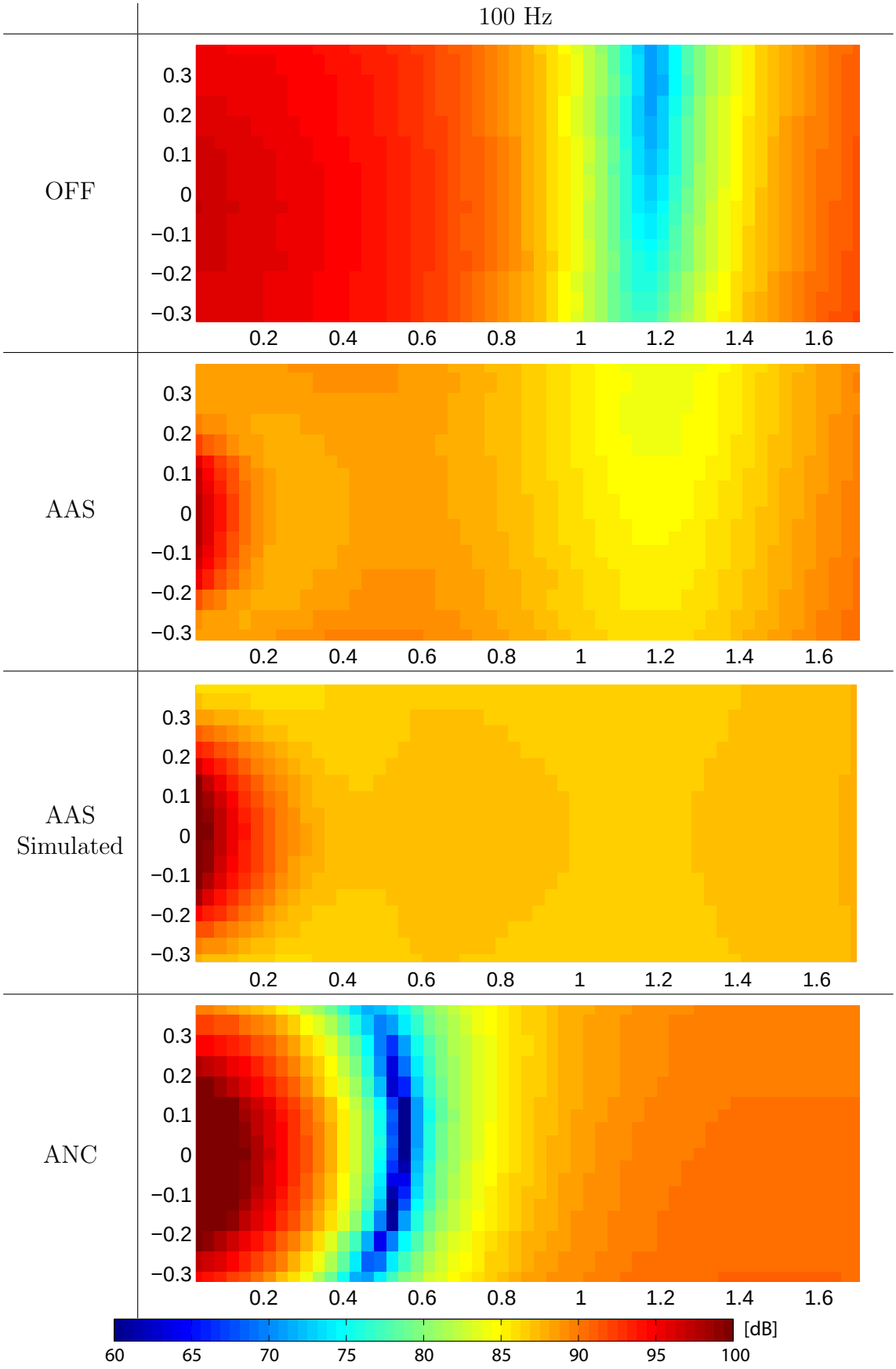

Table 3.12: Measured sound pressure map at 100 Hz: OFF, AAS and ANC. Sound pressure simulation: AAS Simulated. Sensor is located 55 cm away from the secondary source.

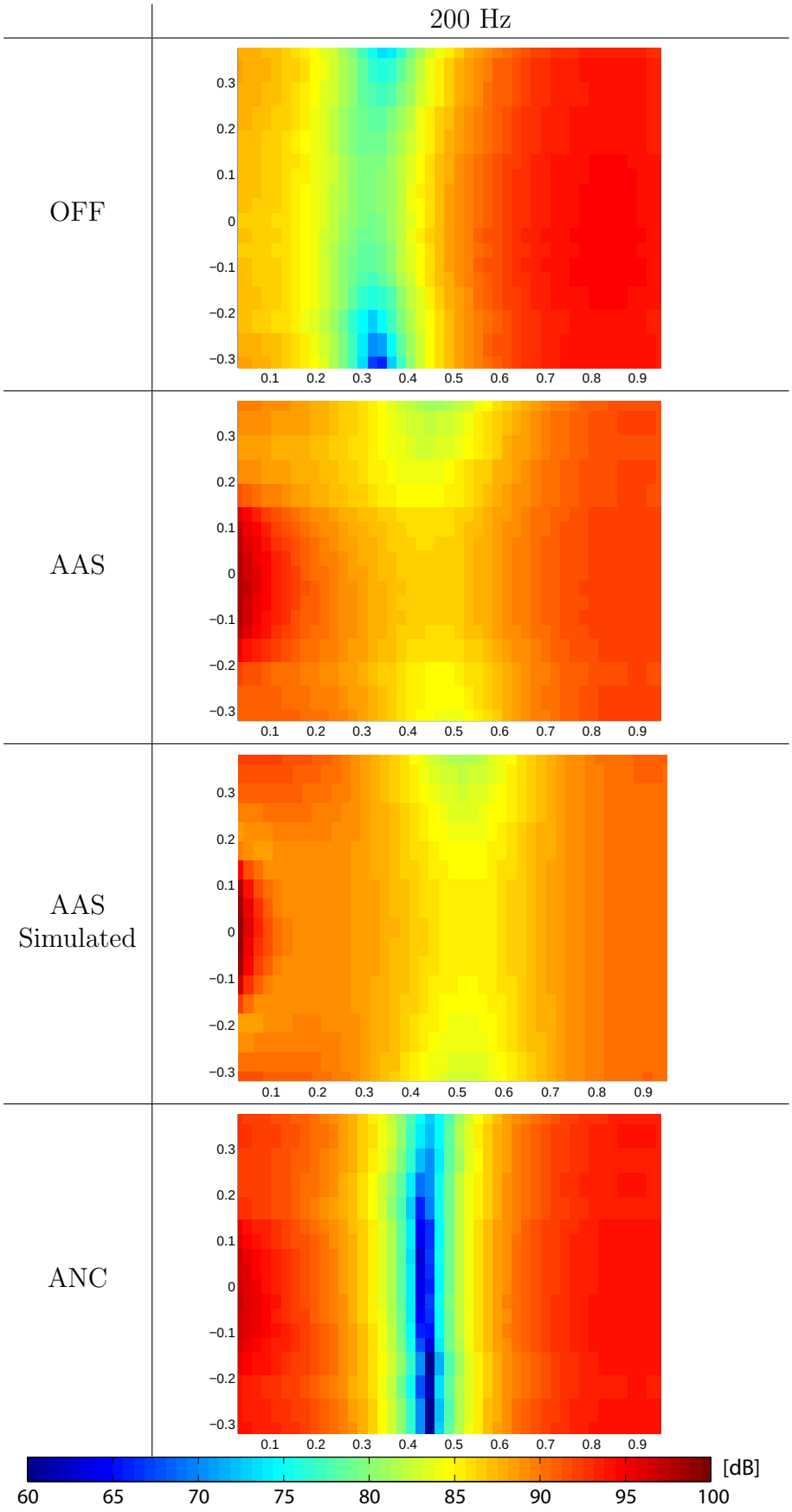

Table 3.13: Measured sound pressure map at 200 Hz: OFF, AAS and ANC. Sound pressure simulation: AAS Simulated. Sensor is located 45 cm away from the secondary source.

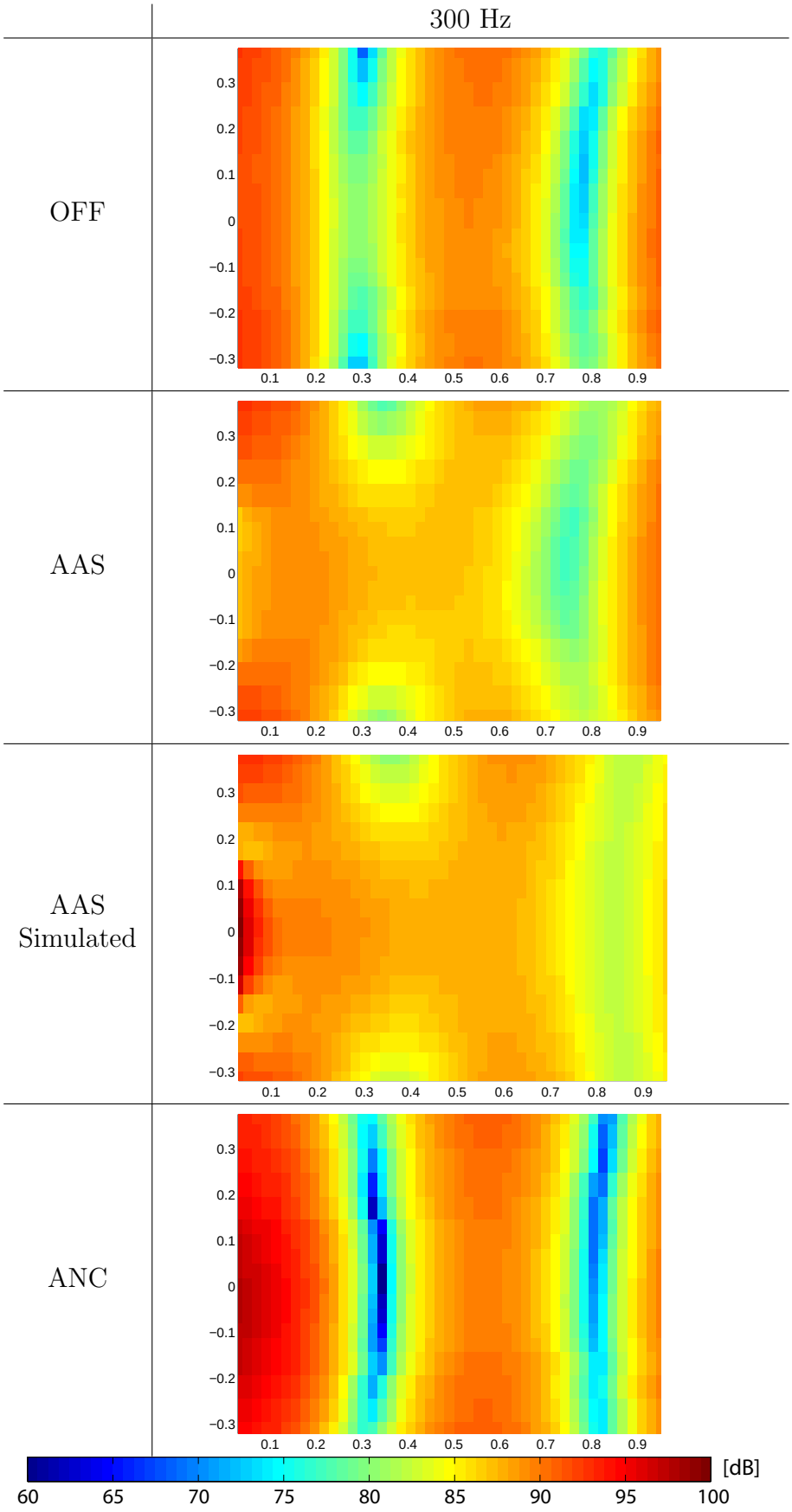

Table 3.14: Measured sound pressure map at 300 Hz: OFF, AAS and ANC. Sound pressure simulation: AAS Simulated. Sensor is located 35 cm away from the secondary source.

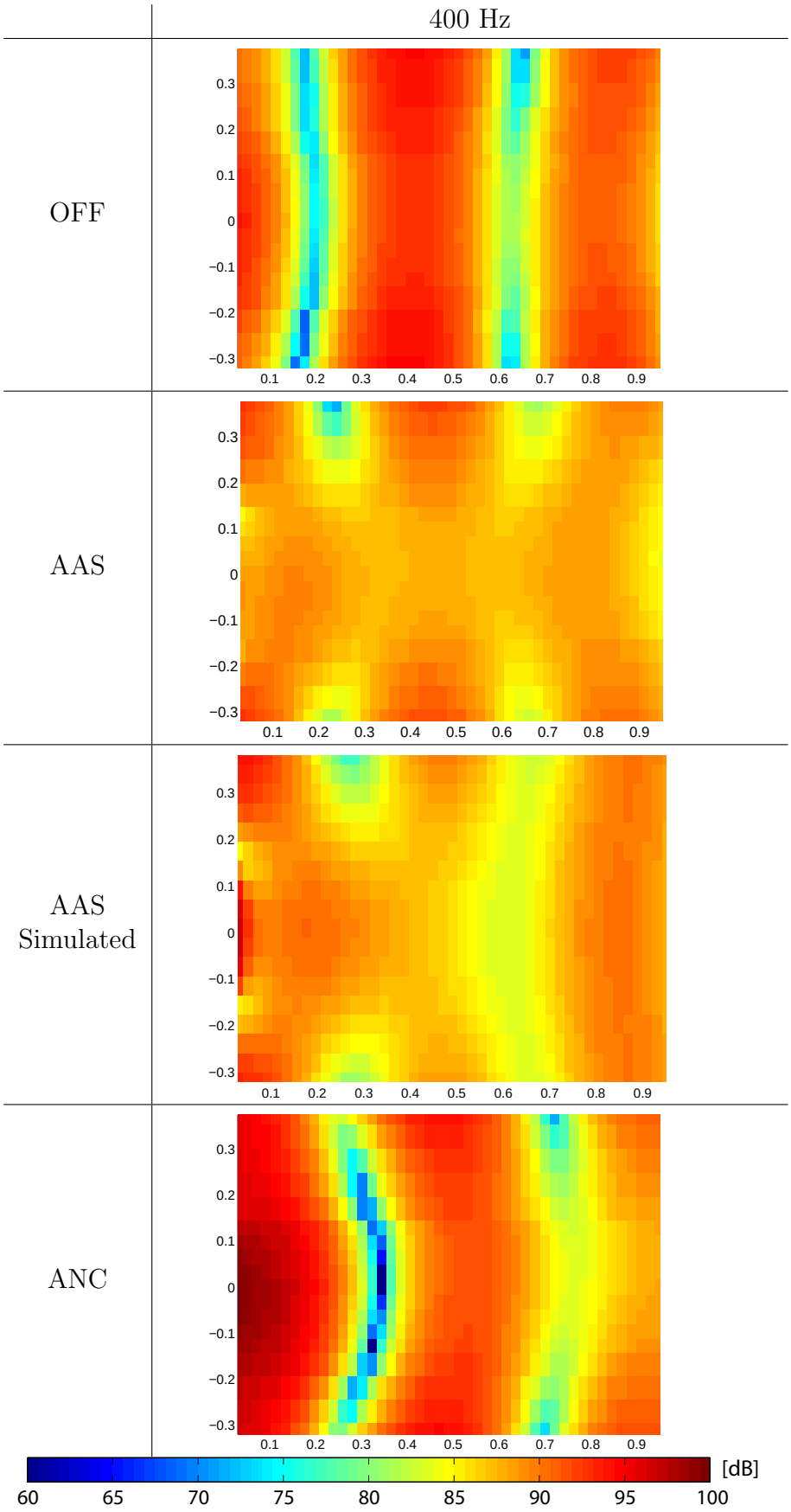

Table 3.15: Measured sound pressure map at 400 Hz: OFF, AAS and ANC. Sound pressure simulation: AAS Simulated. Sensor is located 35 cm away from the secondary source.

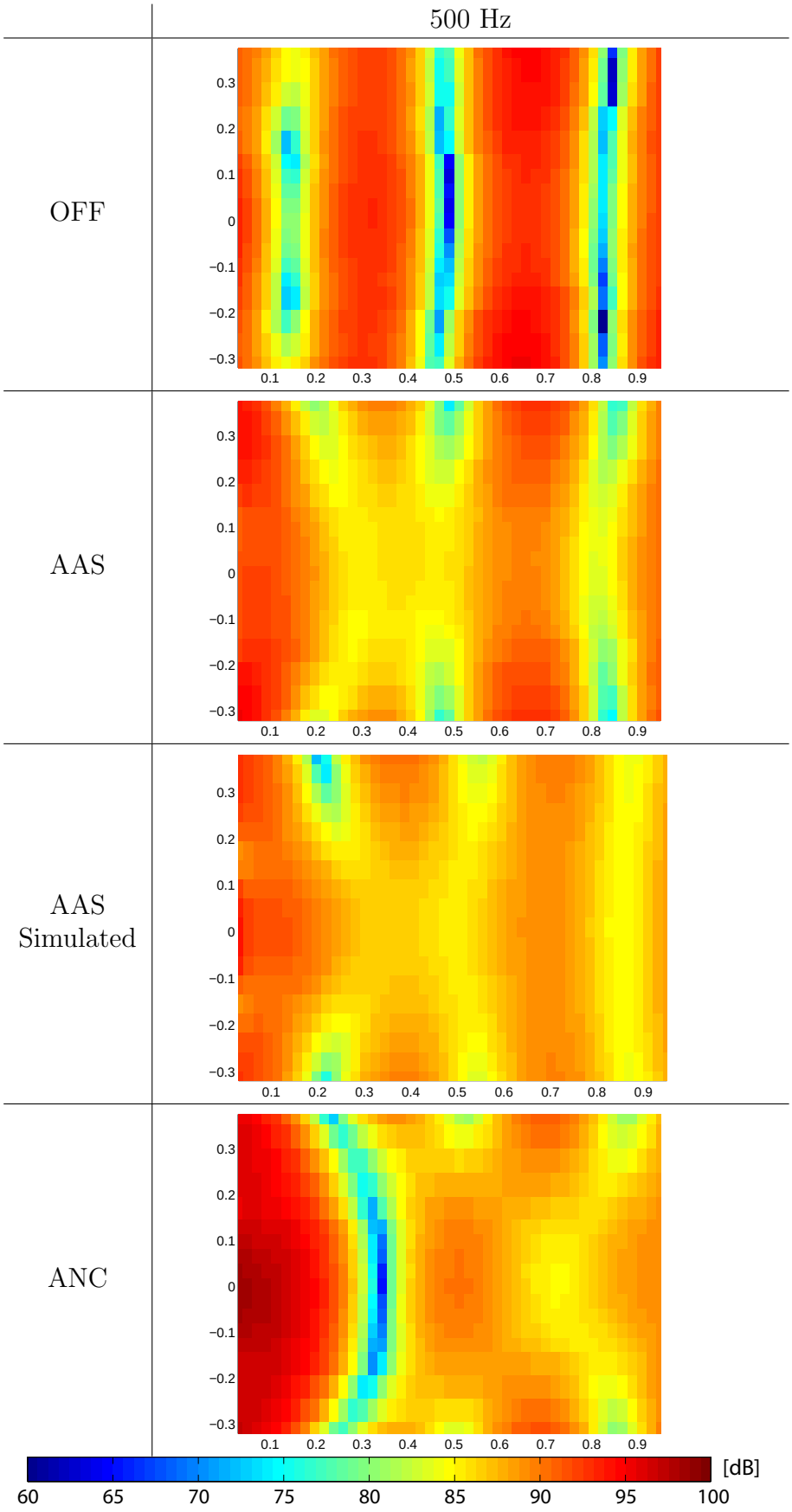

Table 3.16: Measured sound pressure map at 500 Hz: OFF, AAS and ANC. Sound pressure simulation: AAS Simulated. Sensor is located 35 cm away from the secondary source.

Chapter 4

Concluding remarks

Sound absorption is an important property in acoustics. It is one of the parameters that characterize the acoustic quality of a room by its direct influence over the reverberation time. The chance to provide an artificial control of this parameter presents a significant advantage. As seen, the control scheme presented here is not only limited to be applied to simplified sound fields. It has the potential to be implemented under any condition where absorption is required.

Throughout this work a new active absorption method has been presented in details. Every chapter of this theses aimed to answer the questions raised at the beginning. These answers tell that it is possible to create an active absorption system using the knowledge already available from years of development in active noise control (ANC). It was explained how the active absorption uses a particular control criterion that is completely different from typical ANC methods. It was proven that active absorption can be generated for discrete or narrow band frequencies that cover the mid and low spectrum range.

This particular capability of generate absorption at low frequencies offers important benefits. Not only that it is highly efficient in terms of the absorption coefficient that it is able to generate, $\alpha = 1$, but also requires a much smaller constructive volume. This represents always an advantage since it facilitates the implementation and construction of any solution.

A recapitulation of the past chapters helps to emphasize the important aspects of this research.

The wave decomposition method that was presented is based on a simple pair of equations that have crucial importance in the active absorption. They provide the capability to decompose the sound field and *observe* each part independently. These components, the incident and the reflected parts of the sound field, are directly used by the active absorption system. Specifically, the reflected part is used as the control parameter that is minimized. Once the minimization has taken place, only the incident component of the sound field remains, hence generating the active absorption. Although this procedure works correctly, it is just only a special case of a more generalized situation. The latter description assumes that the target absorption coefficient is $\alpha = 1$ and tries to totally minimize the reflected component. However if the required α is smaller, the incident component of the pressure and the reflection coefficient r can be introduced in the equations to generate an arbitrary value of α. In this way a desired α can be obtained introducing a given r, where both quantities are related by $\alpha = 1 - |r|^2$.

Although the wave decomposition is able to separate only one of the directions of the sound field, lets say incident and reflected components of the wave traveling in the positive direction of the x axis, this decomposition can be applied simultaneously to several directions in space. This allows to implement the minimization of the reflected components independently for each direction. The minimization of all these components together generates total absorption in every direction as a result. This extreme case is achieved by applying the decomposition for six directions, positive and negative direction for the x, y and z axis. This is the reason why the cost function J that generates total absorption can be written by the combination of the six independent cost functions as

$$J = J_{x_p} + J_{x_n} + J_{y_p} + J_{y_n} + J_{z_p} + J_{z_n}.$$

It was proven that the active absorption system can be implemented as a manual or as an adaptive controller. Both implementations provided equally positive results. When the primary excitation is known and invariable, e.g. in a ventilation duct, a manual or fixed control offer simplicity and ensures stability. On the other hand when the excitation is constantly changing, e.g. in a music hall or a conference room, the adaptive controller fits the required flexibility to continually adjust the control signal. Naturally both methods offer pros and cons, the right choice must be taken only case by case.

As in every active control system a secondary path is introduced in the algorithm to compensate the transfer function between the output of the controller and the error signal. This is a common task easily solved in most implementations however in the particular case of the active absorption system there is no physical error signal available. Therefore it is not trivial to establish the secondary path. Since in this case the error signal is actually generated inside the algorithm, special attention must be taken to obtain the secondary path in such a way that includes all the components, in the physical and electronic domain.

It was shown that in a one-dimensional waveguide the amount of power absorbed by the active system depends on the impedance of one of the ends of the enclosure. In practice, the best case of absorption is achieved when the impedance of the boundaries are high, i.e. in a rigid closed system. Under these conditions the active system is able to absorb the totality of the incident power, which is translated in the ability to generate an absorption coefficient of $\alpha = 1$.

The active absorption system was combined with the mathematical model of a rectangular three-dimensional room to study the behavior inside a larger enclosure and the influence of the active absorption on the sound field. Simulations showed that the active absorption system is able to replicate a free field condition inside a rigid enclosure.

An extensive set of simulations were carried out to study the effect of different parameters over the efficiency of the active absorption. Special emphasis was put in order to establish the differences between the active absorption system and the widely used ANC systems. The main difference of course lies in the minimization parameter, where for ANC the total sound pressure is used. From the absorption point of view the reduction of this parameter does not contribute to any kind of energy dissipation therefore it does not presents any actual benefit, whereas the active absorption system presents a clear damping of the modes inside the enclosure. This fact is one of the evidences that the system is acting as an absorbent element.

A study of the sensors distribution showed that a certain predefined position must be used to achieve at least some degree of absorption. This remark refers concretely to Figure

2.1 where the best absorption case is obtained when the sensors are regularly distributed near the walls and near the secondary sources. On the other hand a random distribution does not present any utility.

The efficiency of the absorption system was tested under different conditions. One of those condition was a different number and distribution of primary sources. It was established that the system was equally capable to generate efficient absorption under varied conditions of primary sources.

A study of the sound intensity flow near the array of secondary sources showed the dependency between the absorption coefficient generated and the density of sources and sensors. It was found that a minimum density of '3 sources per wavelength' of the excitation signal is required to achieve a high degree of absorption. The similar rule is also required for the number of sensors. As the value of the density approaches to '3 sources per wavelength', the absorption coefficient rapidly increases and reaches approximately 1. This rule provides a valuable evaluation criterion at design time since it allows to calculate the necessary number of sources and sensors required to obtain a high level of absorption for a certain frequency range.

Although the finding of this criterion of '3 sources per wavelength' is a remarkable result, it is not entirely surprising. Nelson describes in his book [19] the problem of discretization of continuos sources and presents the results of several authors regarding this matter. Trying to discretize the Kirchhoff-Helmholtz integral equation method for active absorption it was found that the spacing between an array of secondary sources should be at most $\lambda/2$ to provide a substantial result. However, this is only an approximated value since every author presents slight differences, e.g. $\lambda/\sqrt{\pi}$ or $\lambda^2/(2.5)^2$. This spacing of sources is assumed to be the optimal point between the effective absorption cross-section of a monopole and the distance where mutual interaction would be relatively small. This value presented by Nelson, agrees precisely with the here found criterion of '3 sources per wavelength'.

The evident improvement in the absorption generated above this criterion is not only seen in the absorption coefficient calculated but also in the frequency response and the potential energy. The rule of '3 sources per wavelength' allows to define an upper frequency limit f_{Limit} where the absorption performance is ensured. The simulations of frequency response and potential energy show not only the clear damping of the resonances of the enclosure but also present the difference in the performance below and above f_{Limit}. However it must also be noticed that for near frequencies above f_{Limit} the responses also present a significant degree of damping. This means that f_{Limit} is not a strict frontier for the absorption.

Measurements confirmed in practice the capabilities of the active absorption system. Initially, investigation was carried out using a simple one-dimensional waveguide. This setup helped to establish the real feasibility of the active absorption system driven by the wave decomposition method. The results showed that it was possible to generate high values of absorption coefficients not only for discrete frequencies but also for band-passed signals. The operational bandwidth of active systems has always been a well know issue and it was out of the scope of this work to try to solve this particular problem. However the good result obtained for these band-passed signals indicates that the bandwidth could be improved using a more complex adaptive algorithm. Nevertheless, the simple and commonly used Fx-NLMS algorithm utilized here provided the necessary performance to show the working capabilities of the active absorption system.

Even though the high values of absorption coefficients measured were an important result, the most conclusive evidence came from the mapped sound pressure in front of the secondary source. The comparison between simulations and measurements corroborated the capability of the secondary source to damp the modes of a system, something that is visualized as an homogenization of the sound field. Maxima and minima of pressure in a stationary sound field is defined by the superposition of sound waves traveling in different directions. If the reflected components of that sound field are vanished, the result will be only the presence of the incident traveling component. These incident components should always generate a smooth pressure field. This is exactly the result obtained in simulations and measurements, a homogenization of the sound pressure field. Of course it must be noticed that the effective area of absorption is rather small but this is given by the fact that only one secondary source was used in the experiments.

Appendix

List of symbols

α	Sound absorption coefficient
β_i	*Control complex coefficients* for each i-th sec. source
$\boldsymbol{\beta}$	Vector form of β_i
$\boldsymbol{\beta}_{\text{opt}}$	Optimum set of β_i's that minimize J
A_{pqr}	Modal amplitude
$\mathbf{A}$	Complex matrix part of the hermitian quadratic form
$\mathbf{b}$	Complex vector part of the hermitian quadratic form
c	Speed of sound
c_h	Real value part of the hermitian quadratic form
d	Distance between a secondary source and a sensor point
$d_{pp}, \Delta x$	Distance between two pressure microphones
E_p	Potential energy
γ	*Control complex coefficient* of a sec. source
i	i-th secondary source
I	Total number of secondary sources. ($I = 6 \cdot n^2$, six walls covered)
$\overline{I}_1, \overline{I}_2$	Mean sound intensity
$\Im\{\}$	Imaginary part of a complex quantity
J	Cost function
k	Wavenumber
ℓ	ℓ-th sensor
λ	Wavelength
l_x, l_y, l_z	Room dimensions
L	Total number of sensors
n	Number of secondary sources per direction
$\Psi_{pqr}(\vec{\mathbf{r}})$	Modal shape function
p	Sound pressure
p_0	Reference pressure 20 μPa
p_i	Incident component of the sound pressure
p_r	Reflected component of the sound pressure
p, q, r, l, m, n	Modal indexes

P_0	Acoustic power of the primary source
P_s	Acoustic power of the secondary source
ϱ	Air density
$\Re\{\}$	Real part of a complex quantity
r, r_0	Reflection coefficient
$\vec{\mathbf{r}}$	Vector of cartesian coordinates
σ	Density of secondary sources per wavelength
S	Area or cross section area
v, v_1, v_2	Particle velocity
v_i	Incident component of the particle velocity
v_r	Reflected component of the particle velocity
ω	Angular frequency
x, y, z	Cartesian coordinates
x_p, y_p, z_p	Position of the primary source
Z	Acoustic impedance

Bibliography

[1] F. Orduña-Bustamante and P. A. Nelson. An adaptive controller for the active absorption of sound. *J. Acoust. Soc. Am.*, 91(5):2740–2747, 1992.

[2] Zhen Wu, Vijay K. Varadan, Vasundara V. Varadan, and Kwang Y. Lee. Active absorption of acoustic waves using state-space model and optimal control theory. *The Journal of the Acoustical Society of America*, 97(2):1078–1087, 1995.

[3] H. Takahashi, Y. Suzuki, S. Takane, and F. Asano. A further investigation into the method for active suppression of reflected sound waves based on the state feedback control. *Acoust. Sci. & Tech.*, 23(3):170–172, 2002.

[4] H. Takahashi, Y. Suzuki, S. Takane, and F. Asano. A new method for active supression of the reflected sound wave based on the kirchhoff-helmholtz integral equation with state feedback control. In *Proc. of ACTIVE 2002*, 2002.

[5] S. Takane and T. Sone. A new theory for active suppression of reflected sound waves from the walls based on kirchhoff-helmholtz boundary integral equation. *Acoust. Sci. & Tech.*, 25(1):37–44, 2004.

[6] R. Clark. Active damping of enclosed sound field through direct rate feedback control. *J. Acoust. Soc. Am.*, 97(3):1710–1716, 1995.

[7] S.J. Elliott, P. Joseph, P.A. Nelson, and M.E. Johnson. Power output minimization and power absorption in the active control os sound. *J. Acoust. Soc. Am.*, 90(5): 2501–2512, 1991.

[8] S. Zimmermann. *Control performance of active absorbers in enclosed, harmonic sound fields*. PhD thesis, Institut für Technische Akustik, Technische Universität Berlin, 2003.

[9] S. Ise and H. Tachibana. Active sound absorver using adaptive signal processing. *J. Acoust. Soc. Jpn.*, 17(6):305–310, 1996.

[10] D. Guicking, K. Karcher, and M. Rollwage. Active control of the acoustic reflection coefficient at low frequencies. In *Proc. INTER-NOISE 83*, pages 419–422, 1983.

[11] D. Guicking, K. Karcher, and M. Rollwage. Coherent active methods for applications in room acoustics. *J. Acoust. Soc. Am.*, 78(4):1426–1434, 1985.

[12] H. Zhu, R. Rajamani, and K.A. Stenson. Active control of acoustic reflection, absorption and transmission using thin panel speakers. *J. Acoust. Soc. Am.*, 113(2): 852–870, 2003.

[13] M. Wenzel. *Untersuchungen zur breitbandigen Messung und Regelung der akustischen Wandimpedanz an einer aktiven Schallwand mit adaptiven Filtern*. PhD thesis, Dritten Physikalischen Institut, Georg-August-Universität Göttingen, 1992.

[14] M. Nishimura, K. Ohnishi, W. Patrick, and A. Zander. Development of active acoustic treatment, phase 1: Basic concept and development of aat-cell. In *Proc. of ACTIVE 97*, 1997.

[15] M. Nishimura, K. Ohnishi, W. Patrick, and A. Zander. Development of active acoustic treatment, phase 2: Duct test of aat sheet. In *Proc. of ACTIVE 97*, 1997.

[16] F. Fahy. *Sound intensity*. E & FN SPON, second edition, 1995.

[17] Finn Jacobsen and Hans-Elias de Bree. A comparison of two different sound intensity measurement principles. *The Journal of the Acoustical Society of America*, 118(3): 1510–1517, 2005.

[18] Ning Han and Xiaojun Qiu. A study of sound intensity control for active noise barriers. *Applied Acoustics*, 68(10):1297 – 1306, 2007.

[19] P.A. Nelson and S.J. Elliott. *Active Control of Sound*. Academic Press, 1992.

[20] M. Ochmann. The source simulation technique for acoustic radiation problems. *Acustica*, 81:512 – 527, 1995.

[21] K. Johannsen. *The Influence of Surface Impedances on Sound Radiation Properties of a Shroud-Barrier-Combination - Der Einfluss der Oberflächenimpedanz auf das Abstrahlverhalten eines Schürze-Niedrigstschallschirm-Systems*. PhD thesis, Technische Universität Berlin, 2005.

[22] Michael Möser. Die Wirkung von zylindrischen Aufsätzen an Schallschirmen. *ACUSTICA*, 81:565–586, 1995.

[23] Heinrich Kuttruff. *Room Acoustics*. Elsevier Applied Science. ELSEVIER Science Publishing, third edition, 1991.

[24] P.A. Nelson, A.R.D. Curtis, and S.J. Elliott. Quadratic optimization problem in the active control of free and enclosed sound fields. *Proceedings of the Institute of Acoustics*, 7:45–53, 1985.

[25] ISO 354:2003(E). *Acoustics - Measurement of sound absorption in reverberation room*. International Organization for Standardization, Geneva, Switzerland, 2003.

[26] D.G. Crighton, A.P. Dowling, J.E. Ffowcs Williams, M. Heckl, and F.G. Leppington. *Modern methods in analytical acoustics*. Springer-Verlag, 1942.

[27] Qing-Huo Liu and Jianping Tao. The perfectly matched layer for acoustic waves in absorptive media. *The Journal of the Acoustical Society of America*, 102(4):2072–2082, 1997.

[28] Frank D. Hastings, John B. Schneider, and Shira L. Broschat. Application of the perfectly matched layer (PML) absorbing boundary condition to elastic wave propagation. *The Journal of the Acoustical Society of America*, 100(5):3061–3069, 1996.

[29] COMSOL AB. *Acoustics Module User's Guide*, 2006.

[30] Michael Möser. *Engineering Acoustics: An Introduction to Noise Control*. Springer, 2nd edition, 2009.

[31] Simon Haykin. *Adaptive Filter Theory*. Prentice Hall, Third 1996.

[32] M.R. Schroeder. Integrated-impulse method measuring sound decay without using impulses. *J. Acoust. Soc. Am*, 66(2):497–500, 1979.

[33] A. Carini. Efficient nlms and rls algorithms for perfect and imperfect periodic sequences. *Signal Processing, IEEE Transactions on*, 58(4):2048 –2059, April 2010.

[34] ISO 10534-2:1998. *Acoustics - Determination of sound absorption coefficient and impedance in impedance tubes Part 2: Transfer-function method.* International Organization for Standardization, Geneva, Switzerland, 2001.

[35] Isadore Rudnick. The propagation of an acoustic wave along a boundary. *J. Acoust. Soc. Am.*, 19(2):348–356, Mar. 1947.

[36] Uno Ingard. On the reflection of a spherical sound wave from an infinite plane. *J. Acoust. Soc. Am.*, 23(3):329–335, May 1951.

[37] A.J. Cramond and C.G. Don. Reflection of impulses as a method of determining acoustic impedance. *J. Acoust. Soc. Am.*, 75(2):382–389, Feb. 1984.

[38] C. Nocke, V. Mellert, T. Waters-Fuller, K. Attenborough, and K.M. Li. Impedance deduction from broad-band, point-source measurements at grazing incidence. *Acta Acustica united with Acustica*, 83(6):1085–1090, Nov./Dec. 1997.